Department of Biochemistry, Biotechnologies and Pharmacy

PhD in Biochemistry and Molecular Biology

Cycle XXXIV

Coordinator: Prof. Lorenza Trabalzini

The C-type lectin CD93 in physiological and pathological angiogenesis

Scientific-disciplinary sector: BIO/11

Tutor:

Prof. Maurizio Orlandini

PhD student:

Stefano Barbera

Stefano Barbera Digitally signed by Stefano Barbera Date: 2022.03.07 14:05:00 +01'00'

Academic Year 2021/2022

TABLE OF CONTENTS

LIST OF ARTICLES

Article 1

‘’The C-type lectin CD93 controls endothelial cell migration via activation of the Rho family of small GTPases’’

Barbera, S., Lugano, R., Pedalina, A., Mongiat, M., Santucci, A., Tosi, G.M., Dimberg, A., Galvagni, F., Orlandini, M., 2021a. Matrix Biol. 99, 1–17.

Article 2

‘’CD93 Signaling via Rho Proteins Drives Cytoskeletal Remodeling in Spreading Endothelial Cells’’

Barbera, S., Raucci, L., Lugano, R., Tosi, G.M., Dimberg, A., Santucci, A., Galvagni, F., Orlandini, M., 2021b. Int. J. Mol. Sci. 22, 12417.

Article 3

‘’The small GTPase Rab5c is a key regulator of trafficking of the CD93/Multimerin-2/β1 integrin complex in endothelial cell adhesion and migration’’

Barbera, S., Nardi, F., Elia, I., Realini, G., Lugano, R., Santucci, A., Tosi, G.M., Dimberg, A., Galvagni, F., Orlandini, M., 2019. Cell Commun. Signal. 17, 55.

Article 4

‘’The Binding of CD93 to Multimerin-2 Promotes Choroidal Neovascularization’’

Tosi, G.M., Neri, G., Barbera, S., Mundo, L., Parolini, B., Lazzi, S., Lugano, R., Poletto, E., Leoncini, L., Pertile, G., Mongiat, M., Dimberg, A., Galvagni, F., Orlandini, M., 2020. Investig. Opthalmology Vis. Sci. 61, 30.

ABBREVIATIONS

AMD	Age-Related Macular Degeneration
bFGF	Basic Fibroblast Growth Factor
BMDC	Bone Marrow Derived Cell
CSA	Choroid Sprouting Assay
CNV	Choroidal Neovascularization
CD93	Cluster of Differentiation 93
C1qRp	Complement Component C1q Receptor Protein
CTLD	C-type Lectin Domain
DOCK180	Dedicator of Cytokinesis
DLL4	Delta-like 4
EC	Endothelial Cell
EGF	Endothelial Growth Factor
EGFR	Endothelial Growth Factor Receptor
ECM	Extracellular Matrix
ERM	Ezrin/Radixin/Moesin
HIF	Hypoxia Inducible Factor
F-actin	Filamentous Actin
FDA	Food and Drug Administration
HGF	Hepatocyte Growth Factor
HUVEC	Human Umbilical Vein Endothelial Cell
HIF	Hypoxia Inducible Factor
IPTG	Isopropyl-β-D-thiogalactoside
KO	Knockout
mAb	Monoclonal Antibody
MMRN2	Multimerin-2
NPC	Nasopharyngeal Carcinoma
NK	Natural Killer
nAMD	Neovascular Age-related Macular Degeneration
NEC	Normal Endothelial Cell
NICD	Notch Intracellular Domain
PI3K	Phosphoinositide 3 Kinase
PDGFB	Platelet Derived Growth Factor B
PDGFRβ	Platelet Derived Growth Factor Receptor β
RPE	Retinal Pigment Epithelium
SDS-PAGE	Sodium Dodecyl Sulphate-Polyacrylamide Gel Electrophoresis
sCD93	Soluble Cluster of Differentiation 93
SC	Stalk Cell
TC	Tip Cell
TEC	Tumor Endothelial Cell
TKI	Tyrosine Kinase Inhibitor
VEGF	Vascular Endothelial Growth Factor

ABSTRACT

Formation of blood vessels is required for development, growth and healing. Although quiescent, endothelial cells (ECs) store a potent proliferative and invasive potential that, upon the appropriate *stimuli*, is unleashed and gives rise to neovascularization phenomena.

Disease progression of cancer and neovascular age-related macular degeneration (nAMD) strongly depends on angiogenesis. In cancer, tumor cells are able to stimulate ECs to become angiogenic and form new blood vessels that allow them to fulfill their tendency to grow and escape the site of the primary tumor. In nAMD, instead, inflammation and drusen deposition induce a strong damage to the retinal pigment epithelium (RPE), which in response to the damage triggers abnormal vessel formation that directly causes disease progression and consequent vision loss. In light of the role that angiogenesis plays in these diseases, targeting blood vessels with anti-angiogenic drugs has always been an appealing concept. However, due to the partial failure of anti-angiogenic therapies in the treatment of such diseases, it has become crucial to find alternative strategies that rely on targeting new molecules in a way to show great efficacy with minimal toxic effects.

CD93 is a transmembrane glycoprotein that has been shown to have a prevalent role in controlling EC function, such as cell adhesion and migration. In this work, we investigated the molecular pathways behind the function of CD93 as regulator of EC adhesion and migration, showing that CD93 regulates actin dynamics *via* the small GTPases Rac1, Cdc42 and RhoA in a signaling axis triggered by its phosphorylation and interaction with Cbl phosphorylated on tyrosine 774. We also gained insights on the functional transport of CD93 during adhesion and migration, demonstrating that it is regulated by both its cytoplasmic domain and the Rab5C-dependent early endosome pathway. Importantly, we showed that CD93 is retrieved from and recycled back to the plasma membrane together with its interacting partners Multimerin-2 (MMRN2) and β1 integrin. Due to the relevant role played by the CD93/MMRN2 interaction in controlling EC function, we tested the potential of inhibiting it, by means of a monoclonal antibody, in *ex vivo* human models of nAMD. Finally, for the first time we characterized a CD93 dimeric form in ECs, showing that the CD93 dimer strongly binds to MMRN2, and setup the expression of a soluble recombinant CD93 comprising the CTLD and sushi domains for further protein crystallization and structural analyses.

1 INTRODUCTION

1.1 Angiogenesis and molecular regulation of vessel sprouting

An ancestor of the modern vascular system has evolved as early as 600 million years ago when the first triploblastic organism set foot on earth, a phenomenon that allowed species to overcome the constraint of diffusion (Monahan-Earley et al., 2013). The vascular system forms during development by progenitor endothelial cells (ECs) (angioblasts) by a phenomenon termed vasculogenesis, which leads to the formation of "blood islands". The mature vascular bed consists of a hierarchically organized intertwining of veins, venules, capillaries, arterioles, and arteries which continuously remodels in order to respond to oxygen and nourishment demand (Herbert and Stainier, 2011). Such remodeling process is called angiogenesis. Differently from vasculogenesis, which is the *de novo* formation of blood vessels, angiogenesis (classified in sprouting and intussusceptive) is instead the process by which new blood vessels are formed by pre-existing ones (Carmeliet, 2003). In sprouting angiogenesis, ECs bud from a parental vessel to form a new branch of the network (Adams and Alitalo, 2007; Herbert and Stainier, 2011). To properly exert their physiological function, blood vessels need to be stable and quiescent. However, when a sprouting event is needed, this process must be tightly regulated, because it requires a strong stimulation that drives differentiation, proliferation, and motility of ECs, which destabilize the vessel structure. Hypoxia is the leading *stimulus* of sprouting angiogenesis and triggers the expression and exocytosis of pro-angiogenic molecules by stromal cells. The Hypoxia Inducible Factor (HIF) 1 consists of one α and one β subunit and acts as an O_2 sensor allowing tissues to respond to low oxygen tensions. Indeed, when O_2 levels are low, the HIF-1α subunit accumulates into the cytosol and subsequently enters the *nucleus*, where it interacts with the HIF-1β subunit thus starting the transcription of numerous pro-angiogenic genes (Zimna and Kurpisz, 2015). One of the genes regulated by HIF-1, and probably the strongest inducer of angiogenesis known so far, is the Vascular Endothelial Growth Factor A (VEGFA) (Zimna and Kurpisz, 2015). VEGFA, along with other soluble factors such as: Fibroblast Growth Factor (FGF) 1, FGF2 and FGF4, angiopoietins (1 and 2) and Platelet Derived Growth Factor (PDGF), triggers EC sprouting (Otrock et al., 2007). VEGFA exerts its activity by binding the cognate receptor VEGF receptor (VEGFR) 2 expressed on the EC surface. VEGFR2 is a transmembrane tyrosine kinase receptor which dimerizes and autophosphorylates upon VEGFA binding, thus starting a signaling cascade that culminates in EC proliferation, tube formation and chemotaxis (Herbert and Stainier, 2011; Otrock et al., 2007). ECs that experience the VEGFA-VEGFR2 signaling become tip cells (TC) and acquire a motile and invasive phenotype (Gerhardt et al., 2003). TCs lose their pericyte coverage, degrade the extracellular matrix (ECM) and extend pro-migratory filopodia and lamellipodia, which allow them to sprout out the parental vessel and probe the microenvironment, therefore becoming the lead of the nascent vessel (De Smet et al., 2009; Herbert and Stainier, 2011). Surrounding cues have a dual nature, they are both biochemical and mechanical. Soluble cytokines, such as VEGFA, bind their receptor on the TC surface inducing downstream signaling events, in terms of protein post-translational modifications, important for TC motility and chemotaxis. On the other hand, mechanical cues due to matrix composition

and stiffness are physically sensed by the TC through a paraphernalia of mechanoreceptors among which integrin α5β1 and αvβ3 have shown to play crucial roles in EC-ECM interaction during angiogenesis (De Smet et al., 2009; Neve et al., 2014). Integrins are connected directly to the actin cytoskeleton by a series of adaptor proteins and convert mechanical cues in signaling events that result in either elongation or retraction of the TC (Harburger and Calderwood, 2009). A clear example of such signaling dualism is the cooperation between integrin αvβ3 and VEGFR2, which is regulated by matrix composition and VEGFR2 stimulation, and acts synergistically to promote EC adhesion, migration, and proliferation (Mahabeleshwar et al., 2007; Plow et al., 2000; Somanath et al., 2009). Importantly, the activation of the small GTPases, Rac1, RhoA and Cdc42, essential for filopodia and lamellipodia formation, is regulated by both the VEGFA and integrin signaling triggered upon integrin engagement of the ECM (De Smet et al., 2009; Harburger and Calderwood, 2009). Moreover, Rac1, RhoA and Cdc42 are critical orchestrators in the establishment of TC shape and polarity during the sprouting event (De Smet et al., 2009; Merajver and Usmani, 2005, 2005). While TCs lead the sprout, specialized ECs, termed stalk cells (SCs) trail behind them and allow sprout elongation. Differently from TCs, SCs do not assume an invasive phenotype, but, instead, proliferate, lay down the ECM and form the lumen (De Smet et al., 2009). The balance between TC and SC fate is based on Notch signaling. Indeed, VEGFA stimulation of VEGFR2 in the TC induces the expression of Delta-Like-4 (DLL4), a juxtracrine binding partner of Notch, whose expression is high in SCs (Herbert and Stainier, 2011). The binding of DLL4 to Notch triggers Notch cleavage and the release of the Notch Intracellular Domain (NICD) into the *nucleus* of SCs where it inhibits VEGFR2 expression and induces the expression of VEGFR1, a decoy receptor which sequestrates VEGFA preventing VEGFR2 signaling (De Smet et al., 2009). To form a new connection, TCs need to switch their motile and explorative phenotype when they meet their target, which is usually a TC from another sprout or a capillary. Next, the TC and the target establish stable cell to cell junctions at the joining point, stabilizing the new forming vessel. Moreover, the release of PDGFB from both TCs and SCs allows the recruitment of pericytes, which express high levels of PDGF receptor (PDGFR) β. Pericyte recruitment, together with matrix deposition, promote vessel maturation and quiescence (Herbert and Stainier, 2011). Finally, lumen formation occurs in the cytoplasm of SCs by fusion of large vacuoles. This allows perfusion of the newborn blood vessel which by itself promotes maturation processes such as pericyte attachment, ECM deposition and stabilization of cell junctions (Adams and Alitalo, 2007; Herbert and Stainier, 2011).

1.2 Angiogenesis in disease

Beside oxygen transport, blood vessels deliver hormones, growth factors, neurotransmitters and cells of the immune system (Filipowska et al., 2017; Pober and Tellides, 2012). Therefore, the vascular network is a must in development, growth, endocrine communication, and immunity and it is not surprising that a dysfunction in the vascular system may itself cause or exacerbate pathologies. Defects in the angiogenic mechanisms that culminate in insufficient angiogenesis or in an exaggerate vessel regression cause pathologies in different organs including lungs, kidneys, bones, the nervous system, the gastrointestinal and cardiocirculatory apparatus, the skin, and the reproductive system (Carmeliet, 2003). On the other hand, when vessel growth is uncontrolled, angiogenesis becomes the cause or contributes to the development of numerous diseases (Carmeliet, 2003). In this section, we will focus on the role that angiogenesis plays in cancer and in the neovascular stage of age-related macular degeneration (AMD).

1.2.1 Angiogenesis and cancer

When the American oncologist Judah Folkman in 1971 reported his observations of how tumor cells stimulate EC growth and sprouting, the fact that neovascularization played a role in solid tumors growth was already known, yet not fully appreciated (Folkman, 1971). Nowadays, the important role played by blood vessels in cancer development is well established. In fact, blood vessels allow solid tumors to grow over a certain size and guarantee a highway for either extravasation or co-option of metastatic cancer cells facilitating their escape from the site of the primary tumor (Carmeliet and Jain, 2011a; De Palma et al., 2017; Reynolds AR, 2019). The intrinsic capacity of tumor cells to proliferate allows them to grow indiscriminately. However, after reaching a critical size the tumor bulk undergoes some physical constraints among which two major limitations for tumor expansion are oxygen and nourishment supply. The core of the tumor bulk starts becoming strongly hypoxic and low in pH, increases interstitial pressure and produces potent pro-angiogenic molecules, which are released in the surroundings (Carmeliet and Jain, 2000). Thus, the tumor promotes growth of new blood vessels, which culminates in the disruption of the equilibrium that keeps quiescent the vasculature. This scenario has been named ‘’angiogenic switch’’ and allows tumor cells to exit dormancy and start a rapid growth, which associates with new blood vessels formation (Baeriswyl and Christofori, 2009; Lugano et al., 2020). Tumor cells constantly produce an array of different pro-angiogenic molecules such as VEGFA, bFGF, angiopoietins, hepatocyte growth factor (HGF), chemokines, and PDGF, inducing a constant stimulation of adjacent ECs. Such persistent stimulation of ECs causes dysregulation of quiescent normal vasculature and results in the aberrant morphogenesis typical of tumor blood vessels. Indeed, the tumor vasculature appears chaotic, vessels are tortuous and dilated showing an increased diameter, and loses its pericyte coverage (Carmeliet and Jain, 2000; Hida et al., 2016; Lugano et al., 2020). Ultrastructural analyses have shown that tumor ECs (TECs) are characterized by a discontinuous basement membrane, irregular inter-endothelial junctions, and cell projections into the lumen as consequence of the altered polarity (De Palma et al., 2017). The structure of the tumor vasculature reflects the peculiar phenotype that TECs acquire. The constant angiogenic stimulation in the tumor microenvironment leads

TECs to aneuploidy and centrosome abnormalities as well as acquisition of a protein expression profile compatible with angiogenic ECs (Hida et al., 2016, 2004). Indeed, the expression pattern of TECs highly differs from normal ECs (NECs). TECs express embryonic markers such as PAX2 and high levels of EGFR2, secrete themselves VEGFA thus establishing autocrine loops that lead to self-stimulation of pro-angiogenic signaling pathways (Hida et al., 2016).

1.2.2 Inhibition of angiogenesis in cancer

Due to its central role played in angiogenesis, the VEGFR2-VEGFA axis is considered a suitable target to inhibit tumor angiogenesis and subsequently the tumor growth. Almost two decades ago, the proof of concept that targeting angiogenesis was beneficial to treat cancer came out by a study showing clear survival benefits in patients treated with chemotherapeutic agents in combination with bevacizumab, a monoclonal antibody targeting VEGFA (Hurwitz et al., 2004). This study set a milestone in the anti-angiogenic treatments and nowadays numerous anti-VEGFA and anti-VEGFR2 drugs are Food and Drug Administration (FDA) approved and used in the treatment of cancer. Despite the initial beneficial promises, the success of anti-angiogenic therapies was only partial. Numerous are the reasons why anti-angiogenic therapies did not fulfill the hoped expectations. Due to an extreme heterogeneity of cancer cells, some tumors are intrinsically resistant to anti-angiogenic therapies or in alternative they respond initially and acquire mechanisms of resistance during the course of the treatment (Lupo et al., 2017). During the treatment, sustained blockade of VEGFR2 signaling leads to the formation of highly hypoxic areas within the tumor parenchyma, stimulating the overproduction of pro-angiogenic molecules as compensatory mechanism and converting tumor angiogenesis in VEGF-independent (Carmeliet and Jain, 2011a). Tumor vascularization also relies on the recruitment of bone marrow-derived cells (BMDCs), which start the *de novo* formation of blood vessels, or, alternatively, the tumor co-opts the vessels in a mechanism by which cancer cells migrate toward and along the vasculature (Lugano et al., 2020; Reynolds AR, 2019; Seano and Jain, 2020). Another mechanism of tumor resistance is the vasculogenic mimicry, by which tumor cells form vessel-like structures that allow sufficient tumor perfusion or vessel splitting (Carmeliet and Jain, 2011a). The list of FDA approved drugs for the treatment of angiogenesis is not limited to VEGF blockers. Different tyrosine kinase inhibitors (TKIs) and monoclonal antibodies against other targets are employed in the treatment of different cancer types. However, the therapeutic outcomes are still limited by insufficient efficacy and development of resistance. An interesting avenue would be the normalization of the vascular rather than the tumor vessel depletion. Vascular normalization has been shown to be beneficial in pre-clinical and clinical studies where normalization of vascular abnormalities revealed useful in the treatment of cancer and other angiogenic diseases (Carmeliet and Jain, 2011b). Aiming for vascular normalization rather than pruning promotes tumor perfusion and therefore drug delivery and immune infiltration. Moreover, correcting vessel abnormalities reduces hypoxia in the tumor milieu and prevents the development of more aggressive cancer cells (Magnussen and Mills, 2021; Viallard and Larrivée, 2017).

1.2.3 Angiogenesis and neovascular AMD

The age-related macular degeneration (AMD) is a progressive degeneration of the photoreceptor–retinal pigment epithelial complex and a major cause of irreversible blindness among the elderly population (Al-Zamil and Yassin, 2017). AMD develops in a multi-step way. In the early and intermediate phases (non-exudative AMD) yellowish lipid-rich proteins (known as drusen) accumulate between the retinal pigment epithelium (RPE) and the Brunch's membrane causing an impairment of the retinal photoreceptors function (Yerramothu, 2018). As the disease progresses and drusen accumulates, the damaged RPE releases VEGFA starting a phenomenon called choroidal neovascularization (CNV) which progressively leads to the more severe form of AMD, called neovascular AMD (nAMD) (Ng and Adamis, 2005). As in cancer, in nAMD the new blood vessels proliferate abnormally underneath the retina, which may result in the lift of the retina. Moreover, abnormal vessels are often leaky and are responsible for oedema and loss of vision (Yerramothu, 2018).

1.2.4 Anti-angiogenic therapies for nAMD

The first therapy against nAMD employed corticosteroids as off-label treatment of nAMD due to their angiostatic and anti-inflammatory mechanism of action (Ng and Adamis, 2005). A first trial, based on intravitreal injections of corticosteroids, attempted to evaluate their efficacy in nAMD patients, however no significant improvement has been associated with corticosteroids injections (Frank Billson, 2003). Ocular-related complications can occur after treatment with corticosteroids such as increased ocular pressure, development of cataract and retinal cytotoxicity (Challa et al., 1998; Jonas et al., 2005; Yeung et al., 2004). Due to the central role played by VEGF in regulating angiogenesis, the new era of intervention for nAMD patients was the development of VEGF-inhibitors (Ng and Adamis, 2005). To facilitate the drug delivery and minimize systemic cytotoxicity, VEGF-inhibitors are directly injected into the vitreous (Lai and Landa, 2015; Yerramothu, 2018). New and optimized VEGF therapies are currently used in the treatment of nAMD, however, despite showing good efficacy in slowing down the disease progression, inhibition of VEGF has failed to provide a cure for nAMD patients (Yerramothu, 2018). Repeated administrations of VEGF inhibitors are associated with increase of the intra-ocular pressure, hemorrhage, increase in ocular inflammation (Day et al., 2011), and with high risk of developing retinal scarring and geographic atrophy two to five years after the treatment begins (Daniel et al., 2014; Grunwald et al., 2017). To date the research efforts have led to the identification of new targets and experimentations of alternative administration routs to intraocular injections, but currently the most potent approved therapeutic strategies available rely on the employment of VEGF-inhibitors.

1.2.5 Concluding remarks

Angiogenesis represents a target for cancer and nAMD. Nowadays, several anti-angiogenic drugs have been approved by the FDA but none of them has revolutionized treatments and researchers are still trying to improve drug design and dosage to minimize cytotoxic effects while improving efficacy. Going deep in the

molecular mechanisms and characterizing better the TEC phenotype is mandatory for developing more efficient therapeutical approaches. Transcriptome profiling of pathological blood vessels has allowed us to identify novel and more specific angiogenic markers, which can be targeted for more effective therapeutic benefits.

1.3 The C-type lectin CD93 is a regulator of EC function and angiogenesis

In recent years, the member of the group XIV of C-type lectins CD93 has shown to play a crucial role both in physiological and in pathological angiogenesis.

CD93 is a transmembrane protein which from the N-terminus consists of a conserved C-type lectin domain (CTLD), a sushi domain, five EGF-like domains, a heavily glycosylated mucin-like region, a 21-aminoacid transmembrane domain and a short cytotail (Khan et al., 2019). It is mainly expressed by ECs even though it has been reported to be expressed in various cell types of the hematopoietic system including hematopoietic stem cells, B cells, NK cells, monocytes, neutrophils, naïve T-cells, platelets, and neurons (Danet et al., 2002; Ikewaki et al., 2010; Liu et al., 2014; Løvik et al., 2001; Nepomuceno and Tenner, 1998). Initially, CD93 was studied in the immune system and it was believed able to bind the complement component C1q, hence its alternative name complement component C1q receptor protein (C1qRp) (Steinberger et al., 2002). However, the ability of CD93 to bind the C1q fragment was proven wrong by later functional studies (McGreal et al., 2002). In macrophages and monocytes, CD93 plays a critical role in promoting efferocytosis (clearance of apoptotic cells) both *in vitro* and *in vivo* (Norsworthy et al., 2004). Despite being characterized in the immune system, CD93 has been mainly studied in the endothelium where it plays an essential role in angiogenesis and in controlling EC function (Khan et al., 2019). Early evidences about the importance of CD93 in the endothelium came from knockdown experiments in which CD93-deficitent cells showed defects in the actin cytoskeleton organization and reduced EC adhesion, migration, proliferation and tube formation in different primary ECs (Langenkamp et al., 2015). Such effects were also observed in HUVECs by treating cells with a blocking monoclonal antibody (Orlandini et al., 2014). Defects in EC cytoskeletal organization were observed by time-lapse live imaging showing that cells lacking CD93 present a high density of stress fibers, a phenotype associated with reduced migration velocity and organization of pro-migratory lamellipodia (Barbera et al., 2021a). Importantly, the role of CD93 in regulating EC function and angiogenesis was shown in a *in vivo* model of zebrafish, where knockout (KO) of the homologous gene in embryos caused defects in the vascular system development (Du et al., 2017). In a mouse retina model, despite not causing strong developing defects, the absence of CD93 caused a reduction in the number of TC filopodia (Lugano et al., 2018). Studies carried out on HUVECs have shown that CD93 cytoplasmic domain is phosphorylated in a Src-dependent manner and that this phosphorylation is required for the binding of the adaptor protein Cbl thus promoting EC migration and tube formation (Galvagni et al., 2016). In line with the role of pCD93 in migrating cells, phosphorylation of CD93 increases in migrating ECs compared to confluent cells. Moreover, during EC adhesion and migration, CD93 promotes phosphorylation Cbl on the tyrosine residue 774. CD93 and pY774Cbl bind, associate in lamellipodia and control a signaling axis which culminates with regulation of small GTPases Rac1, Cdc42 and RhoA activity in both adhesion and migration (Barbera et al., 2021a, 2021b; Galvagni et al., 2016). The extracellular domain comprising the CTLD and the sushi domains binds the ECM protein MMRN2 (Galvagni et al., 2017; Khan et al., 2017) and, recently, another extracellular binding partner, the insulin-like growth factor binding protein 7 (IGFBP7), which binds

CD93 via a domain different from that involved in MMRN2 interaction (Sun et al., 2021). The binding of CD93 to MMRN2 promotes EC migration and tube formation (Galvagni et al., 2017; Khan et al., 2017), and triggers activation of the β1 integrin *via* a CD93/MMRN2/active β1 integrin complex formation, which promotes extracellular fibronectin deposition and remodeling both *in vitro* and *in vivo* (Lugano et al., 2018). Importantly, once formed on the plasma membrane, the CD93/MMRN2/active integrin β1 complex are endocytosed in $Rab5C^{+ve}$ endosomes that retrieve and recycle back the proteins during EC spreading and migration (Barbera et al., 2019). Noteworthy, plasma membrane levels of CD93 are also regulated by its intracellular domain that harbors a binding site for the Ezrin/Radixin/Moesin (ERM) protein Moesin, which connects CD93 to the actin cytoskeleton (Zhang et al., 2005). In fact, recombinant CD93 lacking the cytoplasmic domain failed to efficiently reach the plasma membrane during EC migration (Barbera et al., 2019). In addition to its function in signal transduction as a matrix receptor, the extracellular domain of CD93 can be shed from the plasma membrane and released into the extracellular environment (Tunica et al., 2009). The soluble form of CD93 (sCD93) has been detected in the HUVEC supernatant as well as in human plasma (Greenlee et al., 2009). A functional role of sCD93 was found in ECs where a recombinant CD93 encompassing the five EGF-like tandem repeats and the mucin-like domain was found to enhance the EGFR1 and PI3K activity, to increase proliferation and migration as well as to promote angiogenesis *in vivo* (Kao et al., 2012). Although no sheddase involved in CD93 cleavage has been identified to date, a study demonstrated that CD93 proteolytic cleavage is prevented by MMRN2 and that the knockdown of MMRN2 increased sCD93 levels (Lugano et al., 2018), suggesting that extracellular proteases might play a role. Curiously, the antibody used to detect sCD93 in this study targets an epitope spanning from the amino acid 444 to 581, which comprises the whole mucin like region until the beginning of the transmembrane (Lugano et al., 2018). This data, together with the observations that the EGF-like domains and the mucin-like region promote EC function suggest that CD93 shedding might liberate the entire extracellular domain.

1.3.1 CD93 is overexpressed in tumor-associated vessels of numerous cancer types

A study aimed to characterize transcriptome signatures of glioblastoma tumor vessels gave the first evidence that CD93 was highly expressed in tumor-associated vessels while showing a low expression in normal tissues (Dieterich et al., 2012). Further analysis confirmed an elevated expression of CD93 in human glioblastoma-associated vessels and, importantly, in a glioblastoma mouse model, CD93 KO mice showed a better survival and significantly slower tumor progression (Langenkamp et al., 2015). Another study, demonstrated high vessel-specific CD93 expression in human nasopharyngeal carcinoma (NPC) tissues, which negatively correlated with patient survival (Bao et al., 2016). Interestingly, both CD93 and MMRN2 were found upregulated in numerous cancer types, including glioblastoma, but not in healthy tissues (Galvagni et al., 2017; Khan et al., 2017; Lugano et al., 2018) and blocking CD93/MMRN2 binding has shown to impair EC function, suggesting that this interaction could prevent vessel abnormalization and cancer progression (Galvagni et al., 2017). Since high expression of CD93 in tumor-associated vessels has been shown to promote cancer progression in both human patients and mouse models, CD93 is considered an

appealing target for cancer therapy. Recently, it has been demonstrated in two tumor mouse models (the PKC pancreatic ductal adenocarcinoma and the B16 melanoma model) that blockade of CD93 by monoclonal antibodies (mAbs) increased the overall survival outcome. More importantly, blocking CD93 led to tumor vascular normalization without compromising healthy organs and at the same time promoted chemotherapy delivery and anti-PD-L1 immunotherapy as well as enhanced immune cell infiltration in the tumor microenvironment (Sun et al., 2021).

1.3.2 CD93 in nAMD

Tumor and choroidal neovascularization have common signatures and show shared signaling pathways involved in the formation of new blood vessels. As in tumor-blood vessels, elevated levels of CD93 were detected in blood vessels of choroidal neovascular membrane (CNVMs) and high level of sCD93 was found in aqueous humor of AMD patients compared to healthy individuals (Tosi et al., 2017). In a laser-induced CNV murine model CD93 KO mice showed a decreased vascularization of the lesion area compared to the wild-type counterparts. Moreover, employing the choroid sprouting assay (CSA), an *ex vivo* model of CNV, CD93 KO tissues displayed reduced EC sprouting. Importantly, high co-expression of both CD93 and MMRN2 occurs in neovascular membranes of AMD patients and the inhibition of the CD93/MMRN2 interaction with a neutralizing mAb decreased the ability of EC to form sprouts, suggesting that this interaction plays a role in the progression of AMD (Tosi et al., 2020).

1.3.3 Concluding remarks

Due to its endothelial specific expression and its relevance in promoting angiogenesis, CD93 has demonstrated to be an interesting target in the treatment of cancer and AMD. Only recently, the efficacy of an anti-CD93 therapy has been shown to be potentially beneficial for the treatment of cancer, even though the employment of other models is needed. Importantly, in cancer therapy CD93 blockade might only be employed as adjuvant to obtain a vascular normalization rather than a complete inhibition of angiogenesis and should be accompanied with further treatments such as chemotherapy or immunotherapy. On the other hand, since the choroid microenvironment differs from the tumor, targeting CD93 in nAMD might be beneficial *per se* and lead to a better disease progression. However, despite the promises of an anti-CD93 therapy in nAMD further evidence is needed to understand the suitability of an anti-CD93 treatment such as intraocular administration of anti-CD93 mAb in CNV mouse models.

2 AIM OF THE THESIS

Targeting molecules in a complex microenvironment such as in tumors or nAMD has revealed challenging for our generation. The development of novel treatments often is not accompanied by a proper characterization of the target functions in its cellular context. In the present work, we focused on characterizing the functional role of CD93 in endothelial cells. We studied its intracellular associated signaling pathway in the physiological context of EC adhesion and migration. We also investigated how CD93 and its partners MMRN2 and the active form of the β1 integrin are retrieved from and recycled to the plasma membrane during EC attachment on the substrate and during migration. Part of our study was focused on better understand the role of CD93 in nAMD and specifically to investigate the possibility to target the CD93/MMRN2 interaction in nAMD by means of a blocking mAb. Finally, for the first time we identified a dimeric form of CD93 which predominantly binds the MMRN2 and might affect future development of novel anti-CD93 drugs.

3 PUBLISHED RESULTS

3.1 Introduction to articles 1 and 2

In these papers we started from previous findings that CD93 phosphorylation on two tyrosine residues is of fundamental importance for a proper EC migration (Galvagni et al., 2016). Here we demonstrate that CD93 phosphorylation is enhanced during migration and that the presence of CD93 promotes phosphorylation of tyrosine 418 of Src family kinases during adhesion and Cbl on the tyrosine residue 774 during migration as well as in the retina blood vessels during mouse development. In our model, CD93 influences the binding of Cbl to the adaptor protein Crk as well as their cellular localization. Moreover, CD93 is required for the interaction of Crk with the Rac1-GEF DOCK180. We show the importance of the CD93 signaling pathway in the activation of the Rho GTPases Rac1, Cdc42 and RhoA. In absence of CD93, indeed, we observed downregulation of Rac1 and concomitant upregulation of RhoA in both adhesion and migration while Cdc42 activity was dependent on CD93 only during EC migration. Together these articles increase the previous knowledge of the CD93 signaling and shed light on new CD93-dependent intracellular events that culminate in functional EC adhesion and migration.

ARTICLE 1

The C-type lectin CD93 controls endothelial cell migration via activation of the Rho family of small GTPases

Stefano Barbera [a,b], Roberta Lugano [b], Alessia Pedalina [a], Maurizio Mongiat [c], Annalisa Santucci [a], Gian Marco Tosi [d], Anna Dimberg [b], Federico Galvagni [a] and Maurizio Orlandini [a]

***a* - Department of Biotechnology, Chemistry and Pharmacy,** *University of Siena, Italy*
***b* - Department of Immunology, Genetics and Pathology, Science for Life Laboratory,** *Uppsala University, Rudbeck Laboratory, Uppsala, Sweden*
***c* - Department of Research and Diagnosis, Division of Molecular Oncology,** *Centro di Riferimento Oncologico di Aviano (CRO) IRCCS, Italy*
***d* - Department of Medicine, Surgery and Neuroscience, Ophthalmology Unit,** *University of Siena, Italy*

Corresponding to Maurizio Orlandini: *Department of Biotechnology, Chemistry and Pharmacy, University of Siena, Via A. Moro, 2 - 53100 Siena, Italy. maurizio.orlandini@unisi.it.*
https://doi.org/10.1016/j.matbio.2021.05.006

Abstract

Endothelial cell migration is essential to angiogenesis, enabling the outgrowth of new blood vessels both in physiological and pathological contexts. Migration requires the activation of several signaling pathways, the elucidation of which expands the opportunity to develop new drugs to be used in antiangiogenic therapy. In the proliferating endothelium, the interaction between the transmembrane glycoprotein CD93 and the extracellular matrix activates signaling pathways that regulate cell adhesion, migration, and vascular maturation. Here we identify a pathway, comprising CD93, the adaptor proteins Cbl and Crk, and the small GTPases Rac1, Cdc42, and RhoA, which we propose acts as a regulator of cytoskeletal movements responsible for endothelial cell migration. In this framework, phosphorylation of Cbl on tyrosine 774 leads to the interaction with Crk, which acts as a downstream integrator in the CD93-mediated signaling regulating cell polarity and migration. Moreover, confocal microscopy analyses of GTPase biosensors show that CD93 drives coordinated activation of Rho-proteins at the cell edge of migratory endothelial cells. In conclusion, together with the demonstration of the key contribution of CD93 to the migratory process in living cells, these findings suggest that the signaling triggered by CD93 converges to the activation and modulation of the Rho GTPase signaling pathways regulating cell dynamics.

Introduction

Endothelial cell (EC) migration is an integrated molecular process that involves coordinated changes in cell adhesion, signal transduction activation, and cytoskeletal dynamics. ECs of the vascular system are normally stable and quiescent, however when the environment surrounding the endothelium become hypoxic, inflamed, and rich in cytokines and growth factors the ECs turn to a proliferative and motile state leading to the outgrowth of new blood vessels and the expansion of the vascular bed [1,2]. The formation of new capillary sprouts requires the differentiation of ECs into tip cells, which lead the migration and guide the new sprout towards the chemotactic stimulus, and stalk cells that follow immediately behind the tip cells and proliferate to elongate the sprouts [3]. At the cellular level, the constant remodeling of the actin cytoskeleton into filopodia, lamellipodia, and stress fibers is also essential for EC migration [4]. Stimulated endothelia express membrane-bound and activated cytoplasmic proteins, such as integrins, cadherins, and Rho GTPases, which are primarily responsible for

mediating cell-matrix interactions, cell-cell contacts, and cytoplasmic remodeling during cell motility [5-7]. Therefore, given its essential role during angiogenesis EC migration represents a valuable target for antiangiogenic therapy. Hence, the discovery of new molecules crucial for EC migration may lead to the development of new tools to circumvent drug resistance mechanisms and improve the efficacy of antiangiogenic treatments [8–10].

In recent years, the C-type lectin like domain (CTLD) group 14 member CD93 has been proposed to be a potential antiangiogenic target [11–13]. CD93 is a single-pass transmembrane glycoprotein upregulated in the endothelium of different types of vascularized tumors [14,15]. In hyperproliferative ECs, CD93 plays a major role promoting cell adhesion and migration through its interaction with Multimerin-2 [14], an endothelial-specific extracellular matrix (ECM) protein belonging to the EDEN glycoprotein family [16,17]. In the pathological neovascularization of the eye, the binding of CD93 to Multimerin-2 contributes to the progression of age-related macular degeneration while in gliomas it promotes the activation of β1 integrin and the fibrillar organization of fibronectin, increasing the motile properties of proliferating ECs [15,18]. The key role played by membrane receptors is to mediate the transduction of the signals deriving from extracellular cues, which ultimately results in the activation of specific cellular responses [19,20]. Consistently, the short cytoplasmic domain of CD93 interacts with different cytoplasmic proteins. A positively charged motif located in the juxtamembrane region of the CD93 cytotail is responsible for harboring Moesin, an ERM protein that anchors CD93 to F-actin [21]. Deletion of the intracellular domain of CD93 dramatically impairs the endosomal trafficking of CD93, thus preventing its localization at the leading edge of migrating ECs [22]. Upon binding of β-dystroglycan to laminin, the Src kinase phosphorylates the cytoplasmic domain of CD93 on two tyrosine residues, and the mutation of these residues strongly hampers EC migration and tube-like formation [23]. Furthermore, the phosphorylated tyrosine residues in the CD93 cytotail generate consensus motifs for the binding of the adaptor protein c-Cbl, which in turn is phosphorylated on tyrosine 774 [23], a protein modification associated with actin remodeling and enhancement of cell adhesion and migration [24]. However, despite the critical role played by CD93 in EC migration is quite clear, as well as its ability to mediate cellular responses to extracellular cues, the transduction pathway triggered by CD93 during EC migration has not yet been fully elucidated.

In the present work, we dissect the downstream signaling pathway activated by CD93 in primary motile ECs. We show that CD93 phosphorylation, together with the recruitment of phosphorylated Cbl at tyrosine 774 and Crk, trigger a signaling pathway required for the proper localization and activation of Rho-proteins at the leading edge of migrating cells, thus promoting establishment of cell polarity and lamellipodia formation during cell migration.

Results

CD93 as a regulator of EC migration

Both in vitro and in vivo experimental data have previously identified CD93 as an EC transmembrane protein that promotes angiogenesis upon interaction with the extracellular matrix [14,15,18,25]. While these findings highlighted the involvement of CD93 in the process of cell motility, the molecular mechanisms enabling CD93 to promote coordinated cell migration were unclear prior to this investigation. To address this issue, we first verified the contribution of CD93 to cell motility in primary human umbilical vein ECs (HUVECs). Cells were transduced with a lentiviral construct carrying a CD93 specific shRNA sequence and co-transduced with lentiviral constructs expressing the peptide Life-Act, a marker for F-actin visualization [26], conjugated to EGFP (sh-unr) or mScarlet (sh-CD93). Subsequently, cells were let to migrate in all directions and analyzed by time-lapse confocal microscopy. The analyses performed at different tracking times clearly indicated that the motility of CD93-silenced cells was severely impaired compared to the adjacent control-silenced cells (Fig. 1A and Supplementary Video1). In fact, the mean cell velocity (Fig. 1B), the mean square displacements (Fig. 1C), which assess the area explored by cells over time, and the maps of cell trajectories (Fig. 1D), which illustrate the range of migration in a cell population, were strongly hampered in CD93-silenced cells, further indicating that CD93 is key in modulating EC motility.

Cbl is recruited to CD93 and phosphorylated on tyrosine 774 during EC migration

We have previously shown that the CD93-dependent phosphorylation of Cbl on tyrosine 774 is crucial to promote EC adhesion [23], however it was unclear whether this signaling pathway was also involved in the regulation of EC motility. To address this issue, we first set up an in vitro 2-dimensional migration model, in which confluent HUVECs were detached from the plate by using a non-enzymatic solution to prevent CD93 protein breakdown by trypsin treatment (Fig. S1A and S1B) and the reseeded sparse cells, after an adhesion period assessed as late spreading phase [27], were analyzed during the active random migration phase (Fig. S1C) [28]. Consistent with its role played in the activated

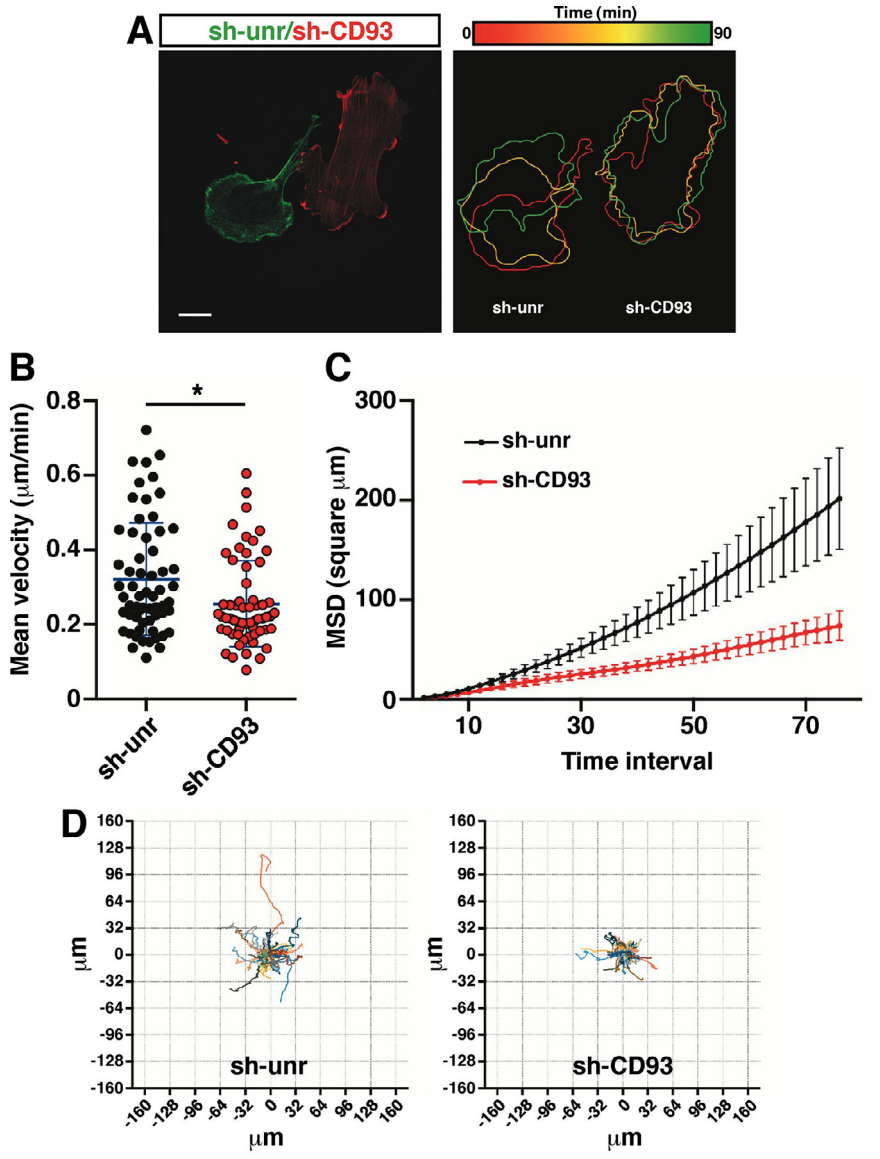

Fig. 1. CD93 drives EC migration. HUVECs were transduced with lentiviral particles expressing unrelated or CD93 shRNAs. Control (sh-unr) or CD93-silenced (sh-CD93) cells were further transduced with lentiviral constructs expressing the peptide LifeAct conjugated to EGFP or mScarlet respectively. Next, cells were detached from culture plates, mixed, replated, and tracked by confocal microscopy during the migration phase. A: Representative images of control and CD93-silenced cells close to each other. The right panel shows three boundaries of the same cells as the left panel tracked over a 90 min time interval. The colored scale represents the image capture time-frames. Scale bar, 30 μm. B: Plot shows the velocity of control and CD93-knockdown cells measured by using ImageJ and the ADAPT plug-in. Data were combined from three independent experiments. Each dot represents a single cell ($n = 63$, sh-unr; $n = 61$, sh-CD93). *$P < 0.05$; Mann-Whitney test. C: Mean square displacement (MSD) was measured by using DiPer software and plotted on a linear scale. The time interval is 40 minutes. $n = 38$ and 36 trajectories for sh-unr and sh-CD93 respectively. Error bars represent standard error of the mean. D: Graphs show the outputs of Plot_At_origin, a DiPer auxillary program, obtained from control or CD93-silenced cells. Trajectories of the cells are relative to the starting position of each cell ($n = 63$, sh-unr; $n = 61$, sh-CD93).

endothelium [13], CD93 phosphorylation levels were enhanced in migrating ECs in comparison to confluent quiescent cells (Fig. 2A, quantified in 2B). Similarly, under the same experimental conditions, the phosphorylation levels of Cbl on tyrosine 774 were also increased (Fig. 2C, quantified in 2D). Of note, Western blotting analyses of co-immunoprecipitation experiments using lysates from migrating ECs showed that CD93 and pY774-Cbl were interacting partners (Fig. 2E). To explore the possibility that the interaction between CD93 and pY774-Cbl was involved in EC migration, we silenced CD93 in

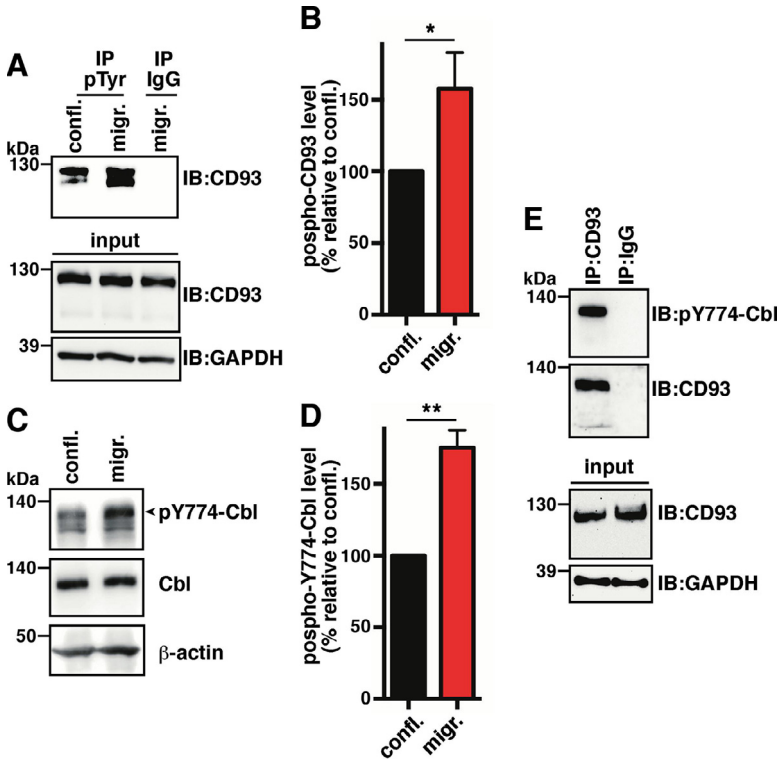

Fig. 2. CD93 binds to pY774-Cbl in migrating ECs. A: Cell lysates from confluent (confl.) or migrating (migr.) ECs were immunoprecipitated (IP) with anti-phosphotyrosine (pTyr) or unrelated mouse (IgG) antibodies. Immunoprecipitates were analyzed by immunoblotting (IB) with anti-CD93 antibodies. To confirm equal loading, whole cell extracts (input) were analyzed by Western blotting with anti-CD93 antibodies. B: Quantification of CD93 phosphorylation levels from independent experiments performed as in A. Values, normalized to CD93 protein levels, represent the percentage of CD93 phosphorylation relative to confluent cells. $^{*}P < 0.05$; paired *t*-test. C: Western blotting analysis of cell extracts from confluent (conf.) and migrating (migr.) ECs using antibodies against pY774-Cbl, Cbl, and β-actin. An arrowhead indicates pY774-Cbl. D: Quantitative analysis of pY774-Cbl levels from experiments performed as in C, normalized to total Cbl and β-actin protein levels and expressed as percentage relative to confluent cells. $^{**}P < 0.01$; paired *t*-test. E: Cell extracts from migrating ECs were immunoprecipitated (IP) with anti-CD93 or unrelated mouse (IgG) antibodies. Immunoprecipitates were analyzed by Western blotting (IB) with anti-pY774-Cbl and anti-CD93 antibodies. To confirm equal loading, whole cell lysates were analyzed by Western blotting using anti-CD93 and anti-GAPDH antibodies.

HUVECs and performed an in vitro scratch assay, analyzing the subcellular localization of the endogenous proteins by immunofluorescence. In agreement with previous findings [15,22], CD93 was strongly expressed and localized at the border of motile ECs. Notably, CD93 colocalized with pY774-Cbl along the lamellipodium edge (Fig. 3A, sh-unr). In contrast, the knockdown of CD93 dramatically impaired the localization of pY774-Cbl along the migrating front and pY774-Cbl showed a punctate redistribution at the terminal ends of the actin filament network as shown in overlapping images using phalloidin staining (Fig. 3A, sh-CD93). These results were further substantiated by quantitative analyses of fluorescent signals along the leading edge of motile cells (Fig. 3B) and by Western blotting analyses of lysates from random migrating control or CD93-depleted ECs (Fig. 3C, quantified in 3D). Interestingly, in the front of migration HUVECs secreted and deposited Multimerin-2, which has been shown to be critical in preventing CD93 proteolytic cleavage [15], in spite of the matrix is usually scraped off in the scratch assay (Fig. S2).

To corroborate the interaction between CD93 and pY774-Cbl in EC migration, we analyzed the developing retinal vasculature in postnatal day 6 (P6) mice by immunofluorescence. In accordance with previous results on the role of CD93 in the regulation of filopodia formation and extension of endothelial sprouts during retinal development [15], we found that CD93 was expressed in the sprouting front of the retinal vasculature and colocalized with pY774-Cbl predominantly in the edges of apical growing vessel sprouts rather than in internal vessels close to the retinal plexus (Fig. 4A, wt). These evidences suggest that the interaction between CD93 and pY774-Cbl mainly occurs during active migration of retinal ECs. To verify if CD93 affects pY774-Cbl localization, we analyzed P6 retinas from *wild-type* and *Cd93*$^{-/-}$ mice by immunofluorescence.

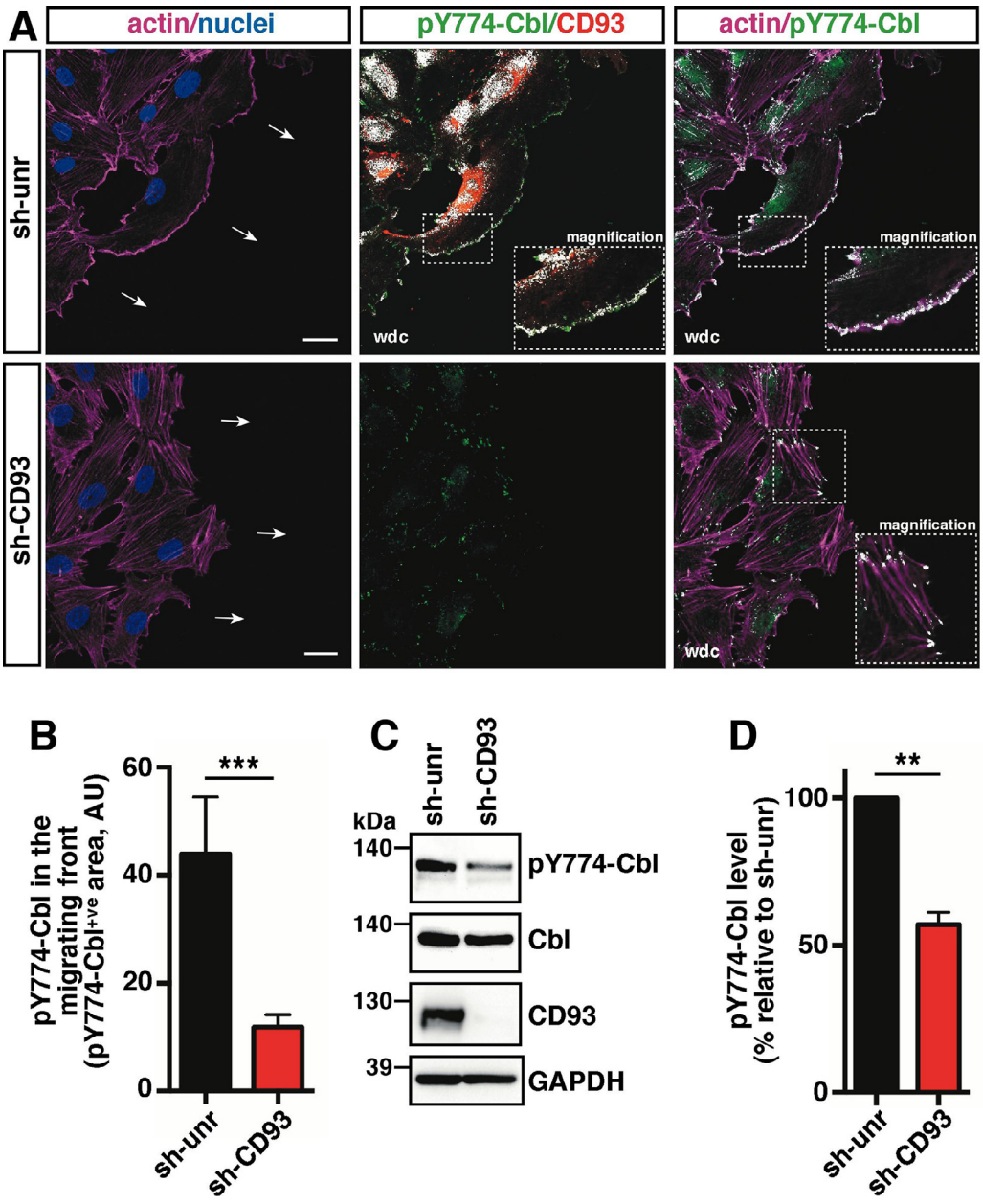

Fig. 3. CD93 drives the localization of pY774-Cbl at the leading edge of migrating ECs. HUVECs were transduced with lentiviral particles expressing unrelated or CD93 shRNAs. A: Representative images of immunofluorescence analysis of control (sh-unr) or CD93-silenced (sh-CD93) HUVECs 5 h after production of a double-sided scratch in the cell monolayer. Cells were stained using phalloidin, Hoechst solution, and antibodies against CD93 and pY774-Cbl. Arrows indicate direction of migration. White dot colocalization (wdc) images between pY774-Cbl and CD93 or F-actin are shown. In the wdc pictures, magnification of the squared areas is shown. Scale bars, 30 μm. B: Quantification of cellular pY774-Cbl in the migrating front area (5 μm from the cell edge) of HUVECs transduced and treated as in A. Bars represent arbitrary units (AU) of the fluorescence intensity of the pY774-Cbl^{+ve} signal per area (n = 7 different areas along the migrating front). ***$P < 0.001$; Mann-Whitney test. C: Western blotting analysis of cell extracts from random migrating control (sh-unr) or CD93-silenced (sh-CD93) ECs using antibodies to CD93, pY774-Cbl, Cbl, and GAPDH to confirm equal loading. D: Graph displaying pY774-Cbl protein levels from experiments performed as in C, normalized to total Cbl and GAPDH levels and expressed as percentage relative to control cells. **$P < 0.01$; paired t-test.

Strikingly, the localization of pY774-Cbl in the angiogenic front of the retinal vasculature was significantly reduced in the *Cd93*$^{-/-}$ mice (Fig. 4A and B). These observations were confirmed by quantitative analyses of fluorescence signals of pY774-Cbl normalized against the CD31 signal in vessel sprouts

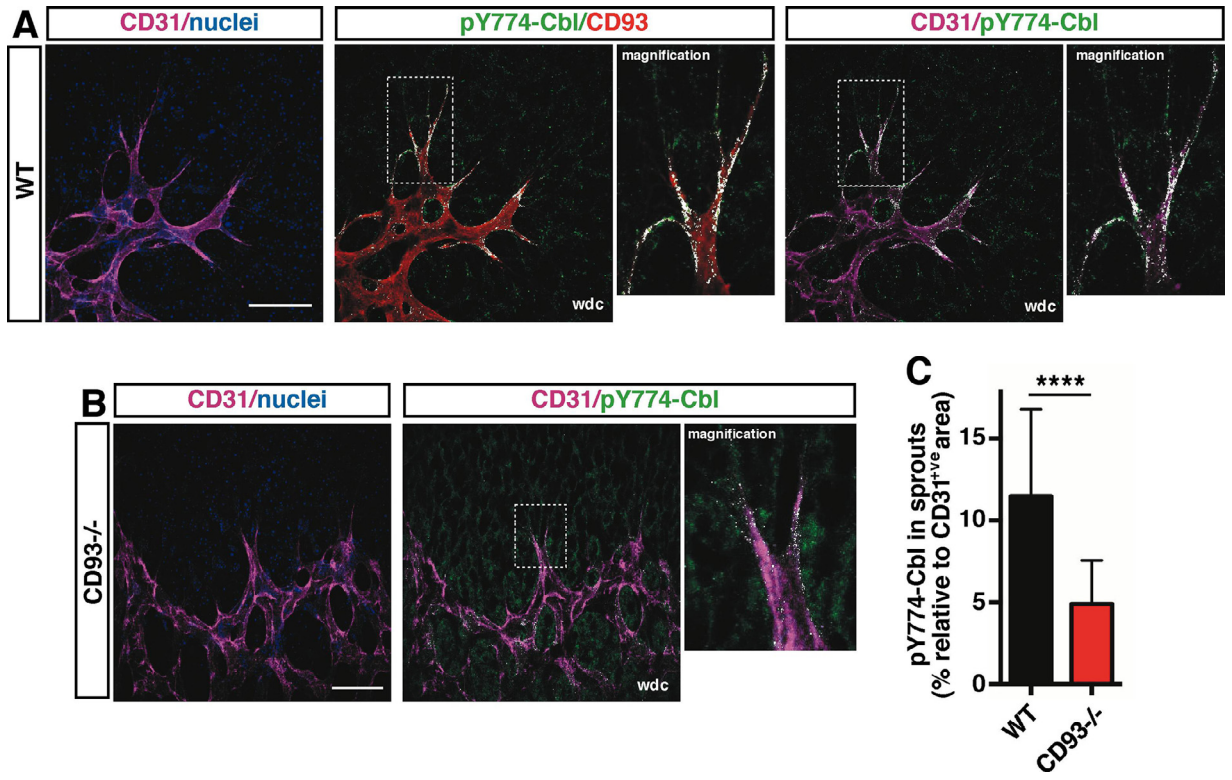

Fig. 4. CD93 drives pY774-Cbl localization in the sprouting front of mouse retinal vasculature. The sprouting front of P6 developing mouse retinas was analyzed by immunofluorescence. The vasculature is visualized by using anti-CD31 antibodies. Hoechst staining highlights nuclei. A: Wild-type (WT) mouse retina stained with antibodies against pY774-Cbl and CD93. White dot colocalization (wdc) pictures between pY774-Cbl and CD93 or CD31 are shown. B: Growing retinal vessels of CD93-deficient ($CD93^{-/-}$) mice stained with antibodies against pY774-Cbl. White dot colocalization (wdc) picture between pY774-Cbl and CD31 is shown. Magnification of the squared areas is shown. Scale bars, 40 μm. C: Quantification of pY774-Cbl in growing retinal vessel sprouts of wild-type ($n = 21$ vessel sprouts from 3 mice) and $CD93^{-/-}$ ($n = 31$ vessel sprouts from 4 mice) mice. Bars represent the percentage of pY774-Cbl fluorescence intensity relative to total $CD31^{+ve}$ area. $^{****}P < 0.0001$; Mann-Whitney test.

(Fig. 4C). Taken together, these data indicate that during angiogenesis phosphorylation of CD93 recruits Cbl, which is in turn phosphorylated on tyrosine 774, thus activating a signaling pathway regulating EC migration.

Crk is a signaling integrator in the CD93 transduction pathway

Since Crk-family proteins are important actors in Cbl-mediated regulation of the actin cytoskeleton rearrangements during cell adhesion and migration [24,29], we hypothesized that Crk was a downstream modulator of the CD93 signaling pathway. To verify this hypothesis, we first studied the effects of CD93 silencing on Crk localization at the leading edge of motile ECs by means of wound healing assays. The confocal microscopy analyses indicated that while Crk broadly colocalized with CD93 along the lamellipodium borders of control ECs, the knockdown of CD93 associated with severe depletion of Crk from the migrating front (Fig. 5A, quantified in 5B). In fact, under this experimental setting, Crk localized in few spots overlapping with the actin filaments, similarly to what observed for pY774-Cbl (compare Fig. 5A to Fig. 3A), suggesting that pY774-Cbl and Crk could be putative binding partners. To verify this possibility we analyzed the localization of these molecules in migrating cells. The immunofluorescence analyses indicated that pY774-Cbl and Crk displayed a strong colocalization along the leading edges of migrating ECs and the silencing of CD93 associated with a dramatic reduction of the pY774-Cbl/Crk overlapping signals in this cell district (Fig. 5C). These observations were further strengthened by immunoprecipitation experiments that highlighted not only pY774-Cbl and Crk interacted during cell migration (Fig. 5D), but also that the interaction was CD93-dependent, since the silencing of the receptor associated with a strong reduction of the pY774-Cbl fraction bound to Crk (Fig. 5E).

To verify if Crk was a downstram mediator of CD93 signaling we interfered with Crk function and

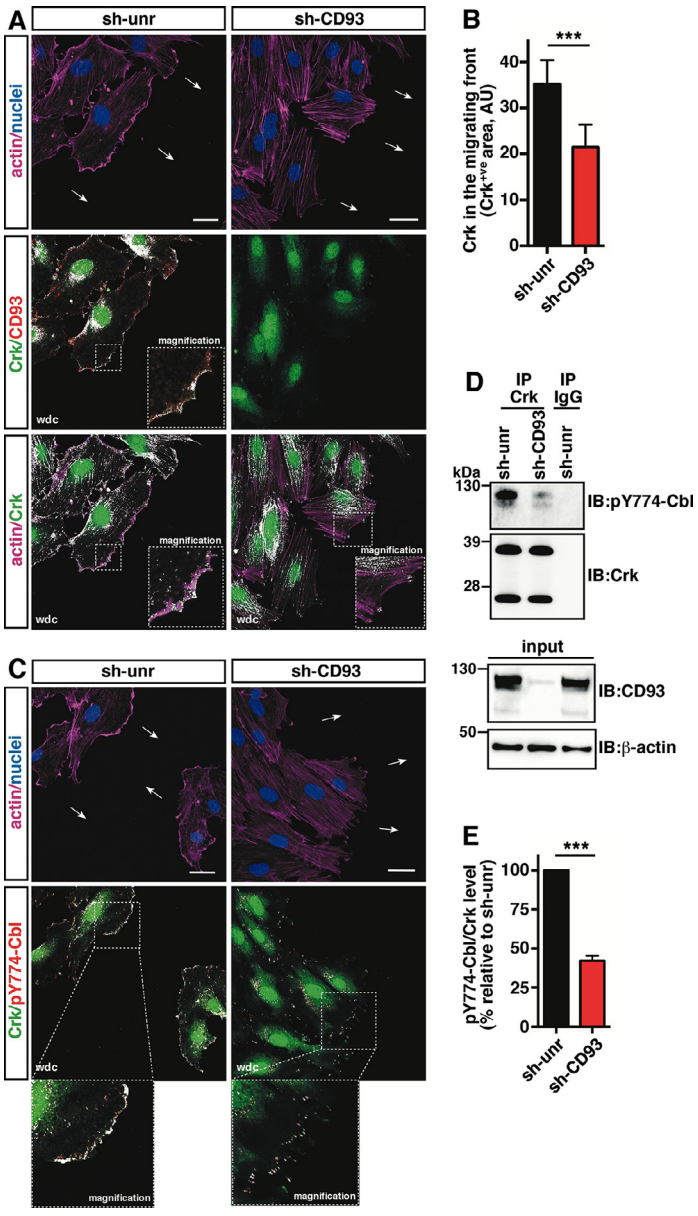

Fig. 5. CD93 knockdown impairs the interaction between pY774-Cbl and Crk at the EC migrating front. HUVECs were transduced with lentiviral particles expressing unrelated or CD93 shRNAs. A: Representative images of immunofluorescence analysis of control (sh-unr) or CD93-silenced (sh-CD93) ECs 5 h after production of a double-sided scratch in the cell monolayer. Cells were stained using phalloidin, Hoechst solution, and antibodies against CD93 and Crk. Arrows indicate direction of migration. White dot colocalization (wdc) images between Crk and CD93 or F-actin are shown. In the wdc pictures, magnification of the squared areas is shown. Scale bars, 30 μm. B: Quantification of Crk in the migrating front area (5 μm from the cell edge) of HUVECs transduced and treated as in A. Bars represent arbitrary units (AU) of the fluorescence intensity of the Crk^{+ve} signal per area ($n = 7$ different areas along the migrating front). $^{***}P < 0.001$; Mann-Whitney test. C: F-actin, nucleus, Crk, and pY774-Cbl were imaged in control (sh-unr) or CD93-silenced (sh-CD93) ECs by confocal microscopy at 5 h after production of a double-sided scratch in the cell monolayer. Arrows indicate direction of migration. White dot colocalization (wdc) images between Crk and pY774-Cbl are shown. In the wdc pictures, magnification of the squared areas is shown. Scale bars, 30 μm. D: Cell extracts from migrating ECs were immunoprecipitated (IP) with anti-Crk (Crk) or unrelated mouse (IgG) antibodies. Immunoprecipitates were analyzed by Western blotting (IB) with antibodies against pY774-Cbl and Crk to confirm equal loading. To check CD93 depletion in sh-CD93 transduced cells, whole cell lysates were analyzed by Western blotting using anti-CD93 and anti-β-actin antibodies. E: Quantitative analysis of the pY774-Cbl protein levels respect to Crk levels from experiments performed as in D. Values represent the percentage of the ratio pY774-Cbl/Crk relative to control cells (sh-unr). $^{***}P < 0.001$; paired *t*-test.

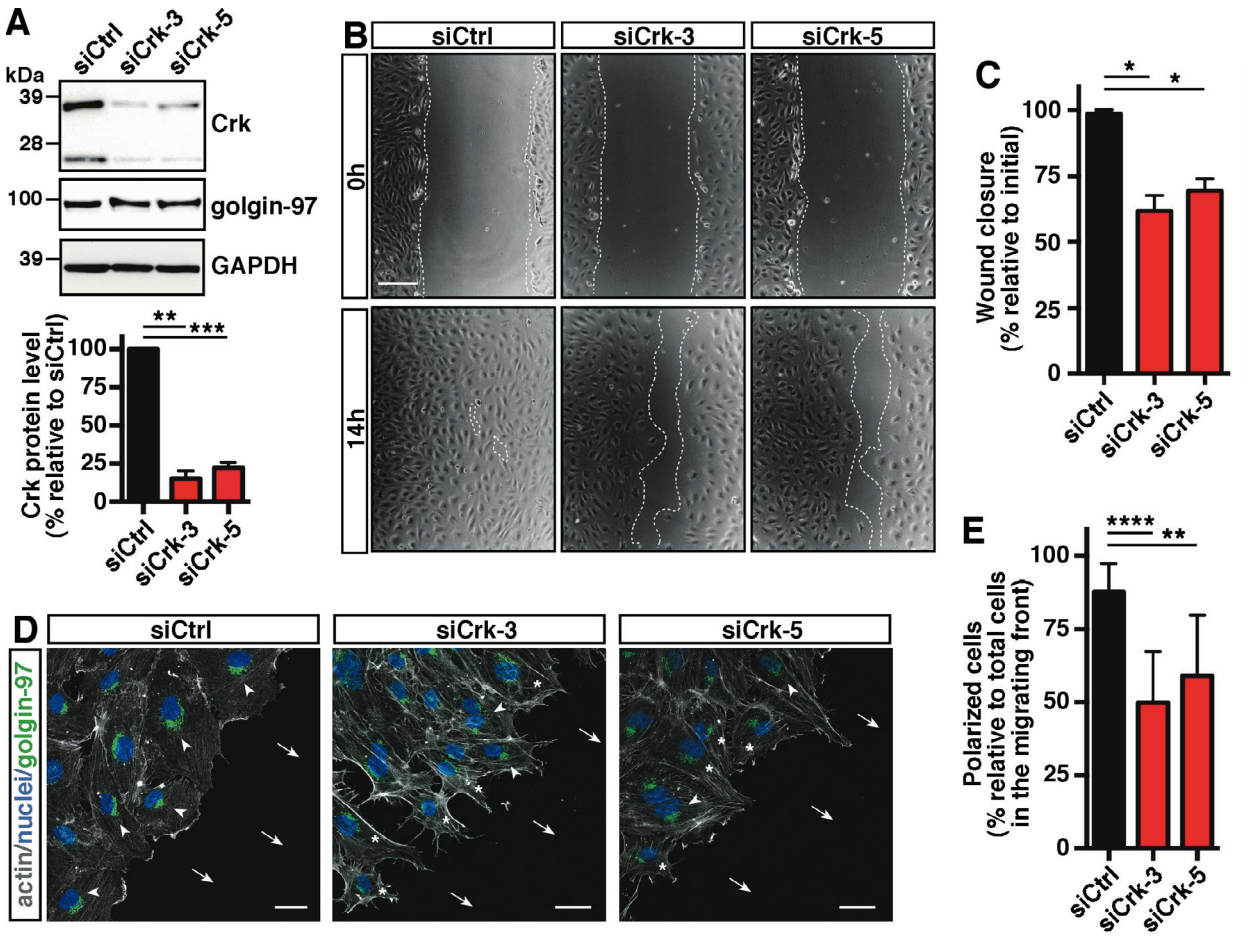

Fig. 6. Crk silencing affects migration and polarization of human ECs. HUVECs were transfected with scrambled control siRNA (siCtrl) or siRNA targeting Crk (siCrk-3 or siCrk-5). A: Cell extracts from siRNA expressing HUVECs were analyzed by Western blotting using anti-Crk and anti-golgin-97 antibodies. Anti-GAPDH antibodies were used to confirm equal loading. Quantification of Crk protein levels is reported. Values, normalized to GAPDH protein levels, were expressed as percentage relative to control cells. $^{**}P < 0.01$ and $^{***}P < 0.001$; paired *t*-test. B: Representative images of wound closure in siRNA transfected HUVECs. Cells were photographed at 0 and 14 h after the scratch. Scale bar, 100 μm. C: Values represent the percentage of wound closure calculated from images acquired at time 0 and 14 h from the scratch ($n = 3$ images per condition pooled from three independent experiments). $^{*}P < 0.05$; paired *t*-test. D: F-actin, nuclei, and golgin-97 were imaged at 5 h after production of a double-sided scratch in the cell monolayer of siRNA-transfected HUVECs. Arrows depict the direction of migration. In the migrating front, polarized (arrowheads) and nonpolarized (asterisks) cells are indicated. Scale bars, 30 μm. E: Quantitative analysis of polarized siRNA-transfected ECs in the leading edge of migration. Bars represent the percentage of polarized cells relative to total cells in the migrating front ($n = 4$ migrating fronts per condition pooled from three independent experiments). $^{****}P < 0.0001$ and $^{**}P < 0.01$; Student *t*-test.

analyzed CD93-regulated processes such as cell motility and polarization [12,23]. To this end, HUVECs were first transfected with two different siRNA targeting Crk, which reduced Crk protein levels with different efficiency (Fig. 6A). Under this condition we analyzed the migration of HUVECs by means of scratch assays. Control-transfected HUVECs completely covered the wounded area 14 hours after the scratch, whereas the down-regulation of Crk expression prevented the healing of the wound within the same time frame (Fig. 6B, quantified in 6C), suggesting that the expression of Crk is required for effective HUVEC cell migration. Since the orientation of the Golgi apparatus along the migration front is considered as a marker of proper cell polarization and migration [30], we asked whether the silencing of Crk could affect the localization of the Golgi apparatus in migrating HUVECs, as previously shown upon the knockdown of CD93 in ECs [12]. Control and Crk silenced cells were stained for the golgin-97 marker, whose expression at the migrating front was not affected by the knockdown of Crk (Fig. 6A). We observed that the majority of control ECs were correctly polarized, whereas loss of Crk significantly increased the number of nonpolarized cells, leading to a disorganized

migrating front (Fig. 6D and E). Of note, the loss of Crk did not affect expression and localization of CD93 in the migrating front of ECs (Fig. S3), suggesting that Crk represents a downstream effector of the CD93-mediated signaling. Importantly, the suppressive effects of CD93 and Crk silencing on EC migration were further substantiated comparing the actin cytoskeleton organization of wild type cells with CD93 and Crk silenced cells at the front of migration. Indeed, while in control ECs the actin cytoskeleton properly organized in broad lammelipodia and pro-migratory stress fibers, both CD93 and Crk knockdown ECs showed a stationary phenotype specified by abundant stress fibers and filopodia (Figs. 3A and 6D).

CD93 drives activation of Rho-proteins at the leading edge of migration

Altogether, the above results led us to hypothesize that activation of the CD93 signaling pathway could represent a novel molecular mechanism to regulate EC migration. To further dissect this signaling pathway, we first investigated the putative involvement of Rac1, crucial regulator of plasma membrane extension in lamellipodia [31,32], in CD93-driven EC motility. Confocal microscopy analyses performed on control HUVECs revealed a sizeable accumulation of Rac1 along the lamellipodial edge where CD93 and F-actin also localize. On the contrary, the knockdown of CD93 associated with a significant reduction of Rac1 in the migration front of ECs (Fig. 7A, quantified in 7B). To further evaluate the possible CD93-dependent activation of Rac1 at the leading edge of migrating cells, control or CD93-silenced ECs were transduced with a lentivirus construct expressing a biosensor (Fig. S3), which produces a localized FRET signal revealing the amount and location of Rac1 activation [33]. Quantitative FRET analysis on transduced cells unveiled a statistically significant decrease of Rac1 activity at the leading edge of CD93-depleted ECs compared to control cells (Fig. 7C, quantified in 7D), suggesting that Rac1 is a downstream effector of the CD93 signaling pathway. Importantly, this assumption was substantiated by immunoprecipitation experiments revealing that the silencing of CD93 prevented the binding between Crk and DOCK180 (Fig. 7E, quantified in 7F), an exchange factor for Rac1 which interacts with Crk and induces lamellipodium extension [34,35], despite the expression of DOCK180 was not affected.

Besides Rac1, also the GTPases Cdc42 and RhoA are activated at the front of migrating cells and act in concert to regulate cell protrusion [36], thus we asked whether their activation at the leading edge of migration was regulated by CD93. To this end, control or CD93-silenced ECs were transduced with lentiviruses expressing Cdc42 and RhoA biosensors (Fig. S4), and were allowed to migrate following a wound scratch. In accordance with previous findings [37,38], FRET analyses revealed that Cdc42 was strongly activated at the leading edge of control cells (Fig. 8A), whereas RhoA activity was concentrated in a sharp band at the edge of the protrusions (Fig. 8B). Notably, in the migrating front the lack of CD93 associated with a severe impairment of Cdc42 activation, whereas RhoA activation was increased compared to control cells (Fig. 8A and 8B, quantified in 8C and 8D). Altogether, these results suggest that the transmembrane molecule CD93, by modulating the activation of Rho GTPases, regulates the actin cytoskeleton dynamics instrumental for a proficient EC migration.

Discussion

Directional migration of ECs is required in both physiological and pathological processes, including embryonic development, tissue repair, and tumor growth [39]. Hence, understanding the signaling pathways that drive cell migration during blood vessel formation may help to elucidate the pathophysiology of angiogenesis-dependent diseases offering novel opportunities for therapeutic intervention. Here, we identify key components that transduce signals from the transmembrane protein CD93 to small GTPases of the Rho family to orchestrate the cytoskeletal movements responsible for EC migration. By tracking living cells we demonstrate that CD93 is a key regulator of EC migration, suggesting that CD93 neutralization may represent a putative new target for the development of potent and effective drugs to inhibit neovessel formation. This especially in light of the fact that, in contrast to quiescent blood vessels, CD93 expression is upregulated in sprouting vessels of the activated endothelium in different pathologies [12–14].

Adaptor proteins are essential components of the signal transduction pathways in all cell types and link activated receptors to specific downstream signals [29]. Accordingly, in this study we show that CD93 associates with the adaptor protein Cbl at the EC migrating front and that Cbl phosphorylation on tyrosine 774 is partially dependent on CD93 expression. Importantly, we demonstrated that during vascularization of the murine retinas, pY774-Cbl is mainly localized in migratory tip cells of the sprouting vascular front and its localization is modulated by the expression levels of CD93. These results, shed more light on the transduction of migratory signals triggered by the engagement of CD93, involving the phosphorylation of the receptor in motile cells and the consequent interaction with pY774-Cbl. The phosphorylation of Cbl on tyrosine 774 provides a docking site for the downstream signaling protein Crk [40] and the exchange factor DOCK180 was identified as a partner for Crk and a mediator of Rho

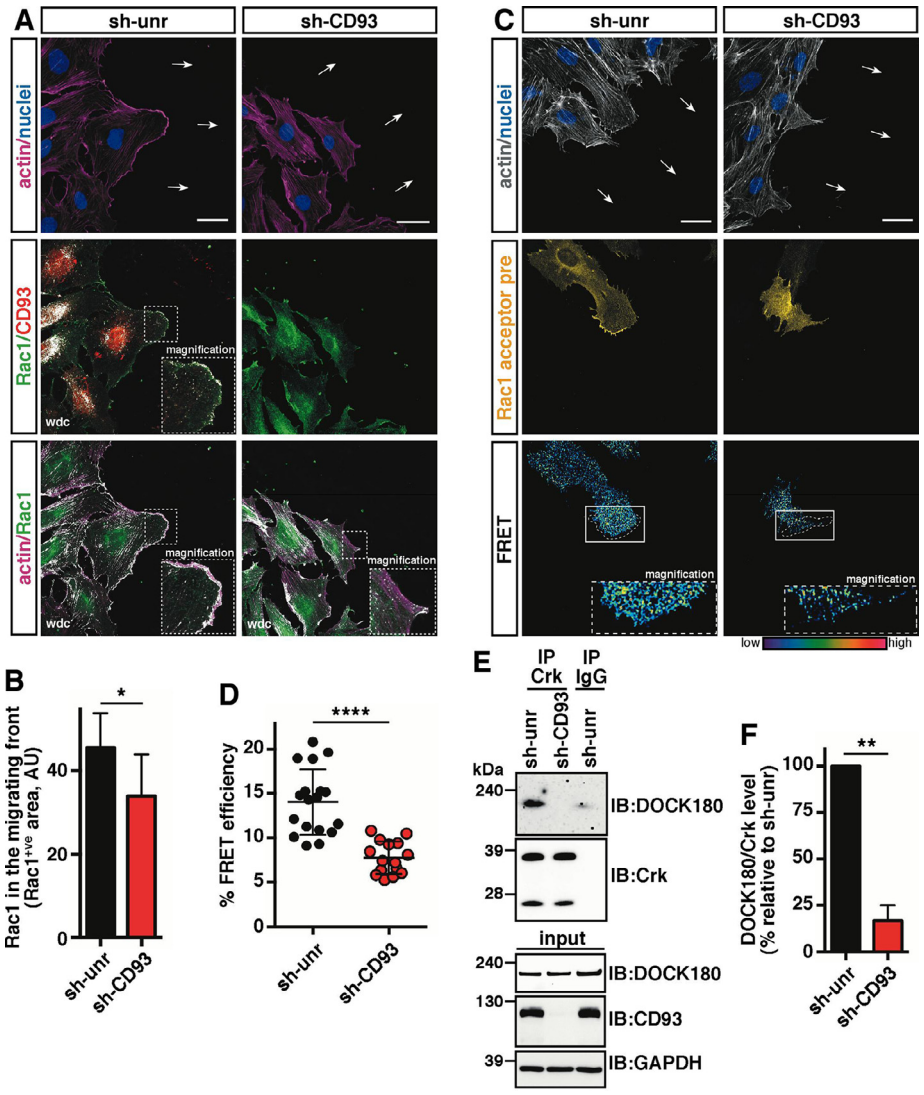

Fig. 7. CD93 signaling activates Rac1 at the leading edge of migration. HUVECs were transduced with lentiviral particles expressing unrelated or CD93 shRNAs. A: Immunofluorescence staining of control (sh-unr) or CD93-silenced (sh-CD93) HUVECs migrating out of a wounded monolayer. Cells were stained using phalloidin, Hoechst solution, and antibodies against Rac1 and CD93. Arrows indicate direction of migration. White dot colocalization (wdc) images between Rac1 and CD93 or F-actin are shown. In the wdc pictures, magnification of the dotted areas is shown. Scale bars, 30 μm. B: Quantification of cellular Rac1 in the migrating front area (5 μm from the cell edge) of HUVECs transduced and treated as in A. Bars represent arbitrary units (AU) of the fluorescence intensity of the $Rac1^{+ve}$ signal per area (n = 8 different areas along the migrating front). *$P < 0.05$; Mann-Whitney test. C: FRET analysis on control (sh-unr) or CD93-silenced (sh-CD93) HUVECs transduced with a lentiviral construct expressing the Rac1 biosensor 5 h after production of a scratch in the cell monolayer. Cells were stained using phalloidin and Hoechst solution. Representative confocal images of transduced cells in the migrating front before photobleaching (acceptor pre) are shown. Rectangles indicate the photobleached cell area and dashed lines the cell edge region used to calculate FRET efficiency. Magnifications of the photobleached leading edge of migrating biosensor-expressing cells are shown. Arrows indicate direction of migration. The colored scale represents the color range of FRET efficiency. Scale bars, 30 μm. D: Plot showing the fluorescence increase (% FRET efficiency) upon photobleaching at the leading edge of migrating ECs (n = 18 cells for sh-unr and n = 15 cells for sh-CD93). Data are presented as scatter plot. ****$P < 0.0001$; Student t-test. E: Cell extracts from migrating ECs were immunoprecipitated (IP) using anti-Crk (Crk) or unrelated mouse (IgG) antibodies. Immunoprecipitates were analyzed by Western blotting (IB) with antibodies against DOCK180 and Crk to confirm equal loading. To check CD93 depletion and DOCK180 expression in sh-CD93 transduced cells, whole cell lysates were analyzed by Western blotting using anti-CD93 and anti-DOCK180 antibodies. Antibodies to GAPDH were used for equal loading control. F: Quantification of DOCK180 protein levels from experiments performed as in E. Values represent the percentage of the ratio DOCK180/Crk relative to control cells (sh-unr). **$P < 0.01$; paired t-test.

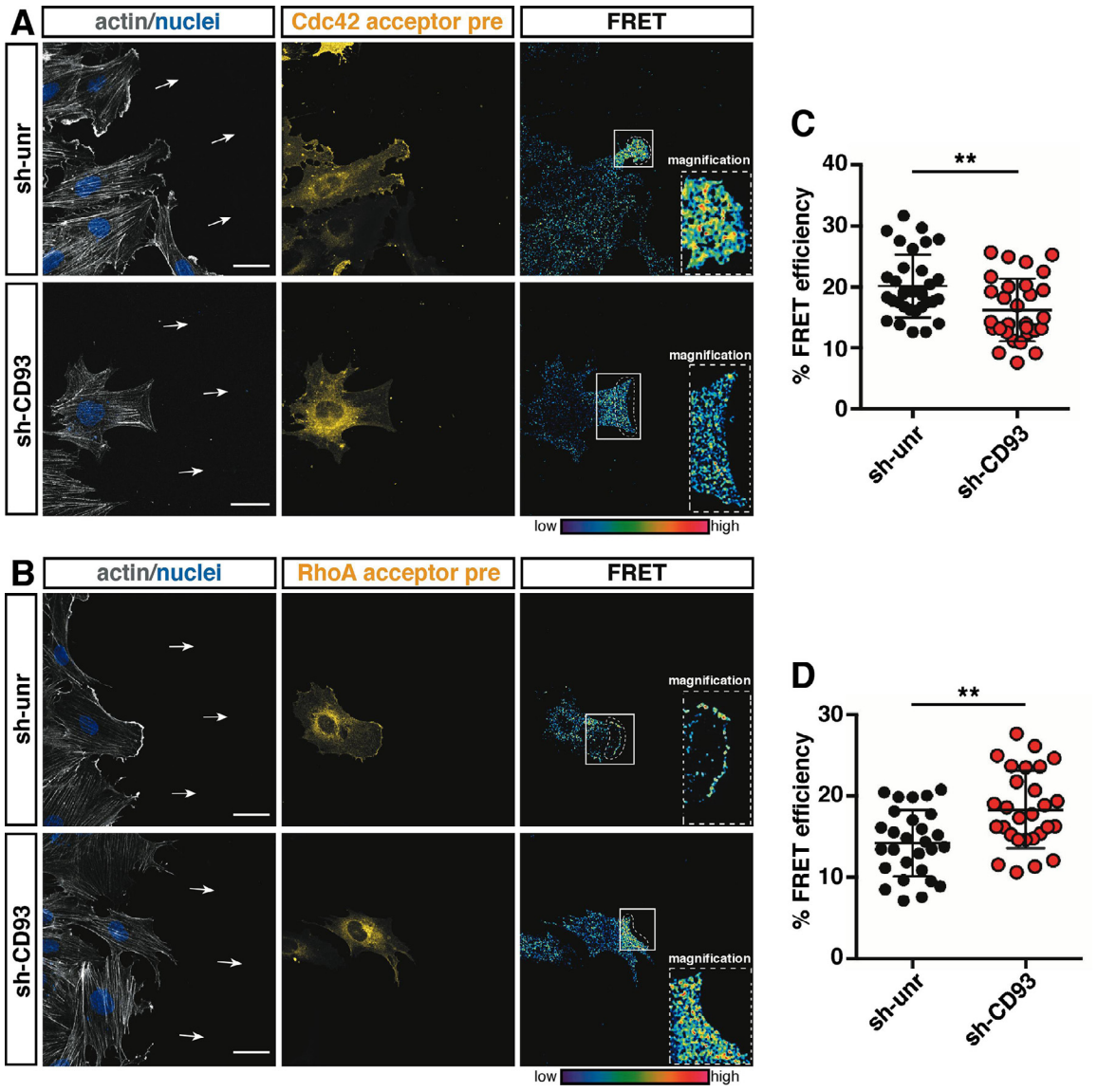

Fig. 8. Cdc42 and RhoA GTPases are modulated by CD93 at the leading edge. FRET analysis on control (sh-unr) or CD93-silenced (sh-CD93) HUVECs migrating out of a wounded monolayer and transduced with a lentiviral construct expressing the Cdc42 (A) or the RhoA (B) biosensors. Cells were stained using phalloidin and Hoechst solution. Representative confocal images of transduced cells in the migrating front before photobleaching (acceptor pre) are shown. Rectangles indicate the photobleached cell area and dashed lines the cell edge region used to calculate FRET efficiency. Magnifications of the photobleached leading edge of migrating biosensor-expressing cells are shown. Arrows indicate direction of migration. The colored scale represents the color range of FRET efficiency. Scale bars, 30 μm. C and D: Graphs showing the fluorescence increase (% FRET efficiency) upon photobleaching at the leading edge of migrating HUVECs transduced with the Cdc42 biosensor (C) (n = 33 cells for sh-unr and n = 30 cells for sh-CD93) or RhoA biosensor (D) (n = 28 cells for sh-unr and n = 28 cells for sh-CD93). Data are presented as scatter plots. $^{**}P < 0.01$; Student t-test.

protein activation at the cell leading edge for lamellipodium formation [34,41]. In line with these findings, we showed that Crk exerts a crucial role in in modulating EC polarized migration, and that CD93 expression is required to mediate the binding between pY774-Cbl and Crk and between Crk and DOCK180 at the leading edge of migrating cells. These findings suggest that CD93 is a crucial receptor modulating the reorganization of the actin cytoskeleton by regulating the Rho GTPase activity via the pY774-Cbl/Crk/DOCK180 signaling axis.

The best studied Rho GTPases, Rac1, Cdc42, and RhoA, contribute to cell migration in all animal models [31]. Specific spatiotemporal regulation of Rho proteins is deeply controlled and is required to mediate membrane protrusion dynamics at the leading edge, necessary for directional cell migration [42]. The use of FRET-based biosensors allowed us

to investigate the activation of the Rho proteins in migrating ECs, demonstrating a clear role for CD93 in the modulation of the spatially-regulated activity of these molecules at the cell migration front. Notably, we show that the loss of CD93 associates with decreased Rac1 activation at the leading edge, and demonstrate that the receptor modulates the interaction between Crk and DOCK180, known to affect Rac1 activation and to represent strategic molecules in transducing pro-migratory signals from different EC receptors [43]. Consistent with a previous study showing the role of Cdc42 in Rac1 activation [44], we found that the loss of CD93 results in a decreased activity of Cdc42 at the cell leading edge, where Cdc42 is known to contribute to actin remodeling necessary for lamellipodium extension [31]. It has been reported that Rac1 and RhoA are mutually inhibitory and higher RhoA activity is localized in a sharp band immediately adjacent to the edge of migrating fibroblasts [36,45]. Accordingly, we found that RhoA activity exhibits the same sharp localization at the leading edge of control migrating ECs, but the loss of CD93 associates with a broaden cell area displaying RhoA activation as well as increased overall RhoA activity, suggesting that the decreased Rac1 activity under these conditions results in increased RhoA activation. Furthermore, we observed that CD93-silenced cells show abnormal actin cytoskeleton organization and an extensive generation and persistence of actin stress fibers, whose formation and turnover is driven by RhoA and its effector ROCK [46]. Importantly, although RhoA is active at the leading edge of lamellipodia, high levels of RhoA/ROCK activity induce actomyosin-mediated retraction of lamellipodia and inhibit this type of migration [47].

In our study, we analyzed the lamellipodium-based migration both during random migration and at the migration front during wound closure. It is known that Cdc42 activity, particularly by controlling filopodia formation, promotes angiogenesis via cytoskeletal regulation in tip cells and that Rac1 is required for proper angiogenic sprouting [48], suggesting that CD93 promotes angiogenesis by finely tuning Rho GTPase activation during EC migration.

Integrin-mediated adhesion is considered essential for lamellipodium-driven migration, in part due to the fact that integrins' engagement at the leading edge stimulates Rac1 activation [45]. Of note, it has been reported that CD93 promotes β1 integrin activation and activated integrins regulate Src activation [15,49], the protein kinase involved in CD93 phosphorylation [23]. Hence, we can speculate that upon engagement by Multimerin-2, the only ECM molecule known to function as a substrate for this receptor, CD93 promotes integrin and Src activation; next the phosphorylation of CD93 leads to the recruitment of Cbl and activation of the Cbl/Crk/DOCK signaling axis, resulting in actin cytoskeletal remodeling and cell movement (Fig. 9).

Angiogenesis is largely regulated by a finely-tuned integration of external cues, which are

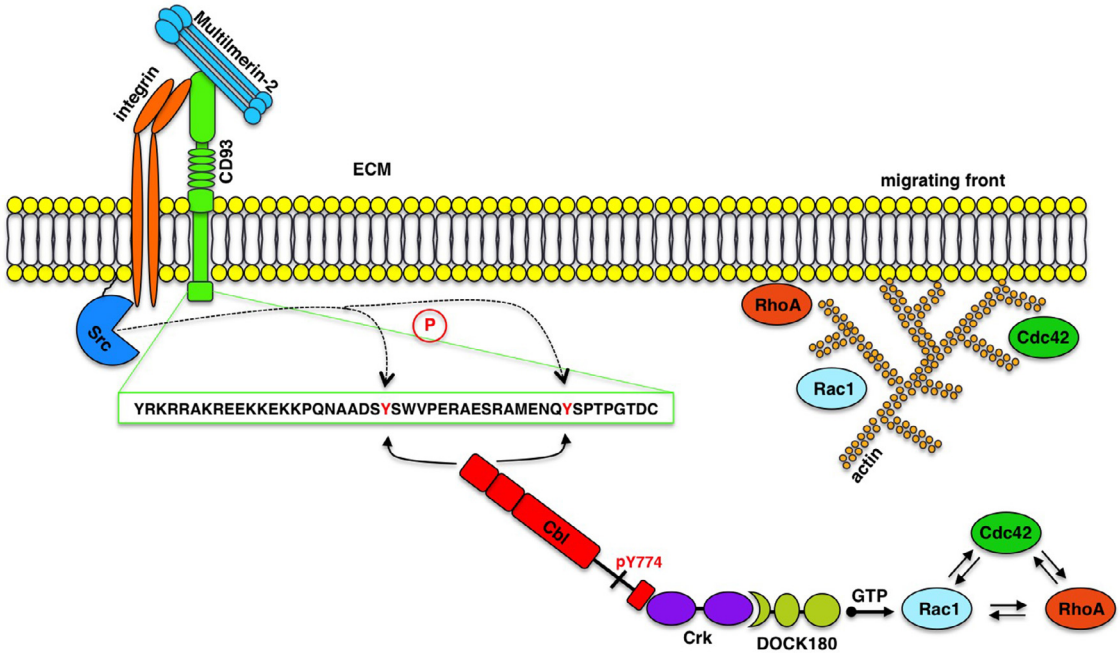

Fig. 9. The CD93 signaling pathway in migrating ECs. The schematic representation shows the proposed molecular mechanisms underlying the regulatory role of CD93 in migrating ECs. The human sequence of the CD93 cytoplasmic tail containing tyrosine 628 and 644 (red) is shown. ECM, extracellular matrix; pY774-Cbl, Cbl phosphorylated on tyrosine 774.

integrated by ECs and culminate in functional cell proliferation and migration. Due to context-dependent variability, ECs use different molecules to control their migratory as well as proliferative behavior. This study provides additional milestones into the understanding of the intricate molecular pathways activated by the microenvironment and translated by CD93 into actin remodeling and effective EC migration during angiogenesis.

Experimental procedures

DNA constructs and RNA interference

The following plasmids were purchased from Addgene (Watertown, MA, USA): pLifeAct-mScarlet-i-N1 plasmid (#85056) [50]; pLJM1-EGFP vector (#19319) [51]; lentiviral negative control vector containing scrambled shRNA (#1864, sh-unr) [52]; Rac1 second generation fluorescence resonance energy transfer (FRET) biosensor for lentivirus production (#66111, pLenti-Rac1-2G) [53]; FRET-based biosensor reporting on Cdc42 activation (#68813, pLenti-Cdc42-2G) [54]; RhoA second generation FRET biosensor for lentivirus production (#40179, pLenti-RhoA-2G) [55]. To obtain the lentiviral vectors expressing LifeAct-EGFP (vLA-EGFP) and LifeAct-mScarlet-i-N1 (vLA-Scar), the actin binding sequence was PCR-amplified from pLifeAct-mScarlet-i-N1 plasmid using the following pairs of primers containing adapters: for1, 5'-TCTATATAAGCAGAGCTGGTTTAGTGAACCGTCAGATCCGCTAGCTCCACCATGGGCGTGGCC-3' and rev1, 5'-AGCTCCTCGCCCTTGCTCACCATGGTGGCGACCGGTAGCGCCTCCTCCTTGCTGATGCTCTCG-3' (vLA-EGFP); for2 5'-TCTATATAAGCAGAGCTGGTTTAGTGAACCGTCAGATCCGCTAGCTCCACCATGGGCGTGGCC-3' and rev2 5'-TTGTGGATGAATACTGCCATTTGTCTCGAGGTCGAGAATTCAGTCGCGGCCGCTTTACTTG-3' (vLA-Scar). The PCR fragments were subcloned into the *Nhe*I (vLA-EGFP) or *Nhe*I/*Eco*RI (vLA-Scar) sites of pLJM1-EGFP vector by using the NEBuilder HiFi DNA assembly cloning kit (New England Biolabs, Ipswich, MA, USA), following manufacturer's instructions. All constructs were checked by sequencing. shRNA-mediated knockdown of CD93 was performed as previously described [11], by using a pLKO.1 retroviral vector from the Mission shRNA Library (Merck KGaA), which expresses a shRNA (clone TRCN0000029085) specific for the silencing of the human protein. Recombinant lentiviruses were produced and used for infection experiments as earlier outlined [56].

For Ckr silencing experiments, HUVECs were incubated with scrambled control siRNA or siRNA to Crk (Hs_Crk_3 or Hs_CRK_5) (FlexiTube, Qiagen, Hilden, Germany) at a concentration of 3 nM in a mixture of 25% Opti-MEM (Thermo Fisher Scientific, Waltham, MA, USA) in EBM-MV2 medium supplemented with 30 μL/mL Lipofectamine RNAiMAX (Thermo Fisher Scientific) for 16 h, after which the medium was replaced with fresh medium. Experiments were performed at day 2 after siRNA transfection.

Cell cultures

HUVECs from single donors were purchased from PromoCell (Heidelberg, Germany) and grown on gelatin-coated plates in antibiotic-free Endothelial Cell Basal Medium (EBM-MV2) with supplements (PromoCell) as previously described [56]. For lentivirus production, human Lenti-X 293T cells (Takara Bio Inc, Kusatsu, Japan) were grown in DMEM containing 10% FBS and 1 mM sodium butyrate (Merck KGaA, Darmstadt, Germany), which increases viral titer [57]. To detach cells from the culture plate by non-enzymatic method, growing cells were washed thrice with PBS, incubated with Cell Dissociation Solution Non-enzymatic (Merck KGaA) for 5 min at 37°C, collected in M199 medium supplemented with 10% FBS, centrifuged, and resuspended in fresh culture medium.

Mice

CD93 knockout (*CD93*$^{-/-}$) mice on the C57BL/6 background [58] were bred in house. C57BL/6 wild-type mice were purchased from Taconic Biosciences (Rensselaer, NY, USA). Animal experiments were performed according to the gudelines for animal experimentation and welfare provided by Uppsala University and approved by the Uppsala County regional ethics committee (license number: 5.8.18-19429_2019).

Antibodies

The following primary antibodies were used: mouse monoclonal anti-CD93 (clone 4E1) [11]; rabbit anti-CD93 (HPA009300, Atlas Antibodies, Bromma, Sweden); sheep anti-CD93 (AF1696, R&D Systems, Minneapolis, MN, USA); mouse anti-β-actin (A2228) and mouse anti-Cbl (05-440, Merck KGaA); rabbit anti-GAPDH (ab9485), rabbit anti-Cbl (ab32027), and mouse anti-phosphotyrosine (ab10321, Abcam, Cambridge, United Kingdom); mouse anti-golgin-97 (CDF4), rabbit anti-pY774-Cbl (8H4L1), rabbit anti-pY774-Cbl (PA5-36734), and hamster anti-CD31 (MA3015, Thermo Fisher Scientific); mouse anti-Crk (610035), mouse anti-Rac1 (610650) and mouse anti-Rho (610990, BD Transduction Laboratories, Franklin Lakes, NJ, USA); mouse anti-Cdc42 (ACD03, Cytoskeleton Inc., Denver, CO, USA); mouse anti-DOCK180 (sc-13163) and normal mouse IgG (sc-2025, Santa Cruz

Biotechnology, Dallas, TX, USA); rabbit anti-Multimerin-2 [59].

Wound healing assay

To capture immunofluorescent images, the scratch test was performed as previously described with slight modifications [22]. Briefly, cells were seeded on gelatin-coated 8-well Nunc Lab-Tek Chamber slides (Thermo Fisher Scientific) and cultured until they reached confluence. A double-sided scratch was created in the monolayer using a sterile pipette tip. The cultures were washed with PBS, grown in supplemented EBM-MV2 medium for 5 h, fixed in 4% paraformaldehyde, and subjected to immunofluorescence analysis.

To test the migratory ability of Crk-silenced HUVECs, cells were assessed for their capability to heal a wound in the cell monolayer. Bright-field images were captured at 14 h from the scratch by using a DM IL LED inverted microscope equipped with a digital DFC405 camera (Leica Microsystems, Wetzlar, Germany). For each condition, images were acquired at three different positions along the scratch and a representative field was shown. The cell-free area was analyzed using ImageJ2 software [60].

Solid-phase binding assay

ELISA-based assay was performed as previously described with slight modifications [14]. Briefly, 96-well plates were coated with gelatin or human Multimerin-2 (1.5 μg/ml) [59]. 1.5×10^4 HUVECs were seeded in gelatin-coated wells, grown in supplemented EBM-MV2 medium for 5 h, fixed in 3% paraformaldehyde, not permeabilized, and subjected to solid phase analysis using anti-Multimerin-2 antibodies. A microtiter plate reader was used to measure color development using *o*-phenylenediamine as HRP substrate.

Immunoprecipitation and immunoblotting analyses

Co-immunoprecipitation experiments were carried out using the Pierce co-immunoprecipitation kit (Thermo Fisher Scientific) according to the manufacturer's instructions. Cell lysates were immunoprecipitated using the primary antibody or normal mouse IgG as negative control, and analyzed by immunoblotting as previously described [61]. To compare protein levels of different samples, densitometric analysis was performed using the gel analyzer tool of ImageJ2.

Immunofluorescent and FRET analyses

Acquisition of fluorescent images, video recording, and FRET experiments were carried out using a Leica TCS SP8 AOBS confocal laser-scanning microscope, following the TCS SP8 and FRET AB manufacturer's software. A Leica HC PL APO 63x/1.40 Oil CS2 objective was used for the acquisition of migrating cell images, highly detailed videos, and FRET analyses and a Leica HC PL APO 63x/1.30 Glyc CORR CS2 glycerol objective was used for the acquisition of retina vasculature images. Diode laser and White Light Laser (WLL) were used to excite fluorochromes and fluorescent molecules at the optimal wavelength ranging from 405 nm to 647 nm and images (1024×1024 pixel resolution) were acquired at a scan speed of 400 Hz image lines/sec. Confocal scanner configuration was set as follows: pinhole at 1.0 Airy diameter and line averaging function at 4.

For live imaging, 48 h after lentivirus transduction, control and CD93-silenced HUVECs were selected with 4 μg/mL of Puromycin for 24 h and then transduced again with lentiviruses expressing LifeAct-EGFP or LifeAct-mScarlet, respectively. 48 h after LifeAct transduction, cells were detached from the plate by a non-enzymatic method, seeded on gelatin-coated Nunc Glass Bottom Dishes (Thermo Fisher Scientific), and grown in EBM-MV2 with supplements during functional migration analyses. Microscopy fields containing multiple cells per each condition were recorded using a Leica Fluotar VISIR 25x/0.95 water objective. Frames (1024×1024 pixel resolution) were recorded at a scan speed of 600 Hz image lines/sec. The pinhole was set at 2 Airy diameter and line averaging function at 6. Mean cell velocity was analyzed using ImageJ and the ADAPT plug-in [62]. Cell trajectories and mean square displacements were measured using the software DiPer and the Plot_At_Origin auxillary program [63].

For immunofluorescent staining, cells were fixed in 4% paraformaldehyde, and treated as previously described [15,56]. The secondary appropriate antibodies were conjugated with Alexa Fluor-488 -568 or -647 (Thermo Fisher Scientific). F-actin staining was performed with Alexa Fluor-647 phalloidin and Hoechst 33342 solution was used to stain nuclei (both from Thermo Fisher Scientific). To show colocalization events by white dots, images were generated using ImageJ2 and the Colocalization plug-in. To quantify protein levels at the migrating front, an area of 5 μm distance from the leading edge was chosen and a minimum of 7 images of the migrating front area per condition were analyzed using ImageJ2.

To analyze and quantify the retinal vasculature, retinas from wild-type and $CD93^{-/-}$ mice were collected at postnatal day 6 (P6), fixed in 4% paraformaldehyde, and stained using primary and conjugated-secondary antibodies. pY774-Cbl levels in mouse retinal sprouts were calculated as follows: first, multiple regions of interest (ROI), each containing an apical sprout, were isolated from acquired images and white dot colocalization (wdc) images between pY774-Cbl and CD31 were generated.

Next, wdc image splitting allowed the isolation of the pY774-Cbl signal overlapping the CD31-positive vessel area. Finally, the isolated pY774-Cbl signal was quantified and plotted against the total $CD31^{+ve}$ signal in the ROI. A number of at least 5 randomly selected images per retina and 3 mice for each genotype were used to perform the analysis.

FRET acceptor photobleaching (apFRET) analyses were carried out on control or CD93-silenced HUVECs transduced with genetically encoded biosensors expressing RhoGTPases Rac1 (pLenti-Rac1-2G), Cdc42 (pLenti-Cdc42-2G), or RhoA (pLenti-RhoA-2G). Confluent cells were double-side scratched, fixed at 5 h from the wound, stained to visualize F-actin and nuclei, and finally analyzed. Acquisition parameters were modified only in the pinhole diameter at 1.40 Airy units. Argon laser lines 476 nm and 514 nm were used to excite mTFP1 and mVenus fluorophores, which represent the donor and the acceptor, respectively. For proper image recording, hybrid detectors HyD were employed by gating a spectral acquisition window of 486-502 nm for the donor and 524-600 nm for the acceptor. In the photobleaching procedure, cells were bleached using the 514 nm argon laser beam at 100% intensity until the acceptor was photobleached down to about 10% of its initial value. FRET analysis was performed using ImageJ2 and the FRETcalc plug-in and FRET efficiency was calculated as previously described [64,65].

Statistical analysis

Data analyses were performed using Prism 6 statistical software (GraphPad, San Diego, CA, USA) and the values represent the mean ± SD obtained from at least three independent experiments. Normality test was performed using D'Agostino & Pearson normality test. The statistical significance of the differences between two groups was determined using the two-tailed Student *t*-test for normally distributed values, or the Mann-Whitney *U* test when the values were not normally distributed. All *P* values reported were two-tailed and $P < 0.05$ was considered statistically significant.

Author contribution

Stefano Barbera: Conceptualization, Methodology, Investigation, Writing; Roberta Lugano and Alessia Pedalina: Investigation, Validation; Anna Dimberg and Federico Galvagni: Resources, Validation, Funding acquisition; Maurizio Mongiat: Writing − Review & Editing; Annalisa Santucci and Gian Marco Tosi: Funding acquisition; Maurizio Orlandini: Conceptualization, Supervision, Writing − Original Draft.

Declaration of Competing Interest

None of the authors has a conflict of interest to declare.

Acknowledgements

This research was partially supported by MIUR Grant Dipartimento di Eccellenza 2018-2022 (L.232,11-12-16); Swedish Cancer Society (CAN 2017/502, 20 1008 PjF); and Swedish Research Council (Dnr 2016-02495, 2020-02563).

Supplementary materials

Supplementary material associated with this article can be found in the online version at doi:10.1016/j.matbio.2021.05.006.

Received 16 March 2021;
Received in revised form 19 May 2021;
Accepted 24 May 2021
Available online 29 May 2021

Keywords:
Cbl;
Crk;
Rac1;
Cdc42;
RhoA

Abbreviations:
HUVEC, human umbilical vein endothelial cell; EC, endothelial cell; ECM, extracellular matrix; CTLD, C-type lectin-like domain; wdc, white dot colocalization; FRET, fluorescence resonance energy transfer

References

[1] M. De Palma, D. Biziato, T.V. Petrova, Microenvironmental regulation of tumour angiogenesis, Nat. Rev. Cancer 17 (2017) 457–474.
[2] G. Eelen, P. de Zeeuw, L. Treps, U. Harjes, B.W. Wong, P. Carmeliet, Endothelial cell metabolism, Physiol. Rev. 98 (2018) 3–58.
[3] X. Li, A. Kumar, P. Carmeliet, Metabolic pathways fueling the endothelial cell drive, Annu. Rev. Physiol. 81 (2019) 483–503.
[4] L. Lamalice, F. Le Boeuf, J. Huot, Endothelial cell migration during angiogenesis, Circ. Res. 100 (2007) 782–794.
[5] C.J. Avraamides, B. Garmy-Susini, J.A. Varner, Integrins in angiogenesis and lymphangiogenesis, Nat. Rev. Cancer 8 (2008) 604–617.

[6] M. Giannotta, M. Trani, E. Dejana, VE-Cadherin and endothelial adherens junctions: active guardians of vascular integrity, Dev. Cell 26 (2013) 441–454.
[7] I. van der Bijl, K. Nawaz, U. Kazlauskaite, A.-M. van Stalborch, S. Tol, A. Jimenez Orgaz, I. van den Bout, N.R. Reinhard, A. Sonnenberg, C. Margadant, Reciprocal integrin/integrin antagonism through kindlin-2 and Rho GTPases regulates cell cohesion and collective migration, Matrix Biol 93 (2020) 60–78.
[8] R. Silva, G. D'Amico, K.M. Hodivala-Dilke, L.E. Reynolds, Integrins: the keys to unlocking angiogenesis, Arterioscler. Thromb. Vasc. Biol. 28 (2008) 1703–1713.
[9] B. Sennino, D.M. McDonald, Controlling escape from angiogenesis inhibitors, Nat. Rev. Cancer 12 (2012) 699–709.
[10] S. Ricard-Blum, S.D. Vallet, Fragments generated upon extracellular matrix remodeling: biological regulators and potential drugs, Matrix Biol 75-76 (2019) 170–189.
[11] M. Orlandini, F. Galvagni, M. Bardelli, M. Rocchigiani, C. Lentucci, F. Anselmi, A. Zippo, L. Bini, S. Oliviero, The characterization of a novel monoclonal antibody against CD93 unveils a new antiangiogenic target, Oncotarget 5 (2014) 2750–2760.
[12] E. Langenkamp, L. Zhang, R. Lugano, H. Huang, T.E.A. Elhassan, M. Georganaki, W. Bazzar, J. Lööf, G. Trendelenburg, M. Essand, F. Pontén, A. Smits, A Dimberg, Elevated expression of the C-type lectin CD93 in the glioblastoma vasculature regulates cytoskeletal rearrangements that enhance vessel function and reduce host survival, Cancer Res 75 (2015) 4504–4516.
[13] G.M. Tosi, E. Caldi, B. Parolini, P. Toti, G. Neri, F. Nardi, C. Traversi, G. Cevenini, D. Marigliani, E. Nuti, T. Bacci, F. Galvagni, M. Orlandini, CD93 as a potential target in neovascular age-related macular degeneration, J. Cell. Physiol. 232 (2017) 1767–1773.
[14] F. Galvagni, F. Nardi, O. Spiga, A. Trezza, G. Tarticchio, R. Pellicani, E. Andreuzzi, E. Caldi, P. Toti, G.M. Tosi, A. Santucci, R.V. Iozzo, M. Mongiat, M. Orlandini, Dissecting the CD93-Multimerin 2 interaction involved in cell adhesion and migration of the activated endothelium, Matrix Biol 64 (2017) 112–127.
[15] R. Lugano, K. Vemuri, D. Yu, M. Bergqvist, A. Smits, M. Essand, S. Johansson, E. Dejana, A. Dimberg, CD93 promotes β1 integrin activation and fibronectin fibrillogenesis during tumor angiogenesis, J. Clin. Invest. 128 (2018) 3280–3297.
[16] M. Mongiat, E. Andreuzzi, G. Tarticchio, A. Paulitti, Extracellular matrix, a hard player in angiogenesis, Int. J. Mol. Sci. 17 (2016) E1822.
[17] R. Pellicani, E. Poletto, E. Andreuzzi, A. Paulitti, R. Doliana, D. Bizzotto, P. Braghetta, R. Colladel, G. Tarticchio, P. Sabatelli, F. Bucciotti, G. Bressan, R.V. Iozzo, A. Colombatti, P. Bonaldo, M. Mongiat, Multimerin-2 maintains vascular stability and permeability, Matrix Biol 87 (2020) 11–25.
[18] G.M. Tosi, G. Neri, S. Barbera, L. Mundo, B. Parolini, S. Lazzi, R. Lugano, E. Poletto, L. Leoncini, G. Pertile, M. Mongiat, A. Dimberg, F. Galvagni, M. Orlandini, The binding of CD93 to Multimerin-2 promotes choroidal neovascularization, Invest. Ophthalmol. Vis. Sci. 61 (2020) 30.
[19] M. Urbanczyk, S.L. Layland, K. Schenke-Layland, The role of extracellular matrix in biomechanics and its impact on bioengineering of cells and 3D tissues, Matrix Biol. 85-86 (2020) 1–14.
[20] R.V. Iozzo, A.D. Theocharis, T. Neill, N.K. Karamanos, Complexity of matrix phenotypes, Matrix Biol. Plus 6-7 (2020) 100038.
[21] M. Zhang, S. Bohlson, Dy S., Tenner M., J A., Modulated interaction of the ERM protein, moesin, with CD93, Immunology 115 (2005) 63–73.
[22] S. Barbera, F. Nardi, I. Elia, G. Realini, R. Lugano, A. Santucci, G.M. Tosi, A. Dimberg, F. Galvagni, M. Orlandini, The small GTPase Rab5c is a key regulator of trafficking of the CD93/Multimerin-2/β1 integrin complex in endothelial cell adhesion and migration, Cell Commun. Signal. 17 (2019) 55.
[23] F. Galvagni, F. Nardi, M. Maida, G. Bernardini, S. Vannuccini, F. Petraglia, A. Santucci, M. Orlandini, CD93 and dystroglycan cooperation in human endothelial cell adhesion and migration, Oncotarget 7 (2016) 10090–10103.
[24] H. Lee, A.Y. Tsygankov, Cbl-family proteins as regulators of cytoskeleton-dependent phenomena, J. Cell. Physiol. 228 (2013) 2285–2293.
[25] K.A. Khan, A.J. Naylor, A. Khan, P.J. Noy, M. Mambretti, P. Lodhia, J. Athwal, A. Korzystka, C.D. Buckley, B.E. Willcox, F. Mohammed, R. Bicknell, Multimerin-2 is a ligand for group 14 family C-type lectins CLEC14A, CD93 and CD248 spanning the endothelial pericyte interface, Oncogene 36 (2017) 6097–6108.
[26] J. Riedl, A.H. Crevenna, K. Kessenbrock, J.H. Yu, D. Neukirchen, M. Bista, F. Bradke, D. Jenne, T.A. Holak, Z. Werb, M. Sixt, R. Wedlich-Soldner, Lifeact: a versatile marker to visualize F-actin, Nat. Methods 5 (2008) 605–607.
[27] A. Pietuch, A. Janshoff, Mechanics of spreading cells probed by atomic force microscopy, Open Biol 3 (2013) 130084.
[28] D.M. Gau, P. Roy, Single cell migration assay using human breast cancer MDA-MB-231 cell line, Bio Protocol 10 (2020) e3586.
[29] A. Braiman, N. Isakov, The role of Crk adaptor proteins in T-cell adhesion and Migration, Front. immunol. 6 (2015) 509.
[30] B. Bisel, M. Calamai, F. Vanzi, F.S. Pavone, Decoupling polarization of the Golgi apparatus and GM1 in the plasma membrane, PLoS One 8 (2013) e80446.
[31] A.J. Ridley, Rho GTPase signalling in cell migration, Curr. Opin. Cell Biol. 36 (2015) 103–112.
[32] M.J. Randles, F. Lausecker, J.D. Humphries, A. Byron, S.J. Clark, J.H. Miner, R. Zent, M.J. Humphries, R. Lennon, Basement membrane ligands initiate distinct signalling networks to direct cell shape, Matrix Biol 90 (2020) 61–78.
[33] V.S. Kraynov, C. Chamberlain, G.M. Bokoch, M.A. Schwartz, S. Slabaugh, K.M. Hahn, Localized Rac activation dynamics visualized in living cells, Science 290 (2000) 333–337.
[34] C.M. Grimsley, J.M. Kinchen, A.-C. Tosello-Trampont, E. Brugnera, L.B. Haney, M. Lu, Q. Chen, D. Klingele, M.O. Hengartner, K.S. Ravichandran, Dock180 and ELMO1 proteins cooperate to promote evolutionarily conserved Rac-dependent cell migration, J. Biol. Chem. 279 (2004) 6087–6097.
[35] J.-F. Côté, K. Vuori, GEF what? Dock180 and related proteins help Rac to polarize cells in new ways, Trends Cell Biol 17 (2007) 383–393.
[36] M. Machacek, L. Hodgson, C. Welch, H. Elliott, O. Pertz, P. Nalbant, A. Abell, G.L. Johnson, K.M. Hahn, G. Danuser, Coordination of Rho GTPase activities during cell protrusion, Nature 461 (2009) 99–103.
[37] P. Nalbant, L. Hodgson, V. Kraynov, A. Toutchkine, K.M. Hahn, Activation of endogenous Cdc42 visualized in living cells, Science 305 (2004) 1615–1619.
[38] O. Pertz, L. Hodgson, R.L. Klemke, K.M. Hahn, Spatiotemporal dynamics of RhoA activity in migrating cells, Nature 440 (2006) 1069–1072.

[39] S.S. Hasan, A.F. Siekmann, The same but different: signaling pathways in control of endothelial cell migration, Curr. Opin. Cell Biol. 36 (2015) 86–92.
[40] R.M. Scaife, S.A. Courtneidge, W.Y. Langdon, The multi-adaptor proto-oncoprotein Cbl is a key regulator of Rac and actin assembly, J. Cell Sci. 116 (2003) 463–473.
[41] G. Gadea, A. Blangy, Dock-family exchange factors in cell migration and disease, Eur. J. Cell Biol. 93 (2014) 466–477.
[42] N.A. Mack, M. Georgiou, The interdependence of the Rho GTPases and apicobasal cell polarity, Small GTPases 5 (2014) 10.
[43] M. Laurin, J.-F. Côté, Insights into the biological functions of Dock family guanine nucleotide exchange factors, Genes Dev. 28 (2014) 533–547.
[44] C.D. Nobes, A. Hall, Rho, rac, and cdc42 GTPases regulate the assembly of multimolecular focal complexes associated with actin stress fibers, lamellipodia, and filopodia, Cell 81 (1995) 53–62.
[45] C.D. Lawson, K. Burridge, The on-off relationship of Rho and Rac during integrin-mediated adhesion and cell migration, Small GTPases 5 (2014) e27958.
[46] S. Tojkander, G. Gateva, P. Lappalainen, Actin stress fibers – assembly, dynamics and biological roles, J. Cell Sci. 125 (2012) 1855–1864.
[47] R.J. Petrie, K.M. Yamada, At the leading edge of three-dimensional cell migration, J. Cell Sci. 125 (2012) 5917–5926.
[48] H.R. Barlow, O. Cleaver, Building blood vessels-one Rho GTPase at a time, Cells 8 (2019) 545.
[49] E.N. Pugacheva, F. Roegiers, E.A. Golemis, Interdependence of cell attachment and cell cycle signaling, Curr. Opin. Cell Biol. 18 (2006) 507–515.
[50] D.S. Bindels, L. Haarbosch, L. van Weeren, M. Postma, K.E. Wiese, M. Mastop, S. Aumonier, G. Gotthard, A. Royant, M.A. Hink, T.W.J Gadella, mScarlet: a bright monomeric red fluorescent protein for cellular imaging, Nat. Methods 14 (2017) 53–56.
[51] Y. Sancak, T.R. Peterson, Y.D. Shaul, R.A. Lindquist, C.C. Thoreen, L. Bar-Peled, D.M. Sabatini, The Rag GTPases bind raptor and mediate amino acid signaling to mTORC1, Science 320 (2008) 1496–1501.
[52] D.D. Sarbassov, D.A. Guertin, S.M. Ali, D.M. Sabatini, Phosphorylation and regulation of Akt/PKB by the rictor-mTOR complex, Science 307 (2005) 1098–1101.
[53] R.D. Fritz, D. Menshykau, K. Martin, A. Reimann, V. Pontelli, O. Pertz, SrGAP2-dependent integration of membrane geometry and Slit-Robo-repulsive cues regulates fibroblast contact inhibition of locomotion, Dev. Cell 35 (2015) 78–92.
[54] K. Martin, A. Reimann, R.D. Fritz, H. Ryu, N.L. Jeon, O. Pertz, Spatio-temporal co-ordination of RhoA, Rac1 and Cdc42 activation during prototypical edge protrusion and retraction dynamics, Sci. Rep. 6 (2016) 21901.
[55] R.D. Fritz, M. Letzelter, A. Reimann, K. Martin, L. Fusco, L. Ritsma, B. Ponsioen, E. Fluri, S. Schulte-Merker, J. van Rheenen, O. Pertz, A versatile toolkit to produce sensitive FRET biosensors to visualize signaling in time and space, Sci. Signal. 6 (2013) rs12.
[56] M. Orlandini, S. Nucciotti, F. Galvagni, M. Bardelli, M. Rocchigiani, F. Petraglia, S. Oliviero, Morphogenesis of human endothelial cells is inhibited by DAB2 via Src, FEBS Lett 582 (2008) 2542–2548.
[57] A.P. Cribbs, A. Kennedy, B. Gregory, F.M. Brennan, Simplified production and concentration of lentiviral vectors to achieve high transduction in primary human T cells, BMC Biotechnol. 13 (2013) 98.
[58] P.J. Norsworthy, L. Fossati-Jimack, J. Cortes-Hernandez, P.R. Taylor, A.E. Bygrave, R.D. Thompson, S. Nourshargh, M.J. Walport, M. Botto, Murine CD93 (C1qRp) contributes to the removal of apoptotic cells in vivo but is not required for C1q-mediated enhancement of phagocytosis, J. Immunol. 172 (2004) 3406–3414.
[59] E. Lorenzon, R. Colladel, E. Andreuzzi, S. Marastoni, F. Todaro, M. Schiappacassi, G. Ligresti, A. Colombatti, M. Mongiat, MULTIMERIN2 impairs tumor angiogenesis and growth by interfering with VEGF-A/VEGFR2 pathway, Oncogene 31 (2012) 3136–3147.
[60] C.T. Rueden, J. Schindelin, M.C. Hiner, B.E. DeZonia, A.E. Walter, E.T. Arena, K.W. Eliceiri, ImageJ2: ImageJ for the next generation of scientific image data, BMC Bioinform. 18 (2017) 529.
[61] F. Galvagni, F. Anselmi, A. Salameh, M. Orlandini, M. Rocchigiani, S. Oliviero, Vascular endothelial growth factor receptor-3 activity is modulated by its association with caveolin-1 on endothelial membrane, Biochemistry 46 (2007) 3998–4005.
[62] D.J. Barry, C.H. Durkin, J.V. Abella, M. Way, Open source software for quantification of cell migration, protrusions, and fluorescence intensities, J. Cell Biol. 209 (2015) 163–180.
[63] R. Gorelik, A. Gautreau, Quantitative and unbiased analysis of directional persistence in cell migration, Nat. Protoc. 9 (2014) 1931–1943.
[64] D. Stepensky, FRETcalc plugin for calculation of FRET in non-continuous intracellular compartments, Biochem. Biophys. Res. Commun. 359 (2007) 752–758.
[65] C. Boscher, V. Gaonac'h-Lovejoy, C. Delisle, J.-P. Gratton, Polarization and sprouting of endothelial cells by angiopoietin-1 require PAK2 and paxillin-dependent Cdc42 activation, Mol. Biol. Cell 30 (2019) 2227–2239.

ARTICLE 2

International Journal of
Molecular Sciences

MDPI

Article

CD93 Signaling via Rho Proteins Drives Cytoskeletal Remodeling in Spreading Endothelial Cells

Stefano Barbera [1,2], Luisa Raucci [1], Roberta Lugano [2], Gian Marco Tosi [3], Anna Dimberg [2], Annalisa Santucci [1], Federico Galvagni [1] and Maurizio Orlandini [1,*]

[1] Department of Biotechnology, Chemistry and Pharmacy, University of Siena, 53100 Siena, Italy; stefano.barbera@student.unisi.it (S.B.); luisa.raucci@unisi.it (L.R.); annalisa.santucci@unisi.it (A.S.); federico.galvagni@unisi.it (F.G.)
[2] Department of Immunology, Genetics and Pathology, Science for Life Laboratory, Uppsala University, Rudbeck Laboratory, SE-75185 Uppsala, Sweden; roberta.lugano@igp.uu.se (R.L.); Anna.Dimberg@igp.uu.se (A.D.)
[3] Ophthalmology Unit, Department of Medicine, Surgery and Neuroscience, University of Siena, 53100 Siena, Italy; gianmarco.tosi@unisi.it
* Correspondence: maurizio.orlandini@unisi.it

Abstract: During angiogenesis, cell adhesion molecules expressed on the endothelial cell surface promote the growth and survival of newly forming vessels. Hence, elucidation of the signaling pathways activated by cell-to-matrix adhesion may assist in the discovery of new targets to be used in antiangiogenic therapy. In proliferating endothelial cells, the single-pass transmembrane glycoprotein CD93 has recently emerged as an important endothelial cell adhesion molecule regulating vascular maturation. In this study, we unveil a signaling pathway triggered by CD93 that regulates actin cytoskeletal dynamics responsible of endothelial cell adhesion. We show that the Src-dependent phosphorylation of CD93 and the adaptor protein Cbl leads to the recruitment of Crk, which works as a downstream integrator in the CD93-mediated signaling. Moreover, confocal microscopy analysis of FRET-based biosensors shows that CD93 drives the coordinated activation of Rac1 and RhoA at the cell edge of spreading cells, thus promoting the establishment of cell polarity and adhesion required for cell motility.

Keywords: Src; Cbl; Crk; Rac1; Cdc42; RhoA

Citation: Barbera, S.; Raucci, L.; Lugano, R.; Tosi, G.M.; Dimberg, A.; Santucci, A.; Galvagni, F.; Orlandini, M. CD93 Signaling via Rho Proteins Drives Cytoskeletal Remodeling in Spreading Endothelial Cells. *Int. J. Mol. Sci.* **2021**, *22*, 12417. https://doi.org/10.3390/ijms222212417

Academic Editor: Richard L. Hoover

Received: 6 October 2021
Accepted: 13 November 2021
Published: 17 November 2021

1. Introduction

Migration of endothelial cells (ECs) is essential for the outgrowth of new blood vessels both in physiological and pathological conditions. ECs of the vascular bed are usually stable and quiescent; however, when the environment surrounding the endothelium becomes hypoxic, the ECs switch to a proliferative and migratory state, leading to vascular remodeling [1]. In migrating cells, the integration of several cues, largely provided by adhesion to the substrate, is critical to activate intracellular signals that bias cytoskeletal remodeling, cell shape, and polarity [2]. Therefore, uncovering the molecular mechanisms that underpin the regulation of EC adhesion could allow a better understanding of both physiological and pathological angiogenesis.

In addition to integrins, stimulated endothelia express alternative adhesive proteins that can bind extracellular matrix (ECM) components and activate signaling pathways during cell motility [3]. Among these proteins, the C-type lectin transmembrane protein CD93, predominantly expressed in ECs, has been extensively proven to play important roles in vascular biology [4–6]. CD93 is upregulated in the endothelium of different types of vascularized tumors where it promotes its proangiogenic activities regulating cell adhesion and migration through interaction with different proteins [7,8]. Indeed, CD93 interacts with β-dystroglycan, which is a laminin-binding protein found to be

upregulated in ECs of growing blood vessels within malignant tumors [9,10]. Moreover, the binding of CD93 to Multimerin-2, an endothelial-specific ECM protein [11], contributes to progression of the neovascular form of age-related macular degeneration, while in gliomas, it promotes β1 integrin activation and the fibrillar organization of fibronectin, increasing the motility of proliferating ECs [7,8,12]. Furthermore, the pathway activated by the interaction between CD93 and insulin-like growth factor binding protein 7 (IGFBP7), an ECM protein upregulated in tumor blood vessels, contributes to abnormal tumor vasculature [13]. As a membrane receptor, CD93 mediates the transduction of signals from the extracellular milieu into the cell. Consistently, the cytoplasmic domain of CD93 interacts with different proteins and is essential for the endosomal trafficking of CD93 to the leading edge of migrating ECs [14,15]. In spreading cells, the Src kinase phosphorylates the cytotail of CD93 on two tyrosine residues, which generate consensus motifs for the binding of the adaptor protein c-Cbl that drives the regulation of in vitro angiogenesis [9]. In migrating cells, the phosphorylation of Cbl on tyrosine 774 triggers a signaling cascade that leads to the activation of Rho-proteins and remodeling of the cytoskeleton [16]. However, although the critical role played by CD93 in mediating cellular responses to extracellular cues is quite clear, the transduction pathway triggered by CD93 during EC adhesion has not yet been fully elucidated.

In the present work, we analyze the downstream signaling pathway regulated by CD93 in primary spreading ECs. We show that CD93-dependent Src activation, together with the recruitment of phosphorylated Cbl on tyrosine 774, triggers the activation of small GTPases at the cell edge of spreading cells, thus promoting cytoskeletal reorganization required for proper EC adhesion.

2. Results

2.1. CD93 Modulates Activation and Localization of Src Kinase

We have previously shown that in ECs adhering to the substrate, Src-dependent phosphorylation of the CD93 cytotail on tyrosines 628 and 644 generates two consensus sequences for the binding of the adaptor protein Cbl [9]. While these findings outlined the involvement of CD93 in the activation of a signaling pathway regulating cell adhesion, CD93-dependent regulation of Src activity was unclear prior to this investigation. To address this issue, human umbilical vein ECs (HUVECs) were transduced with a lentiviral construct carrying a CD93 specific shRNA sequence, detached from the plate, and the reseeded sparse cells, after an adhesion period assessed as early spreading phase [17], were analyzed by immunoblotting. Analyses of cell lysates from early spreading HUVECs showed decreased levels of Src phosphorylated at tyrosine 418, which is a protein modification that is closely correlated with kinase activity, in CD93-silenced cells compared to control ECs (Figure 1a, quantified in Figure 1b). These observations were further substantiated by immunofluorescence analyses showing that active Src was strongly decreased at the cell border of CD93-silenced ECs compared to ECs transduced with a lentivirus expressing an unrelated shRNA (Figure 1c). Furthermore, immunofluorescence analysis, showing the colocalization of F-actin with active Src in early adhering ECs, highlighted that the activation of Src was significantly decreased at the cell edge of CD93-depleted ECs in comparison to control cells (Figure 1d, quantified in Figure 1e). These data, together with previous findings showing that CD93 silencing strongly affected adhesion and actin cytoskeletal organization of ECs [5,7], suggest that CD93 drives Src activation and its recruitment to the cell edge to allow proper EC adhesion.

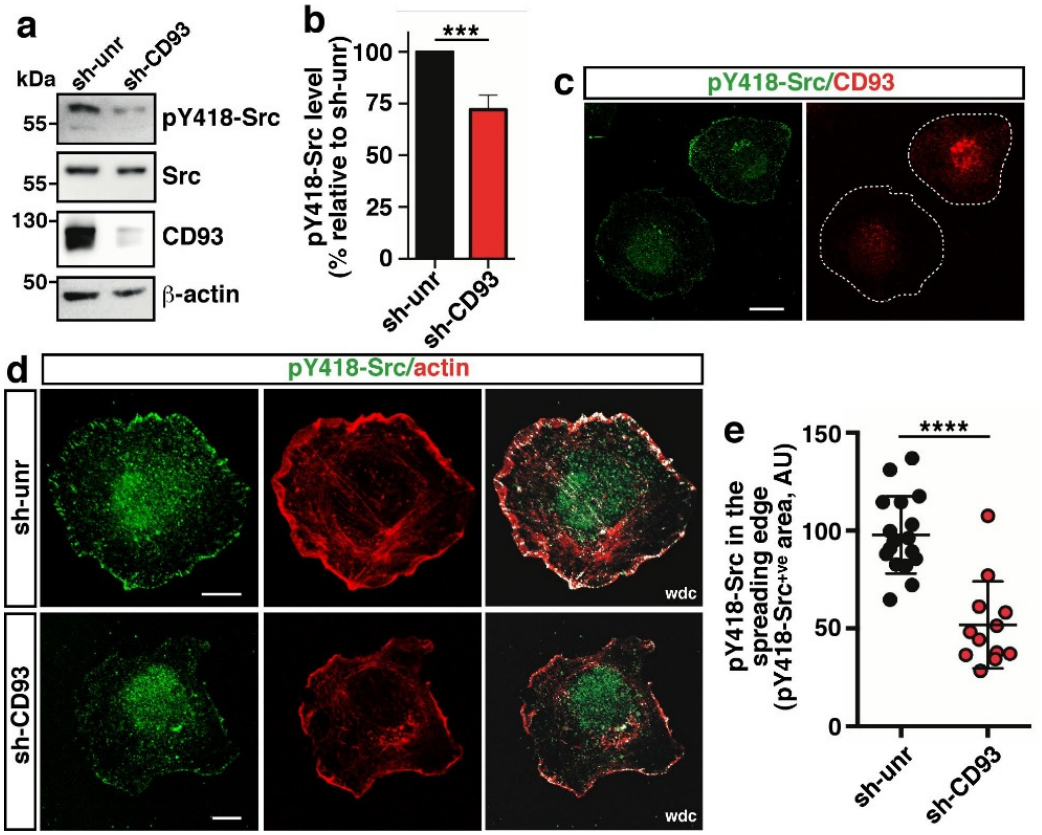

Figure 1. CD93 regulates the activation of Src in adhering ECs. HUVECs were transduced with lentiviral particles expressing unrelated (sh-unr) or CD93 (sh-CD93) shRNAs. (**a**) Total cell extracts from early spreading transduced HUVECs were analyzed by Western blotting with antibodies against pY418-Src, Src, and CD93. Anti-β-actin antibodies were used to confirm equal loading. (**b**) Quantitative analysis of pY418-Src levels from independent experiments performed as in (**a**). Values, normalized to total Src and β-actin protein levels, represent the percentage of Src phosphorylation in CD93-silenced cells (sh-CD93) relative to control (sh-unr). *** $p < 0.001$; paired *t*-test. (**c**) Transduced HUVECs were detached from the plate by a non-enzymatic method, resuspended in complete medium, mixed, reseeded, and fixed at the early phases of spreading. Cells were stained using antibodies against pY418-Src and CD93. White dashed lines indicate cell boundaries. Scale bar, 20 μm. (**d**) Representative images of immunofluorescence analysis of transduced ECs in the early phase of adhesion. Cells were stained using phalloidin and antibodies against pY418-Src. White dot colocalization (wdc) images between pY418-Src and F-actin are shown. Scale bar, 10 μm. (**e**) Quantification of cellular pY418-Src in the spreading border area (5 μm from the cell edge) of control cells ($n = 17$, sh-unr) and CD93-silenced cells ($n = 12$, sh-CD93). Data are presented as a scatter plot, and the fluorescence intensity of the pY418-Src^{+ve} signal per area is reported as arbitrary units (AU). **** $p < 0.0001$; Mann–Whitney test.

2.2. CD93 Controls Phosphorylation and Cellular Localization of Cbl

We have previously shown that the CD93-dependent phosphorylation of Cbl on tyrosine 774 is an important event in promoting EC adhesion [9]; however, it was unclear whether this regulation was also dependent on Src activation. To explore this possibility, we investigated the effect of PP2, a selective Src family kinase (SFK) inhibitor, on Cbl phosphorylation. Western blot analysis of cell lysates from spreading HUVECs revealed that the treatment with PP2 strongly impaired the activation of Src kinase and importantly the phosphorylation of Cbl on tyrosine 774, suggesting that this specific adaptor modification is SFK-dependent in ECs flattening out on the surface (Figure 2a, quantified in Figure 2b). Since in the migration front of ECs, the binding of pY774-Cbl to CD93 triggers a signaling cascade regulating cell dynamics [16], we asked whether this signaling path-

way was also activated during cell spreading. To address this issue, we silenced CD93 in HUVECs and analyzed by immunofluorescence the subcellular localization of previously identified CD93-dependent signaling players [16]. Consistent with our previous results on EC migration [16], while CD93 colocalized with pY774-Cbl and the downstream modulator Crk at the cell edge (Figure 2c,d, sh-unr), the knockdown of CD93 dramatically impaired the localization of pY774-Cbl and Crk along the cell edge of ECs adhering to the substrate (Figure 2c,d, sh-CD93). These findings were further corroborated by quantitative analyses of pY774-Cbl and Crk at the cell edge of spreading cells (Figure 2e,f), providing further evidence of the key role played by CD93 in the regulation of the signaling pathway that controls EC adhesion and migration.

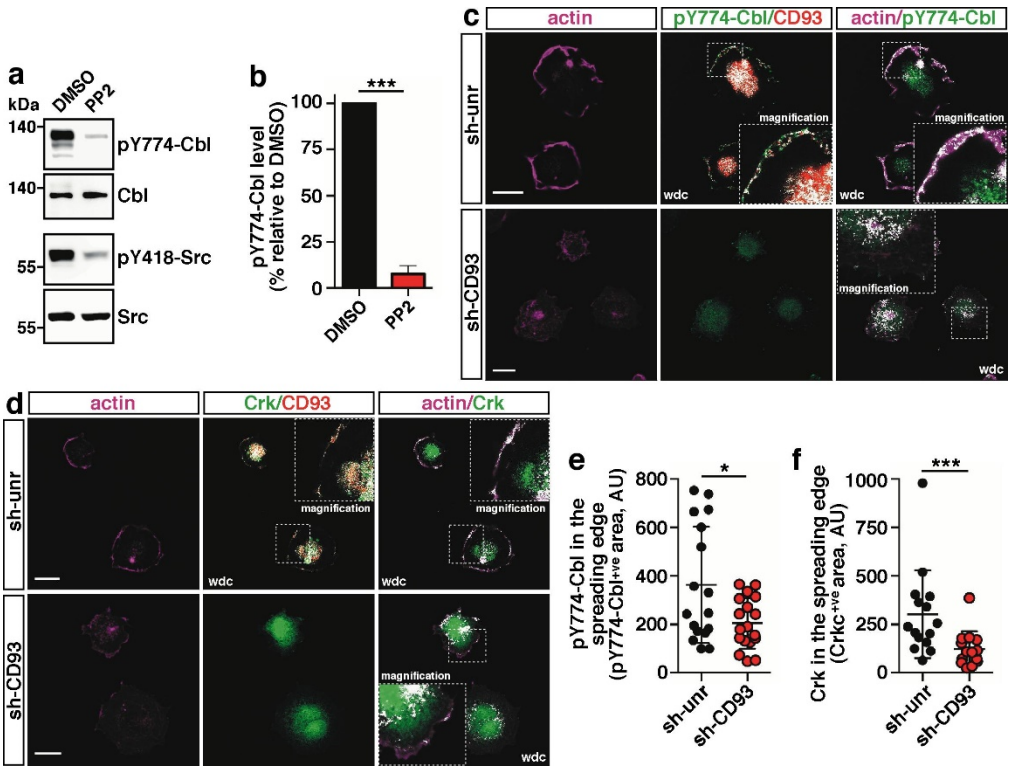

Figure 2. CD93 triggers the pY774-Cbl-dependent signaling pathway in spreading ECs. (**a**) Cell lysates from early spreading HUVECs pretreated for 30 min with vehicle alone (DMSO) or 10 μM PP2 were analyzed by Western blotting using antibodies against pY774-Cbl and pY418-Src to confirm PP2 activity. Equal loading was confirmed by using anti-Cbl and anti-Src antibodies. (**b**) Quantification of pY774-Cbl phosphorylation levels from independent experiments performed as in (**a**). Values, normalized to Cbl protein levels, represent the percentage of pY774-Cbl levels relative to vehicle-treated cells (DMSO). *** $p < 0.001$; paired *t*-test. (**c**,**d**) HUVECs were transduced with lentiviral particles expressing unrelated (sh-unr) or CD93 shRNA (sh-CD93). Cells were detached from the plate, resuspended in complete growth medium, plated on the substrate, and fixed at early phases of spreading. Cells were analyzed by immunofluorescence using phalloidin, anti-CD93 antibody, and antibodies against pY774-Cbl (**c**) and Crk (**d**). White dot colocalization (wdc) images are shown as indicated. In the wdc pictures, magnification of the squared areas is shown (2.5×). Scale bars, 20 μm. (**e**,**f**) Quantification of cellular pY774-Cbl (**e**) and Crk (**f**) in the spreading border area (5 μm from the cell edge) of HUVECs transduced and treated as in (**c**) (n = 14 cells for sh-unr and n = 16 cells for sh-CD93) and (**d**) (n = 15 cells for sh-unr and n = 14 cells for sh-CD93). Data are presented as scatter plots and the fluorescence intensity of the pY774-Cbl^{+ve} and Crk^{+ve} signals per area is reported as arbitrary units (AU). * $p < 0.05$; Student *t*-test (**e**). *** $p < 0.001$; Mann–Whitney test (**f**).

2.3. CD93 Regulates Activity of Rho-Proteins along the Cell Edge of Spreading ECs

Since in motile ECs, the signaling triggered by CD93 converges to the activation and modulation of the Rho GTPase signaling pathways [16], we questioned whether the Rho-proteins Rac1, RhoA, and Cdc42 were CD93-dependent regulators of plasma membrane dynamics also during the early events of EC adhesion to the ECM. To address this possibility, control or CD93-silenced ECs were transduced with lentivirus constructs expressing biosensors that produce localized FRET signals, revealing the amount and location of Rac1, Cdc42, or RhoA activity [18–20]. Quantitative FRET analysis on the early spreading cells unveiled a statistically significant decrease in Rac1 activity at the cell edge of CD93-silenced ECs compared to control cells (Figure 3a, quantified in Figure 3b), suggesting that Rac1 is a downstream effector of the CD93 signaling pathway.

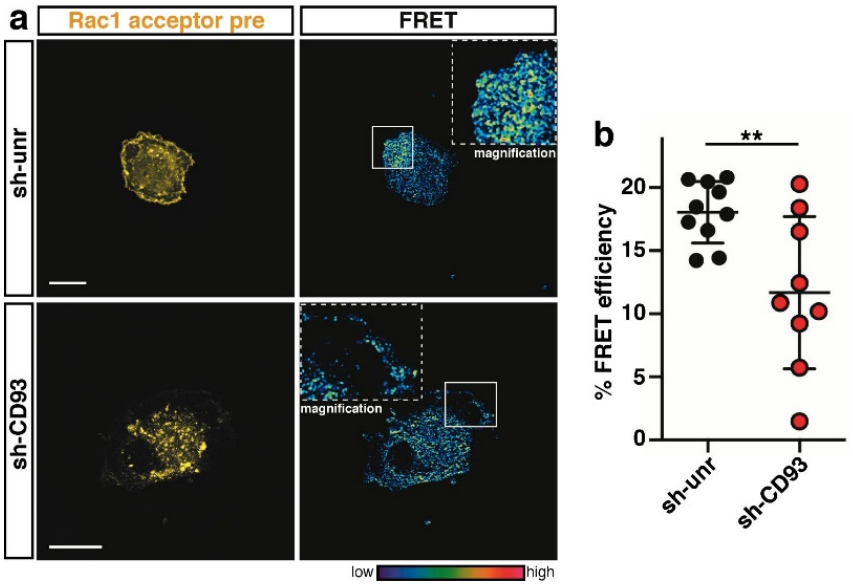

Figure 3. CD93 signaling activates Rac1 at the cell edge of spreading cells. (**a**) FRET analysis on control (sh-unr) or CD93-silenced (sh-CD93) HUVECs transduced with a lentiviral construct expressing the Rac1 biosensor. Cells were fixed at the early phase of adhesion to the ECM. Representative confocal images of transduced cells before photobleaching (acceptor pre) are shown. Rectangles indicate the photobleached cell area. Magnifications of the photobleached area are shown (2.5×). The colored scale represents the color range of FRET efficiency. Scale bars, 20 μm. (**b**) Plot showing the fluorescence increase (% FRET efficiency) upon photobleaching at the cell edge of early spreading ECs (n = 10 cells for sh-unr and n = 9 cells for sh-CD93). Data are presented as scatter plot. ** $p < 0.01$; Student t-test.

Consistent with its role played in the establishment of epithelial apicobasal polarity [21], Cdc42 was strongly activated at the cell edge of control spreading cells (Figure 4a, sh-unr); however, in contrast to Rac1 regulation, Cdc42 activation did not decrease in ECs lacking CD93 (Figure 4a, quantified in Figure 4b), suggesting that in the early phase of EC adhesion, the signaling pathway activated by CD93 does not affect Cdc42 activity. Importantly and in accordance with previous data on mouse fibroblasts [22], RhoA activity was concentrated in a narrow band at the cell edge of control cells (Figure 5a, sh-unr), whereas the lack of CD93 induced a statistically significant increase in RhoA activation at the cell edge of spreading ECs (Figure 5a, quantified in Figure 5b). Collectively, these results suggest that CD93, by modulating the activation of Rac1 and RhoA, controls the actin cytoskeleton dynamics necessary for a coordinated adhesion of ECs to the ECM.

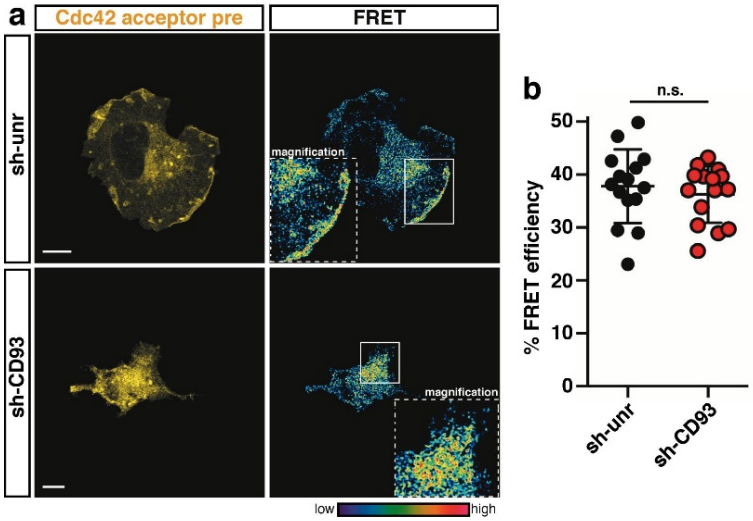

Figure 4. Cdc42 is not modulated by CD93 at the cell edge of adhering ECs. (**a**) FRET analysis on control (sh-unr) or CD93-silenced (sh-CD93) HUVECs transduced with a lentiviral construct expressing the Cdc42 biosensor. Cells were fixed at the early phase of adhesion to the ECM. Representative confocal images of transduced cells before photobleaching (acceptor pre) are shown. Rectangles indicate the photobleached cell area. Magnifications of the photobleached area are shown (1.6× sh-unr; 2.5× sh-CD93). The colored scale represents the color range of FRET efficiency. Scale bars, 10 µm. (**b**) Graph showing the fluorescence increase (% FRET efficiency) upon photobleaching at the cell edge of early spreading ECs (n = 15 cells for sh-unr and n = 15 cells for sh-CD93). Data are presented as scatter plot. n.s., not significant; Student t-test.

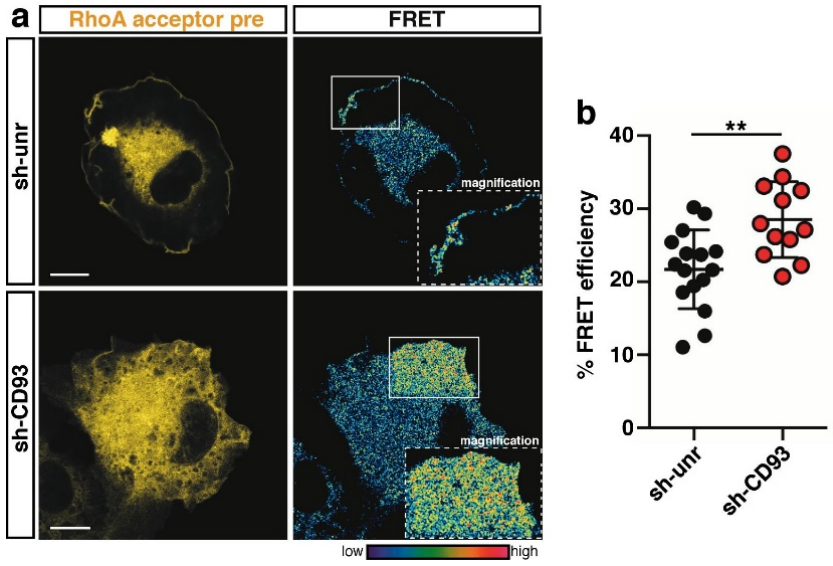

Figure 5. CD93 modulates RhoA activation at the cell edge of spreading ECs. (**a**) FRET analysis on control (sh-unr) or CD93-silenced (sh-CD93) HUVECs transduced with a lentiviral construct expressing the RhoA biosensor. Cells were fixed at the early phase of adhesion to the ECM. Representative confocal images of transduced cells before photobleaching (acceptor pre) are shown. Rectangles indicate the photobleached cell area. Magnifications of the photobleached area are shown (1.8× sh-unr; 1.5× sh-CD93). The colored scale represents the color range of FRET efficiency. Scale bars, 10 µm. (**b**) Plot showing the fluorescence increase (% FRET efficiency) upon photobleaching at the cell edge of early spreading ECs (n = 16 cells for sh-unr and n = 12 cells for sh-CD93). Data are presented as scatter plot. ** $p < 0.01$; Student t-test.

3. Discussion

The adhesion of ECs to the ECM plays a critical role in modulating essential cellular functions such as migration, proliferation, and survival, via the activation of a complex network of intracellular signaling pathways. Hence, elucidating the signaling pathways that manage EC adhesion to the ECM may help to understand the physiology of angiogenesis-dependent diseases, offering the opportunity to unveil novel antiangiogenic targets. In the present work, we show that, similarly to what has been observed in migrating ECs [16], the transmembrane protein CD93 activates a signaling cascade involving Rac1 and RhoA small GTPases to control cytoskeletal movements responsible for EC spreading. This appears particularly interesting in view of the fact that, differently from quiescent blood vessels, CD93 is mainly expressed in ECs of growing new blood vessels in different types of neovascular pathologies [5,7,23].

Integrins are transmembrane proteins essential in mediating cellular responses downstream of ECM engagement [24]. Importantly, it has been shown that the binding of CD93 to the ECM promotes β1 integrin activation and activated integrins regulate Src activation [8,25], which is the protein kinase involved in the phosphorylation of the CD93 cytotail [9]. Consistent with these observations, we demonstrate that in spreading ECs, the activation and localization of Src on the cell edge depends on CD93 expression, suggesting that CD93 itself promotes the phosphorylation of its cytoplasmic domain via an integrin/Src signaling axis, which generates consensus sequences for the binding of the adaptor protein Cbl [9]. Of note, we show that the phosphorylation of Cbl on tyrosine 774 is also dependent on SFK activity, suggesting that the activation of Rho GTPases in adhesion signaling involves extensive crosstalk between integrins and Src kinases [26].

Adaptor proteins are crucial components of the signaling pathways and link activated receptors to specific downstream signals. We have previously shown that the CD93-dependent phosphorylation of Cbl on tyrosine 774, a protein modification associated with actin remodeling and enhancement of cell adhesion [27], is essential to promote EC ahesion [9]. Accordingly, we show that CD93 drives the reorganization of the actin cytoskeleton by controlling the proper localization of pY774-Cbl and its binding partner Crk on the cell edge of spreading ECs and by transducing intracellular signals similar to those observed in motile ECs [16], thus reinforcing the notion that cell adhesion and migration are tightly connected processes [28].

Rac1 activation and RhoA inhibition are specific characteristics of the early cell adhesion phase [17]. The use of FRET-based biosensors allowed us to investigate the activation of the Rho proteins in early spreading ECs, demonstrating a clear role for CD93 in the regulation of the spatially modulated activity of these molecules. It has been shown that Rac1 and RhoA are mutually inhibitory, and higher RhoA activity is localized in a narrow band at the cell border of migrating cells [16,22]. Consistent with these requirements, we show that RhoA activity exhibits the same sharp localization at the cell edge of control spreading ECs, but the loss of CD93 associates with a broadened cell area with increased RhoA activity and a consequent decreased of Rac1 activation at the cell edge, suggesting that the crosstalk between Rac1 and RhoA is crucial for the regulation of early adhesion events in ECs. Interestingly, elevated RhoA activity may suppress Rac1 activity and lamellipodium formation both via the activation of FilGAP, which is a Rac GTPase-activating protein, and via the restriction of the interaction between Rac1 and its guanine nucleotide exchange factor (GEF) β-Pix [29,30]. However, since the fine balance that exists between the opposing activities of Rac1 and RhoA is dictated by the spatiotemporal activation of several specific GAPs and GEFs, more work is required to understand how Rho-proteins signal to control specific phases of adhesion and spreading in ECs [17].

Angiogenesis is largely regulated by a finely tuned integration of external cues, which are integrated by ECs. Although speculative, we propose a molecular mechanism of how ECs attach and spread on ECM. When cells adhere on the substrate, they derive spatial cues from integrin signaling, which induces Src activation. At the same time, CD93 interacts with the ECM and promotes integrin activation, which leads to Src-dependent

phosphorylation of the CD93 cytoplasmic domain. Phosphorylated CD93 recruits Cbl, which in turn undergoes SFK-dependent phosphorylation at tyrosine 774, generating a binding site for Crk and a signaling cascade for the reorganization of the actin cytoskeleton by modulating the Rho GTPases activity. In conclusion, this study sheds light into the understanding of the intricate molecular pathways activated by the microenvironment and translated by CD93 into actin dynamics during the adhesion process.

4. Materials and Methods

4.1. DNA Constructs and RNA Interference

The following plasmids were purchased from Addgene (Watertown, MA, USA): a lentiviral negative control vector containing scrambled shRNA (#1864, sh-unr) [31]; Rac1 generation fluorescence resonance energy transfer (FRET) biosensor for lentivirus production (#66111, pLenti-Rac1-2G) [32]; FRET-based biosensor reporting on Cdc42 activation (#68813, pLenti-Cdc42-2G) [33]; RhoA second-generation FRET biosensor for lentivirus production (#40179, pLenti-RhoA-2G) [34].

shRNA-mediated knockdown of CD93 was performed as previously outlined [4] by using a pLKO.1 retroviral vector from the Mission shRNA Library (Merck KGaA, Darmstadt, Germany), which expresses a shRNA (clone TRCN0000029085) specific for the silencing of the human protein. Recombinant lentiviral particles were produced and used for infection experiments as earlier described [35].

4.2. Cell Culture

HUVECs from single donors were purchased from PromoCell (Heidelberg, Germany) and grown on gelatin-coated plates in Endothelial Cell Basal Medium (EBM-MV2) with supplements (PromoCell) as previously described [35]. For lentivirus production, human Lenti-X 293T cells (Takara Bio Inc, Kusatsu, Japan) were grown in DMEM containing 10% FBS and 1 mM sodium butyrate (Merck KGaA), which increases the viral titer [36]. To detach cells from the culture plate by the non-enzymatic method, growing cells were washed thrice with PBS, incubated with Cell Dissociation Solution Non-enzymatic (Merck KGaA) for 5 min at 37 °C, collected in M199 medium supplemented with 10% FBS, centrifuged, and resuspended in fresh culture medium.

4.3. Antibodies and Reagents

The following primary antibodies were used: mouse monoclonal anti-CD93 (clone 4E1) [4]; rabbit anti-phospho-Cbl(Tyr774) (04-334) and mouse anti-β-actin (A2228, Merck KGaA); mouse anti-Cbl (sc-1651) and normal mouse IgG (sc-2025, Santa Cruz Biotechnology, Dallas, TX, USA); rabbit anti-Src (32G6) and rabbit anti-phospho-Src(Tyr416) (D49G4, Cell Signaling Technology, Danvers, MA, USA).

The Src family tyrosine kinase inhibitor PP2 was purchased from Merck KGaA.

4.4. Western Blotting Analyses

Immunoblotting experiments were performed as previously described [37]. To compare protein levels of different samples, densitometric analysis was performed using the gel analyzer tool of ImageJ2.

4.5. Immunofluorescent and FRET Analyses

Acquisition of fluorescent images and FRET experiments were carried out using a Leica TCS SP5 AOBS confocal laser-scanning microscope, following the TCS SP5 and FRET AB manufacturer's software. A Leica HC PL APO 63x/1.40 Oil CS2 objective was used for the acquisition of cell images and FRET analyses. A diode laser and argon laser were used to excite fluorochromes and fluorescent molecules at the optimal wavelength ranging from 405 to 647 nm, and images (1024 × 1024 pixel resolution) were acquired at a scan speed of 400 Hz image lines/sec. Confocal scanner configuration was set as follows: pinhole at 1.0 Airy diameter and line averaging function at 4.

For immunofluorescent staining, cells were fixed in 3% paraformaldehyde and treated as previously described [35]. The secondary appropriate antibodies were conjugated with Alexa Fluor-488 or -568 (Thermo Fisher Scientific, Waltham, MA, USA). F-actin staining was performed with Alexa Fluor-647 phalloidin (Thermo Fisher Scientific). To show colocalization events by white dots, images were generated using ImageJ2 and the Colocalization plug-in. To quantify protein levels at the cell border, an area of 5 µm distance from the cell edge was chosen, and images were analyzed using ImageJ2.

FRET acceptor photobleaching (apFRET) analyses were carried out on control or CD93-silenced HUVECs transduced with genetically encoded biosensors expressing RhoGTPases Rac1 (pLenti-Rac1-2G), Cdc42 (pLenti-Cdc42-2G), or RhoA (pLenti-RhoA-2G). Transduced cells were detached from the plate, resuspended in complete growth medium, plated on the substrate, fixed at early phases of spreading (from 30 to 40 min), and analyzed. Acquisition parameters were modified only in the pinhole diameter at 2.0 Airy units. Argon laser lines 458 nm and 514 nm were used to excite mTFP1 and mVenus fluorophores, which represent the donor and the acceptor, respectively. For proper image recording, hybrid detectors HyD were employed by gating a spectral acquisition window of 468–502 nm for the donor and 524–600 nm for the acceptor. In the photobleaching procedure, cells were bleached using the 514 nm argon laser beam at 100% intensity until the acceptor was photobleached down to about 10% of its initial value. FRET analysis was performed using ImageJ2, and the FRETcalc plug-in and FRET efficiency was calculated as previously described [38,39].

4.6. Statistical Analysis

Data analyses were performed using Prism statistical software (GraphPad, San Diego, CA, USA), and the values represent the mean ± SD obtained from at least three independent experiments. A normality test was performed using the D'Agostino & Pearson normality test. The statistical significance of the differences between two groups was determined using the two-tailed Student *t*-test for normally distributed values or the Mann–Whitney *U* test when the values were irregularly distributed. All *p*-values shown were two-tailed, and $p < 0.05$ was considered statistically significant.

Author Contributions: Conceptualization, S.B. and M.O.; methodology, S.B.; validation, F.G. and M.O.; investigation, S.B., L.R. and R.L.; resources, G.M.T., A.D. and A.S.; data curation, S.B. and M.O.; writing—original draft preparation, S.B. and M.O.; writing—review and editing, G.M.T., A.D., F.G. and A.S.; visualization, M.O.; supervision, M.O.; funding acquisition, G.M.T., A.D., F.G., A.S. and M.O. All authors have read and agreed to the published version of the manuscript.

Funding: This research was partially funded by MIUR, grant Dipartimento di Eccellenza 2018–2022 number L.232,11-12-16; Tuscany Region (Bando Regionale Ricerca Salute 2018—MAGIC) number D78D20000910002; Swedish Cancer Society number CAN 2017/502, 20 1008 PjF; and Swedish Research Council number Dnr 2016-02495, 2020-02563.

Institutional Review Board Statement: Not applicable.

Informed Consent Statement: Not applicable.

Acknowledgments: We thank Alessia Pedalina for her excellent technical assistance.

Conflicts of Interest: The authors declare no conflict of interest. The funders had no role in the design of the study; in the collection, analyses, or interpretation of data; in the writing of the manuscript, or in the decision to publish the results.

References

1. De Palma, M.; Biziato, D.; Petrova, T.V. Microenvironmental regulation of tumour angiogenesis. *Nat. Rev. Cancer* **2017**, *17*, 457–474. [CrossRef] [PubMed]
2. Lamalice, L.; Le Boeuf, F.; Huot, J. Endothelial cell migration during angiogenesis. *Circ. Res.* **2007**, *100*, 782–794. [CrossRef]
3. Schmidt, S.; Friedl, P. Interstitial cell migration: Integrin-dependent and alternative adhesion mechanisms. *Cell Tissue Res.* **2010**, *339*, 83–92. [CrossRef] [PubMed]

4. Orlandini, M.; Galvagni, F.; Bardelli, M.; Rocchigiani, M.; Lentucci, C.; Anselmi, F.; Zippo, A.; Bini, L.; Oliviero, S. The characterization of a novel monoclonal antibody against CD93 unveils a new antiangiogenic target. *Oncotarget* **2014**, *5*, 2750–2760. [CrossRef]
5. Langenkamp, E.; Zhang, L.; Lugano, R.; Huang, H.; Elhassan, T.E.A.; Georganaki, M.; Bazzar, W.; Lööf, J.; Trendelenburg, G.; Essand, M.; et al. Elevated expression of the C-type lectin CD93 in the glioblastoma vasculature regulates cytoskeletal rearrangements that enhance vessel function and reduce host survival. *Cancer Res.* **2015**, *75*, 4504–4516. [CrossRef]
6. Khan, K.A.; McMurray, J.L.; Mohammed, F.; Bicknell, R. C-type lectin domain group 14 proteins in vascular biology, cancer and inflammation. *FEBS J.* **2019**, *286*, 3299–3332. [CrossRef]
7. Galvagni, F.; Nardi, F.; Spiga, O.; Trezza, A.; Tarticchio, G.; Pellicani, R.; Andreuzzi, E.; Caldi, E.; Toti, P.; Tosi, G.M.; et al. Dissecting the CD93-Multimerin 2 interaction involved in cell adhesion and migration of the activated endothelium. *Matrix Biol.* **2017**, *64*, 112–127. [CrossRef] [PubMed]
8. Lugano, R.; Vemuri, K.; Yu, D.; Bergqvist, M.; Smits, A.; Essand, M.; Johansson, S.; Dejana, E.; Dimberg, A. CD93 promotes β1 integrin activation and fibronectin fibrillogenesis during tumor angiogenesis. *J. Clin. Investig.* **2018**, *128*, 3280–3297. [CrossRef]
9. Galvagni, F.; Nardi, F.; Maida, M.; Bernardini, G.; Vannuccini, S.; Petraglia, F.; Santucci, A.; Orlandini, M. CD93 and dystroglycan cooperation in human endothelial cell adhesion and migration. *Oncotarget* **2016**, *7*, 10090–10103. [CrossRef]
10. Hosokawa, H.; Ninomiya, H.; Kitamura, Y.; Fujiwara, K.; Masaki, T. Vascular endothelial cells that express dystroglycan are involved in angiogenesis. *J. Cell Sci.* **2002**, *115*, 1487–1496. [CrossRef] [PubMed]
11. Pellicani, R.; Poletto, E.; Andreuzzi, E.; Paulitti, A.; Doliana, R.; Bizzotto, D.; Braghetta, P.; Colladel, R.; Tarticchio, G.; Sabatelli, P.; et al. Multimerin-2 maintains vascular stability and permeability. *Matrix Biol.* **2020**, *87*, 11–25. [CrossRef]
12. Tosi, G.M.; Neri, G.; Barbera, S.; Mundo, L.; Parolini, B.; Lazzi, S.; Lugano, R.; Poletto, E.; Leoncini, L.; Pertile, G.; et al. The binding of CD93 to Multimerin-2 promotes choroidal neovascularization. *Investig. Ophthalmol. Vis. Sci.* **2020**, *61*, 30. [CrossRef] [PubMed]
13. Sun, Y.; Chen, W.; Torphy, R.J.; Yao, S.; Zhu, G.; Lin, R.; Lugano, R.; Miller, E.N.; Fujiwara, Y.; Bian, L.; et al. Blockade of the CD93 pathway normalizes tumor vasculature to facilitate drug delivery and immunotherapy. *Sci. Transl. Med.* **2021**, *13*, eabc8922. [CrossRef] [PubMed]
14. Zhang, M.; Bohlson, S.S.; Dy, M.; Tenner, A.J. Modulated interaction of the ERM protein, moesin, with CD93. *Immunology* **2005**, *115*, 63–73. [CrossRef] [PubMed]
15. Barbera, S.; Nardi, F.; Elia, I.; Realini, G.; Lugano, R.; Santucci, A.; Tosi, G.M.; Dimberg, A.; Galvagni, F.; Orlandini, M. The small GTPase Rab5c is a key regulator of trafficking of the CD93/Multimerin-2/β1 integrin complex in endothelial cell adhesion and migration. *Cell Commun. Signal.* **2019**, *17*, 55. [CrossRef]
16. Barbera, S.; Lugano, R.; Pedalina, A.; Mongiat, M.; Santucci, A.; Tosi, G.M.; Dimberg, A.; Galvagni, F.; Orlandini, M. The C-type lectin CD93 controls endothelial cell migration via activation of the Rho family of small GTPases. *Matrix Biol.* **2021**, *99*, 1–17. [CrossRef]
17. Lawson, C.D.; Burridge, K. The on-off relationship of Rho and Rac during integrin-mediated adhesion and cell migration. *Small GTPases* **2014**, *5*, e27958. [CrossRef]
18. Kraynov, V.S.; Chamberlain, C.; Bokoch, G.M.; Schwartz, M.A.; Slabaugh, S.; Hahn, K.M. Localized Rac activation dynamics visualized in living cells. *Science* **2000**, *290*, 333–337. [CrossRef]
19. Nalbant, P.; Hodgson, L.; Kraynov, V.; Toutchkine, A.; Hahn, K.M. Activation of endogenous Cdc42 visualized in living cells. *Science* **2004**, *305*, 1615–1619. [CrossRef]
20. Pertz, O.; Hodgson, L.; Klemke, R.L.; Hahn, K.M. Spatiotemporal dynamics of RhoA activity in migrating cells. *Nature* **2006**, *440*, 1069–1072. [CrossRef]
21. Mack, N.A.; Georgiou, M. The interdependence of the Rho GTPases and apicobasal cell polarity. *Small GTPases* **2014**, *5*, 10. [CrossRef] [PubMed]
22. Machacek, M.; Hodgson, L.; Welch, C.; Elliott, H.; Pertz, O.; Nalbant, P.; Abell, A.; Johnson, G.L.; Hahn, K.M.; Danuser, G. Coordination of Rho GTPase activities during cell protrusion. *Nature* **2009**, *461*, 99–103. [CrossRef]
23. Tosi, G.M.; Caldi, E.; Parolini, B.; Toti, P.; Neri, G.; Nardi, F.; Traversi, C.; Cevenini, G.; Marigliani, D.; Nuti, E.; et al. CD93 as a potential target in neovascular age-related macular degeneration. *J. Cell. Physiol.* **2017**, *232*, 1767–1773. [CrossRef] [PubMed]
24. Hynes, R.O. Integrins: Bidirectional, allosteric signaling machines. *Cell* **2002**, *110*, 673–687. [CrossRef]
25. Pugacheva, E.N.; Roegiers, F.; Golemis, E.A. Interdependence of cell attachment and cell cycle signaling. *Curr. Opin. Cell Biol.* **2006**, *18*, 507–515. [CrossRef]
26. Huveneers, S.; Danen, E.H.J. Adhesion signaling—Crosstalk between integrins, Src and Rho. *J. Cell Sci.* **2009**, *122*, 1059–1069. [CrossRef]
27. Lee, H.; Tsygankov, A.Y. Cbl-family proteins as regulators of cytoskeleton-dependent phenomena. *J. Cell. Physiol.* **2013**, *228*, 2285–2293. [CrossRef]
28. Vicente-Manzanares, M.; Choi, C.K.; Horwitz, A.R. Integrins in cell migration–the actin connection. *J. Cell Sci.* **2009**, *122*, 199–206. [CrossRef]
29. Shifrin, Y.; Arora, P.D.; Ohta, Y.; Calderwood, D.A.; McCulloch, C.A. The role of FilGAP-filamin A interactions in mechanoprotection. *Mol. Biol. Cell* **2009**, *20*, 1269–1279. [CrossRef] [PubMed]

30. Kuo, J.-C.; Han, X.; Hsiao, C.-T.; Yates Iii, J.R.; Waterman, C.M. Analysis of the myosin-II-responsive focal adhesion proteome reveals a role for β-Pix in negative regulation of focal adhesion maturation. *Nat. Cell Biol.* **2011**, *13*, 383–393. [CrossRef]
31. Sarbassov, D.D.; Guertin, D.A.; Ali, S.M.; Sabatini, D.M. Phosphorylation and regulation of Akt/PKB by the rictor-mTOR complex. *Science* **2005**, *307*, 1098–1101. [CrossRef]
32. Fritz, R.D.; Menshykau, D.; Martin, K.; Reimann, A.; Pontelli, V.; Pertz, O. SrGAP2-dependent integration of membrane geometry and Slit-Robo-repulsive cues regulates fibroblast contact inhibition of locomotion. *Dev. Cell* **2015**, *35*, 78–92. [CrossRef]
33. Martin, K.; Reimann, A.; Fritz, R.D.; Ryu, H.; Jeon, N.L.; Pertz, O. Spatio-temporal co-ordination of RhoA, Rac1 and Cdc42 activation during prototypical edge protrusion and retraction dynamics. *Sci. Rep.* **2016**, *6*, 21901. [CrossRef]
34. Fritz, R.D.; Letzelter, M.; Reimann, A.; Martin, K.; Fusco, L.; Ritsma, L.; Ponsioen, B.; Fluri, E.; Schulte-Merker, S.; van Rheenen, J.; et al. A versatile toolkit to produce sensitive FRET biosensors to visualize signaling in time and space. *Sci. Signal.* **2013**, *6*, rs12. [CrossRef] [PubMed]
35. Orlandini, M.; Nucciotti, S.; Galvagni, F.; Bardelli, M.; Rocchigiani, M.; Petraglia, F.; Oliviero, S. Morphogenesis of human endothelial cells is inhibited by DAB2 via Src. *FEBS Lett.* **2008**, *582*, 2542–2548. [CrossRef] [PubMed]
36. Cribbs, A.P.; Kennedy, A.; Gregory, B.; Brennan, F.M. Simplified production and concentration of lentiviral vectors to achieve high transduction in primary human T cells. *BMC Biotechnol.* **2013**, *13*, 98. [CrossRef]
37. Galvagni, F.; Anselmi, F.; Salameh, A.; Orlandini, M.; Rocchigiani, M.; Oliviero, S. Vascular endothelial growth factor receptor-3 activity is modulated by its association with caveolin-1 on endothelial membrane. *Biochemistry* **2007**, *46*, 3998–4005. [CrossRef] [PubMed]
38. Stepensky, D. FRETcalc plugin for calculation of FRET in non-continuous intracellular compartments. *Biochem. Biophys. Res. Commun.* **2007**, *359*, 752–758. [CrossRef]
39. Boscher, C.; Gaonac'h-Lovejoy, V.; Delisle, C.; Gratton, J.-P. Polarization and sprouting of endothelial cells by angiopoietin-1 require PAK2 and paxillin-dependent Cdc42 activation. *Mol. Biol. Cell* **2019**, *30*, 2227–2239. [CrossRef] [PubMed]

3.2 Introduction to article 3

In this article, we highlighted the importance of Rab5C in regulating the retrieving and recycling of CD93 and its interacting partners MMRN2 and the active form of integrin β1. Rab5C-depleted cells had reduced surface levels of both CD93 and active β1 integrin and showed less migratory capabilities compared to wild-type cells. Moreover, accordingly to the importance of the positively charged RKRR motif in the juxtamembrane region of CD93 important for Moesin binging and therefore connection with the actin cytoskeleton (Zhang et al., 2005), recombinant CD93 lacking the cytoplasmic tail failed to properly localize in the apical bud during cell spreading and at the plasma membrane in migrating ECs.

ARTICLE 3

Barbera et al. Cell Communication and Signaling (2019) 17:55
https://doi.org/10.1186/s12964-019-0375-x

Cell Communication and Signaling

RESEARCH Open Access

The small GTPase Rab5c is a key regulator of trafficking of the CD93/Multimerin-2/β1 integrin complex in endothelial cell adhesion and migration

Stefano Barbera[1], Federica Nardi[1], Ines Elia[1], Giulia Realini[1], Roberta Lugano[2], Annalisa Santucci[1], Gian Marco Tosi[3], Anna Dimberg[2], Federico Galvagni[1*] and Maurizio Orlandini[1*]

Abstract

Background: In the endothelium, the single-pass membrane protein CD93, through its interaction with the extracellular matrix protein Multimerin-2, activates signaling pathways that are critical for vascular development and angiogenesis. Trafficking of adhesion molecules through endosomal compartments modulates their signaling output. However, the mechanistic basis coordinating CD93 recycling and its implications for endothelial cell (EC) function remain elusive.

Methods: Human umbilical vein ECs (HUVECs) and human dermal blood ECs (HDBEC) were used in this study. Fluorescence confocal microscopy was employed to follow CD93 retrieval, recycling, and protein colocalization in spreading cells. To better define CD93 trafficking, drug treatments and transfected chimeric wild type and mutant CD93 proteins were used. The scratch assay was used to evaluate cell migration. Gene silencing strategies, flow citometry, and quantification of migratory capability were used to determine the role of Rab5c during CD93 recycling to the cell surface.

Results: Here, we identify the recycling pathway of CD93 following EC adhesion and migration. We show that the cytoplasmic domain of CD93, by its interaction with Moesin and F-actin, is instrumental for CD93 retrieval in adhering and migrating cells and that aberrant endosomal trafficking of CD93 prevents its localization at the leading edge of migration. Moreover, the small GTPase Rab5c turns out to be a key component of the molecular machinery that is able to drive CD93 recycling to the EC surface. Finally, in the Rab5c endosomal compartment CD93 forms a complex with Multimerin-2 and active β1 integrin, which is recycled back to the basolaterally-polarized cell surface by clathrin-independent endocytosis.

Conclusions: Our findings, focusing on the pro-angiogenic receptor CD93, unveil the mechanisms of its polarized trafficking during EC adhesion and migration, opening novel therapeutic opportunities for angiogenic diseases.

Keywords: Cell polarity, Cell spreading, Moesin, C1qRp

* Correspondence: federico.galvagni@unisi.it; maurizio.orlandini@unisi.it
[1]Department of Biotechnology, Chemistry and Pharmacy, University of Siena, Via A. Moro, 2, 53100 Siena, Italy
Full list of author information is available at the end of the article

Background

Physiological processes such as development, wound healing, and growth are strictly dependent on vasculature dynamics and require angiogenesis, the branching of new blood vessels from pre-existing ones [1]. As a result, dysregulation of vessel growth has a strong impact on health and contributes to the etiopathogenesis of several disorders, including cancer progression, psoriasis, atherosclerosis, blindness, and infectious disease [2, 3]. Despite several promising drugs have been developed against the main molecules involved in angiogenesis, conventional anti-angiogenic therapies still need to resolve issues such as efficacy, resistance, and toxicity to give long-term meaningful outcomes [4]. Therefore, a better understanding of the mechanisms underlying angiogenesis is mandatory to intervene in pathological processes. Numerous efforts have been made to identify new biomarkers for anti-angiogenic therapy [5]. Recently, molecules belonging to the group XIV family of C-type lectin-like domain (CTLD)-containing proteins have been identified as potential anti-angiogenic targets [6, 7].

CD93 is a single-pass transmembrane protein, which, from the N- to C-terminus, consists of a CTLD domain, five EGF-like repeats, a mucin-like domain, a transmembrane domain, and a cytoplasmic domain. In the juxtamembrane region, CD93 contains a positively charged motif (RKRR), shared with other adhesion molecules, which harbors a binding site for the FERM domain of Moesin, a member of the Ezrin/Radixin/Moesin (ERM) family, involved in the regulation of membrane-cortex interactions and signaling [8, 9]. Since ERM proteins link membrane proteins to actin filaments [10], the interaction between CD93 and Moesin contributes to the reorganization of cytoskeleton, which is essential during cell adhesion and migration [11].

CD93 is predominantly expressed in endothelial cells (ECs) and several data are consistent with a role for CD93 as pro-angiogenic molecule in the vascular endothelium [6, 12–14]. Importantly, CD93 is highly expressed in hyperproliferative ECs of blood vessels within different cancer types and choroidal neovascular membranes of age-related macular degeneration patients [13, 15, 16]. In the activated endothelium, CD93 plays a dual role both operating as adhesion molecule and soluble growth factor [17]. As adhesion molecule, CD93 contributes to EC adhesion and migration through its interaction with Multimerin-2 (MMRN2), an endothelial-specific member of the EDEN family, consistently deposited in the extracellular environment of tumor vasculature [7, 16, 18]. Notably, in tumor angiogenesis the CD93-MMRN2 interaction is required for activation of β1 integrin and formation of a fibrillar fibronectin network [18], which is essential to promote angiogenesis through its continuous turn over and remodeling [19].

Adhesion receptors are endocytosed and recycled through the endosomal pathway and this can fine-tune their spatiotemporal signaling outputs [20]. Moreover, cell adhesion molecule turnover and sorting play a key role during dynamic processes such as cytokinesis, migration, angiogenesis and invasion [21–23] . Within such a framework, Rab GTPases are the major coordinators of endosomal trafficking and regulate vesicle budding, motility, and their tethering to the target compartment, also conferring transport specificity and organelle identity [24, 25]. Here, we investigate the trafficking of CD93 in dynamically active primary ECs to unveil its consequences in angiogenesis regulation. We show the retrieval and recycling of CD93 during EC spreading and migration, identify the cytoplasmic domain of CD93 as a key domain in the endosomal trafficking of CD93 and demonstrate the major role of Rab5c isoform in driving CD93 and β1 integrin delivering to the cell surface to support EC migration.

Methods

Cell culture and transfection

Human umbilical vein ECs (HUVECs) and human dermal blood ECs (HDBECs) were purchased from PromoCell (Heidelberg, Germany). Cells were grown on gelatin-coated plates as previously described [18, 26]. For spreading analyses, cells were detached from the culture plate by using enzyme-free cell dissociation buffer (Thermo Fisher Scientific, Waltham, MA, USA), plated on gelatin-coated coverslips, and allowed to spread for different times. Cells at specific phases of spreading were fixed, labeled, and imaged by microscopy. Transient transfection experiments were performed by electroporation as previously described [12].

DNA constructs

The chimeric construct expressing human CD93 fused to YFP was previously described [12]. The deletion mutant CD93ΔC (covering the amino acid residues from 1 to 604 of the human CD93 sequence) fused to YFP was obtained by PCR amplification of a cDNA clone corresponding to the human *CD93* gene, using the following oligonucleotides: 5′-GAGAATTCATGGCCACCTCCATGGG-3′ and 5′-GAGGATCCACCAGTAGCCCCAGAGCC-3′. PCR fragments were cloned into pEYFP-N1 vector (Clontech Labs, Fremont, CA, USA). The construct was confirmed by sequencing.

Reagents and antibodies

Latrunculin B (Calbiochem-Novabiochem Corp., San Diego, CA, USA) and nocodazole (Sigma-Aldrich, Saint Louis, MO, USA) were used as previously described to

disrupt actin and microtubule cytoskeleton integrity, respectively [27]. Cycloheximide (Sigma-Aldrich) was used to inhibit protein synthesis in HUVECs at the concentration of 50 μg/mL.

The following primary antibodies were used: mouse monoclonal anti-CD93 (mAb 4E1) [6], rabbit anti-MMRN2 (generously provided by M. Mongiat), rabbit anti-CD93 (HPA009300, Atlas Antibodies, Bromma, Sweden), mouse anti-CD93 (MBL International Corporation, Woburn, MA, USA), rabbit anti-Giantin, mouse anti-β1 integrin (12G10), and mouse anti-Rab7 (Abcam, Cambridge, UK), rabbit anti-Moesin (Cell Signaling Technology, Danvers, MA, USA), mouse anti-Rab5 (BD Biosciences, Franklin Lakes, NJ, USA), mouse anti-β-actin (Sigma-Aldrich), rabbit anti-CD93 (H-190), mouse anti-COPD (E-12), mouse anti-Sec31A (H-2), mouse anti-β-Adaptin (A-5), mouse anti-Rab5a (E-11), mouse anti-Rab5b (F-9), mouse anti-Rab5c (H-3), mouse anti-β1 integrin (4B7R), mouse anti-Rab11a (D-3), rabbit anti-caveolin-1 (N-20), and mouse anti-MMRN2 (H572) (Santa Cruz Biotechnology, Dallas, TX, USA). Alexa Fluor-488 and -647 phalloidin (Thermo Fisher Scientic) were used for F-actin labeling.

Immunofluorescence microscopy

Cells were seeded onto gelatin-coated glass coverslips, fixed in 3% paraformaldehyde, and treated as previously described [18, 28]. The secondary antibodies used were conjugated with Alexa Fluor-488 and Alexa Fluor-568 (Thermo Fisher Scientific). Fluorescent images were captured using a Leica TCS SP2 AOBS confocal laser-scanning microscope and overlaid images were produced. A Leica HCX PL APO lbd.BL 63x/1.40 oil objective was used. Fluorochromes and fluorescent proteins were excited at the optimal wavelength ranging from 458 nm to 633 nm and images (512 × 512 resolution) acquired at a scan speed of 400 Hz image lines/sec. Confocal scanner configuration was set as follows: pinhole at 1.0 Airy diameter and line averaging function at 4. To better dissect the labeled cellular structure, some cells were shown as lateral views, corresponding to single *xz* planes. These images were processed as previously described [27]. Cell distribution of exogenous CD93 proteins and protein localization at the migrating front were measured using NIS-Elements image analysis software (Nikon Instruments, Melville, NY, USA). For protein quantification at the migrating front, an area of 20 μm distance from the leading edge was chosen, and a minimum of 5 images of the migrating front area per condition were used. Similarly, exogenous CD93 was quantified in the migrating front area of single transfected cells. The quantitative colocalization analyses were performed pre-processing the images and using ImageJ 2.0 and the JACoP plug-in to determine Manders coefficients and Costes randomization values as previously described [29]. Costes *P* values ≥95% were considered as a colocalization signal. To show colocalization events by white dots, images were generated using ImageJ and the Colocalization plug-in.

RNA interference, immunoblotting analysis, and flow cytometry

Silencing experiments were performed using pLKO.1 retroviral vectors from the MISSION shRNA Library (Sigma-Aldrich) expressing specific shRNAs for human Rab5c (SHCLNG-NM_004583, clone TCRN0000380031, referred to as 31; clone TCRN0000072933, referred to as 33) and human CD93 (clone TRCN0000029085) [6]. Recombinant lentiviruses were produced and used for infection experiments as previously described [28]. Immunoblotting experiments were performed as previously described [30]. Flow cytometry analysis was performed as previously described with slight modifications [31]. Briefly, living cells were detached from the culture plate using enzyme-free cell dissociation buffer, incubated with an anti-CD93 (mAb 4E1) antibody followed by an anti-mouse Alexa Fluor 488-conjugated secondary antibody, and analyzed on GUAVA flow cytometer (Merck Millipore, Burlington, MA, USA).

Wound healing assay

The scratch test was performed as previously described with slight modifications [16]. Briefly, transfected or lentivirus transduced HUVECs were seeded on glass coverslips in a 24-well plate and cultured until they reached confluency. A straight scratch was created in the monolayer using a sterile pipette tip. The cultures were washed with PBS and grown in complete medium. Bright-field images were captured using an inverted microscope equipped with a digital camera. For each condition, images were acquired at three different positions along the scratch and a representative field was shown. For immunofluorescence analysis, after the scratch cells were washed with PBS, grown in complete medium for 5 h, fixed in 3% paraformaldehyde, and subjected to immunofluorescence analysis.

Statistical analysis

In this study, the data analysis was performed using Prism 6 software (Graphpad Software, La Jolla, CA, USA). Differences between samples were estimated using the two-tailed student's *t*-test or 2-way ANOVA followed by Dunnett's test. Values were expressed as the mean ± SD and $P < 0.05$ was considered statistically significant.

Results

In early spreading ECs, CD93 is channeled to the actin-rich apical bud

During the early phases of EC adhesion, the cooperation between F-actin and Moesin leads to the assembly of an actin-rich apical domain (also known as apical bud or apical membrane insertion site) that drives apical-basolateral polarization [27, 32]. Since Moesin orchestrates cytoskeletal remodeling and links transmembrane CD93 to the actin cytoskeleton [11], we questioned whether the localization of CD93 was polarized during spreading of human primary ECs. To address this issue, exponentially growing HUVECs were detached from the plate, allowed to adhere on the substrate, and analyzed by immunofluorescence. Interestingly, at early degrees of cell spreading CD93 showed a pattern of localization similar to Moesin, being mainly confined into the apical bud and colocalizing with F-actin (Fig. 1, upper panels). Moreover, CD93 was also localized in small vesicles clustered directly beneath the apical bud (Fig. 1, upper panels), which in turn colocalized with caveolin-1 (Additional file 1: Figure S1), a key player in promoting EC polarization [33]. To assess whether such distribution depended on F-actin, ECs were let to settle on the substrate in the presence of latrunculin B, which disrupts microfilament organization. Consistent with our previous findings [27], disruption of the F-actin cytoskeleton resulted in the impairment of apical bud structure, thus hampering cell polarity and eliciting a random distribution of CD93 throughout the adhering cell (Fig. 1, lower panels).

Next, to better explore the trafficking of CD93 in spreading cells, HUVECs were transfected with an expression vector encoding wild type CD93 fused with YFP at its C-terminus [12]. Fluorescent confocal microscopy was employed to analyze cells fixed at different stages of cell flattening against the substrate. The tagged wild type protein behaved as the endogenous CD93 and it resulted localized to the apical bud (Fig. 2a, 5 min). Importantly, confocal microscopy analysis at increasing times of cell spreading showed that small vesicles containing CD93-YFP moved from the apical bud towards the middle of the cell (Fig. 2a, 10 min, 15 min, and 20 min, quantified in Fig. 2b). This localization was further corroborated by confocal *xz* scans that created a cross-sectional view through a spreading cell (Fig. 2c). Since the cytoplasmic domain of CD93 interacts with the FERM domain of Moesin [11], we questioned whether the cytoplasmic domain was involved in the apical bud localization of CD93. To address this possibility, we generated a YFP-tagged CD93 deletion mutant (CD93ΔC-YFP) lacking the cytoplasmic tail and transfected it into HUVECs (Fig. 2d). Imaging of cells fixed at early attachment stages showed that CD93ΔC-YFP was diffusely distributed throughout the cytoplasm and the small vesicles containing the deletion mutant were not polarized (Fig. 2e). These observations were further substantiated by quantitative analysis of exogenous CD93 and CD93ΔC levels in the apical bud and cytoplasm of early spreading cells (Fig. 2f). Taken together, these findings indicate that in ECs undergoing early spreading, the cytoplasmic domain of CD93 through interaction with Moesin and F-actin drives the localization of CD93 to the polarizing apical bud and its endocytic movements towards the middle of the cell.

F-actin is involved in the endocytic trafficking of CD93

As EC flattening against the substrate increased, we observed the appearance of numerous, large and round-shape CD93-positive ($CD93^{+ve}$) vesicles arranged in the perinuclear region (Fig. 3a). Of note, also in spreading

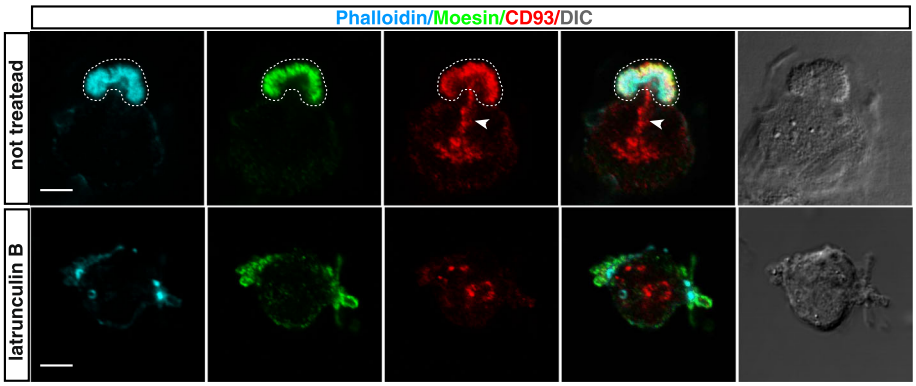

Fig. 1 During the initial phases of spreading, CD93 is sorted towards the actin-rich apical bud. HUVECs were pretreated or not for 30 min with latrunculin B, then they were detached from the plate, resuspended in complete growth medium, and plated on the substrate in the presence or not of latrunculin B. 5 min after plating, cells were fixed and analyzed by immunofluorescence using phalloidin, anti-Moesin, and anti-CD93 antibodies. The apical bud is delimited by a dotted line. Arrowheads indicate small vesicles beneath the apical bud. Differential interference contrast (DIC) images of stained cells are shown. Scale bars represent 5 μm

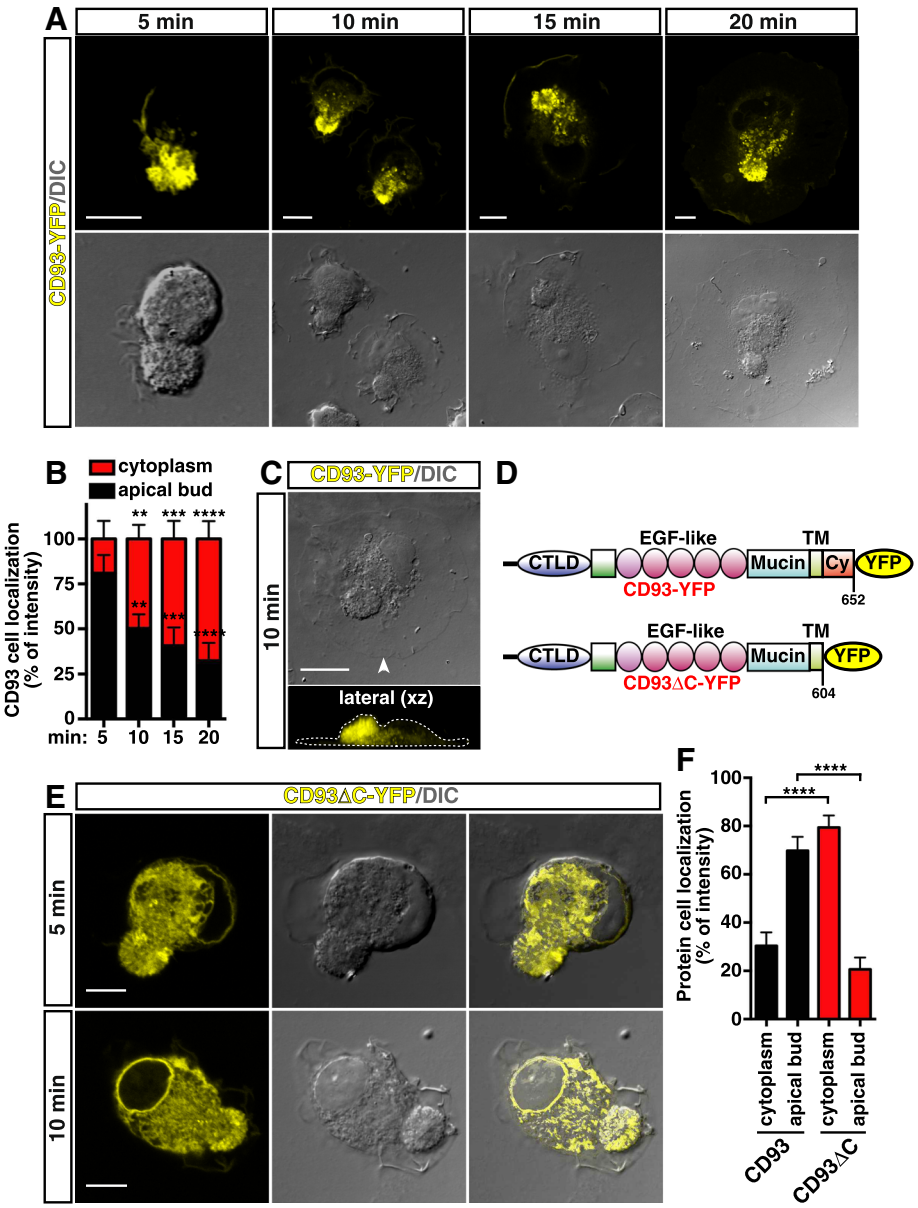

Fig. 2 Retrieval of CD93 is regulated through its cytoplasmic domain. **a**: Time course image analysis of CD93 localization during cell spreading. CD93-YFP was transiently transfected into HUVECs. Cells were detached from the plate, resuspended in complete growth medium, plated on the substrate, and fixed at different spreading times as indicated. Exogenous CD93 was imaged as yellow. Scale bars, 10 μm. **b**: Quantification of exogenous CD93 levels in the apical bud and cytoplasm of ECs treated as in **a**. Bars represent the percentage of total fluorescence intensity/area. Data are presented as the mean/cell ± SD of three independent experiments ($n = 3$ cells per group). $^{**}P < 0.01$, $^{***}P < 0.001$, $^{****}P < 0.0001$ vs. 5 min; 2-way ANOVA with Dunnett's post-test. **c**: Periodic *z*-series of cells treated as in **a** were acquired at 10 min after plating to generate a vertical section (lateral *xz*, 90 *z*-sections of 115 nm each). The corresponding cell boundary is indicated by a dotted line. An arrowhead indicates the point of view of the lateral *xz* image. Scale bar, 15 μm. **d**: The schematic diagram illustrates CD93 wild type (CD93-YFP) and the deletion mutant (CD93ΔC-YFP) lacking the cytoplasmic domain fused with YFP. The deleted amino acid residues are indicated. CTLD, C-type lectin-like domain; EGF-like, Epidermal Growth Factor repeats; Mucin, Mucin-like domain; TM, transmembrane domain; Cy, cytoplasmic domain. **e**: CD93ΔC-YFP deletion mutant was transiently transfected into HUVECs. Cells were detached from the plate, resuspended in complete growth medium, plated on the substrate, and fixed at early phases of spreading (from 5 to 10 min). Exogenous CD93ΔC-YFP was imaged as yellow. Scale bars, 8 μm. Merged and DIC images are shown. **f**: Quantification of exogenous wild type and mutant CD93 levels in the apical bud and cytoplasm of transfected cells as in **a** and **e**. Bars represent the percentage of total fluorescence intensity/area. Data are presented as the mean/cell ± SD of three independent experiments ($n = 15$ cells per group). $^{****}P < 0.0001$; unpaired *t*-test

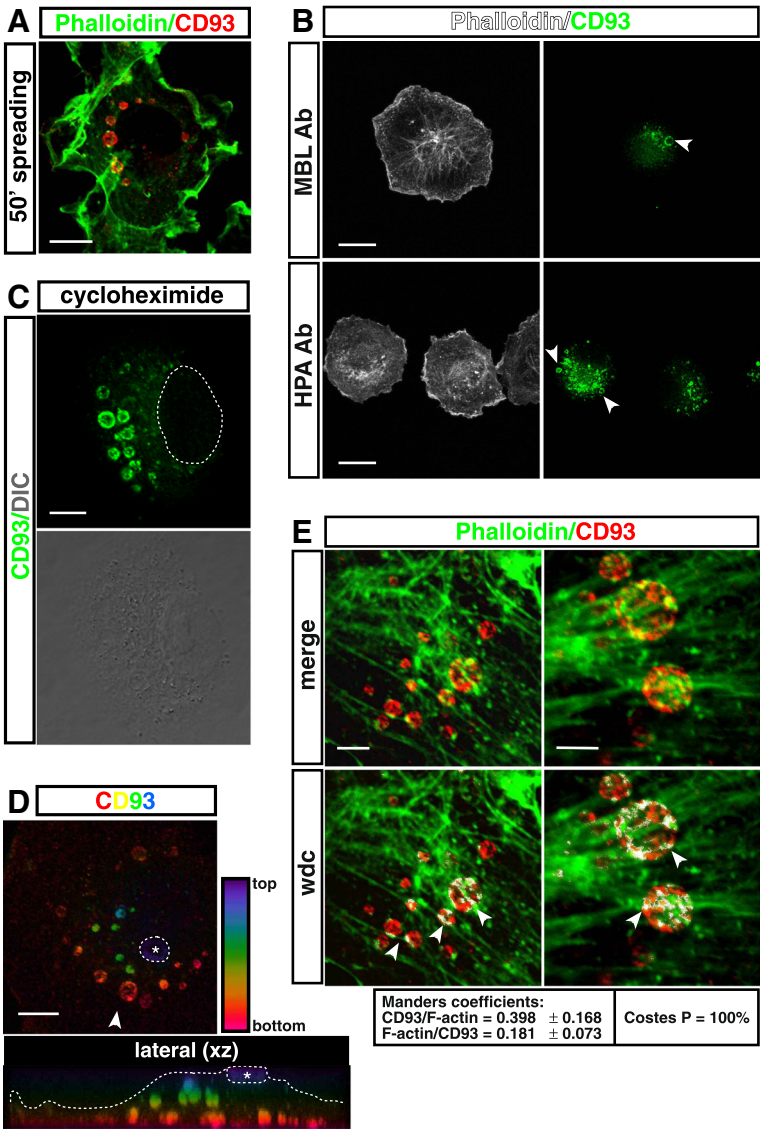

Fig. 3 CD93 is recycled via large vesicles moving along F-actin cables. **a**: Exponentially growing HUVECs were detached from the plate, resuspended in complete growth medium, plated on the substrate, and fixed at late phases of spreading (from 30 to 50 min). Cells were analyzed by immunofluorescence using phalloidin and an anti-CD93 (4E1) antibody. Scale bar, 11 μm. **b**: Exponentially growing HDBECs were treated as in **a**. Cells were analyzed by immunofluorescence using phalloidin and two different anti-CD93 antibodies as indicated. Arrowheads indicate $CD93^{+ve}$ vesicles. Images were acquired using a Leica SP8 confocal microscope equipped with Leica White Light Laser, notch filters (488 nm, 568 nm, and 647 nm) and a HC PL APO CS2 63x/1.40 oil objective. Images were taken in 1024 × 1024 format, speed 400 Hz, and pinhole set at 1.0 Airy diameter. Scale bars, 20 μm. **c**: HUVECs were pretreated for 4 h with 50 μg/mL cycloheximide, then they were detached from the plate, resuspended in complete growth medium, and plated on the substrate in the presence of cycloheximide. Cells were analyzed by immunofluorescence at late phases of spreading using anti-CD93 antibodies. DIC image of stained cells is shown. The dotted line indicates nucleus boundary. Scale bar, 8 μm. **d**: Periodic *z*-series of ECs treated as in **a** were acquired at 50 min after plating to generate a color-coded projection such that the basal cell surface, which adheres to the substrate is red and the apical cell surface is violet. A vertical section (lateral *xz*, 47 *z*-sections of 115 nm each) obtained from the same images is shown. A dotted ring containing an asterisk indicates apical bud boundary. In the *xz* view, a dotted line indicates the cell boundary and an arrowhead the point of view of the image. Scale bar, 8 μm. **e**: Details of late spreading HUVECs. Cells treated as in **a** were stained for F-actin and CD93. Overlay of stained cells and white dot colocalization (wdc) images are shown. Arrowheads indicate colocalization between $CD93^{+ve}$ vesicles and actin cables. Manders and Costes quantitative analyses of CD93 colocalization with F-actin and vice versa are shown ($n = 8$ cells). Scale bars are 4 μm

HDBECs and with the use of different antibodies against CD93, confocal microscopy analysis revealed the appearance of large round-shape $CD93^{+ve}$ vesicles (Fig. 3b), suggesting that the formation of large $CD93^{+ve}$ recycling vesicles is a typical trait in spreading primary ECs. HUVECs treated with cycloheximide showed regular

formation of CD93^{+ve} vesicles during the late spreading phases (Fig. 3c), suggesting that these vesicles contain a recycled pool of pre-existing CD93 and their origin is not due to new protein synthesis. Furthermore, confocal color-coded *xz* sectioning localized the smaller CD93^{+ve} vesicles near and around the apical bud and the largest ones close to the basolateral membrane (Fig. 3d), suggesting that the CD93^{+ve} vesicles move from the apical bud towards the cell-substrate interface. Importantly, high-resolution fluorescence confocal microscopy analysis of CD93^{+ve} vesicles showed their alignment with the actin cables (Fig. 3e). Since actin dynamics ensure efficient endocytosis and direct the trafficking of vesicles to the cell surface [34], we hypothesized a role for F-actin in the transport of CD93^{+ve} vesicles. To explore this hypothesis, ECs were let to spread in the presence of latrunculin B. Accordingly, addition of this drug to the culture medium impaired the formation of CD93^{+ve} vesicles and CD93 resulted mislocalized in several cytosolic regions (Additional file 1: Figure S2). By contrast, when the microtubule cytoskeleton was disrupted by nocodazole, no effects were observed on the formation and localization of CD93^{+ve} vesicles (Additional file 1: Figure S3). Since recent studies have demonstrated that internalized adhesion molecules may transit through the *trans*-Golgi network (TGN) before being delivered to the cell surface [19], we asked whether also CD93 could be involved in the route from or to the Golgi apparatus. To address this possibility, we performed immunofluorescence analyses on early and late spreading HUVECs by staining coatomers involved in the secretory pathway, such as COPI, COPII, and clathrin. However, protein involved in the secretory pathway did not show significant colocalization with CD93 (Additional file 1: Figure S4). Altogether, these data indicate that in spreading ECs, endocytosed CD93 is directly recycled back to the cell-substrate interface via vesicles moving along F-actin cables.

MMRN2 and β1 integrin are recycled together with CD93

Several adhesion molecules are often internalized together with their ligands and other associated proteins in functional domains on the membrane surface. Such associations allow the coordination of ligand-receptor recycling and degradation thus controlling their bioavailability and function [35]. Hence, we sought to investigate whether endocytosed CD93 was associated with its ligand MMRN2 in internalized vesicles. To this end, endogenous CD93 and transfected CD93-YFP were analyzed by fluorescence confocal microscopy at different degrees of cell adhesion. Interestingly, both endogenous and exogenous CD93 were colocalized with MMRN2 at early and late spreading phases (Fig. 4). Such colocalization was also observed in early and late spreading HDBECs (Additional file 1: Figure S5). Since CD93 and MMRN2 cooperate to stabilize α5β1 integrin and β integrin subunits are mainly associated with regulatory and signal transducing proteins [18, 36], we asked whether β1 integrin was also internalized in association with the CD93-MMRN2 complex during cell spreading. Notably, both endogenous and exogenous CD93 were colocalized with β1 integrin, which followed the same endocytic route of CD93 during early and late cell spreading (Fig. 5a-d). Moreover, internalized β1 integrin resulted partly bound to ECM, as assessed by immunofluorescent staining using an antibody that specifically recognizes the active conformation of β1 integrin (Fig. 5e and f). Taken together, these findings indicate that during EC adhesion, endocytosed CD93 forms an active complex with MMRN2 and β1 integrin and the whole complex is retrieved and recycled directly back to the plasma membrane.

Rab5c promotes CD93 recycling

To investigate the nature of CD93 recycling in spreading ECs, we focused on Rab GTPases, which have been demonstrated to regulate endocytic trafficking and contribute to the structural and functional identity of intracellular organelles [25]. To this end, HUVECs were transfected or not with CD93-YFP, fixed, and stained for Rab5, Rab7, and Rab11 at different degrees of attachment to the substrate. CD93^{+ve} vesicles formed during early and late spreading showed a strong colocalization of endogenous and exogenous CD93 with the early endosomal marker Rab5 (Fig. 6), but not with Rab7 and only slightly with Rab11 in the large vesicles (Additional file 1: Figure S6), suggesting that Rab11 contributes to the transition of CD93^{+ve} vesicles from early to recycling endosomes [37]. We hence infer that Rab5 is involved in the regulation of CD93 recycling. Since Rab5 has three isoforms (Rab5a, b, c) that cooperate in the regulation of endocytosis in eukaryotic cells [38], we first investigated whether all isoforms were expressed in HUVECs. Interestingly, only a strong Rab5c signal was detected by both immunofluorescence and immunoblotting analyses (Additional file 1: Figure S7). Next, to directly explore the role of Rab5c in CD93 recycling, we sought to impair Rab5c expression in HUVECs by lentiviral constructs expressing two independent shRNAs (clones 31 and 33). ECs transduced with lentiviruses expressing both Rab5c shRNAs showed a strong decrease in Rab5c protein levels as compared to ECs transduced with a lentivirus expressing an unrelated shRNA (Fig. 7a). Importantly, the silencing of Rab5c did not increase the expression pattern of the other Rab5 isoforms (Fig. 7a), suggesting that in HUVECs Rab5 isoforms do not undergo evident genetic compensation in

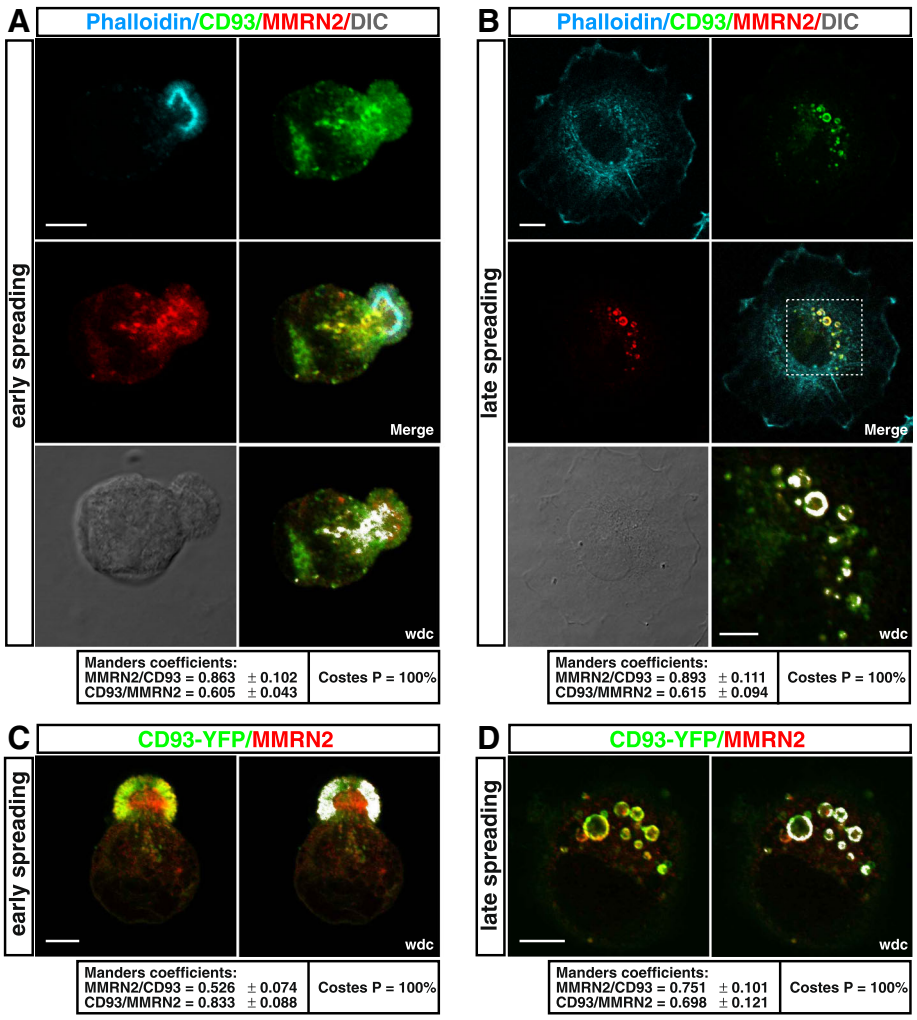

Fig. 4 CD93 colocalizes with MMRN2 in endocytic vesicles. The CD93-YFP construct was transfected or not into HUVECs. Cells were detached from the plate, resuspended in complete growth medium, plated, fixed at different times after plating, and analyzed by confocal microscopy. **a**, **b**: Untransfected ECs at early and late phases of spreading were stained using phalloidin, anti-CD93, and anti-MMRN2 antibodies. Merged, DIC, and wdc images between CD93 and MMRN2 are shown. Scale bars, 7 μm. In **b**, the wdc picture shows a high magnification of the $CD93^{+ve}$ vesicles displayed into the dashed square. Scale bar, 4 μm. **c**, **d**: Transfected early and late spreading cells were stained for MMRN2. Exogenous CD93 was imaged as green. Overlay of stained cells and wdc images are shown. Scale bars, 7 μm. For each condition, Manders and Costes quantitative analyses of MMRN2 colocalization with CD93 and vice versa are reported (n = 5–7 cells)

response to gene knockdown [39]. Moreover, confocal microscopy analysis on Rab5c-silenced HUVECs showed that in early spreading cells, CD93 was regularly distributed in small vesicles beneath the apical bud (Fig. 7b, upper panels). By contrast, in late spreading ECs, confocal microscopy and quantitative analyses showed that Rab5c downregulation resulted in a remarkable disappearance of large $CD93^{+ve}$ vesicles (Fig. 7b lower panels, and 7c), suggesting that Rab5c is involved in the intracellular trafficking and size increase of $CD93^{+ve}$ vesicles but not in the internalization of CD93 from the apical bud. To evaluate further the involvement of Rab5c in the regulation of CD93 recycling, we analyzed plasma membrane and total cellular levels of CD93 in control and Rab5c-silenced ECs by flow cytometry and Western blotting. Notably, we observed that, although the total CD93 cellular levels remained unchanged, less CD93 protein was exposed on the plasma surface of Rab5c-silenced cells in comparison to control (Fig. 7d).

Next, to assess the role of Rab5c in the trafficking of CD93 during EC migration, we employed an in vitro wound healing assay and used confocal microscopy to detect the subcellular localization of CD93 in the leading edge of migrating cells. Similarly to what has been previously reported for HDBECs [18], CD93 was strongly localized in the migrating edge of HUVECs transduced with a lentivirus expressing an unrelated shRNA (Fig. 7e, upper panels). On the

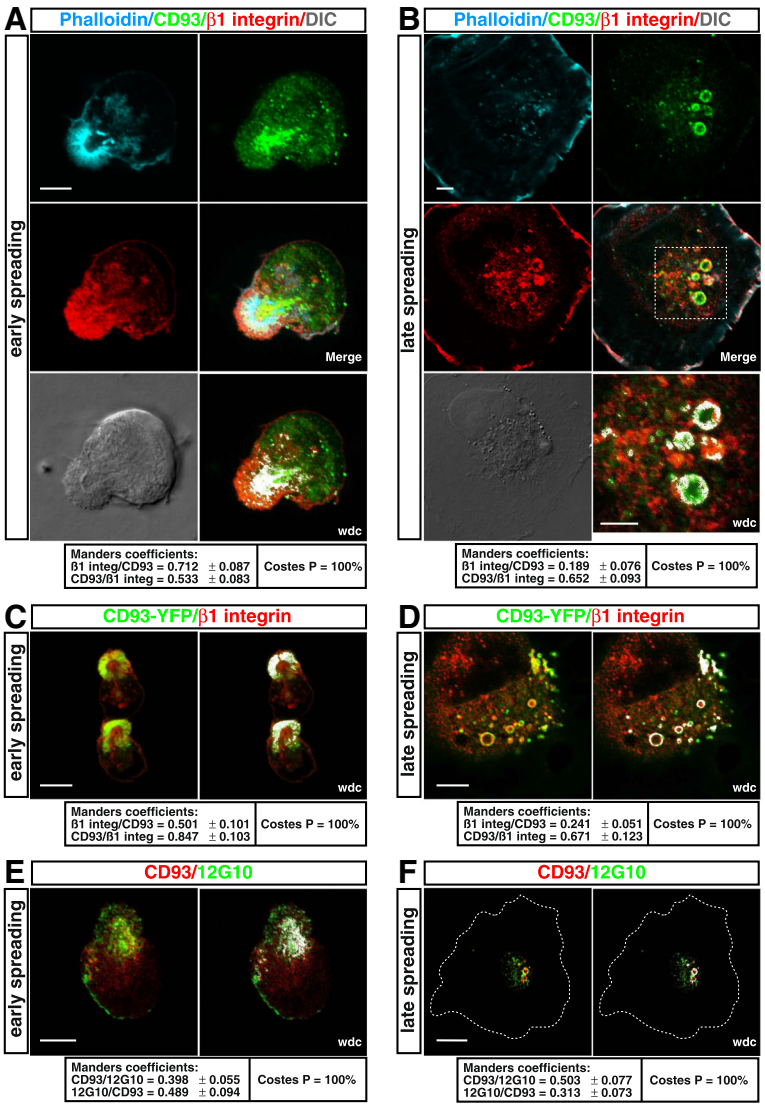

Fig. 5 The CD93-MMRN2 complex is recycled in association with β1 integrin. The CD93-YFP construct was transfected or not into HUVECs. Cells were detached from the plate, resuspended in complete growth medium, plated, fixed at different times after plating, and imaged by immunofluorescence. **a**, **b**: Untransfected cells at early and late phases of spreading were stained using phalloidin, anti-CD93 and anti-β1 integrin antibodies. Merged, DIC, and wdc images between CD93 and β1 integrin are shown. In **b**, the wdc picture shows a high magnification of the $CD93^{+ve}$ vesicles visible into the dotted square. Scale bars, 6 μm (**a**), 4 μm (**b**). **c**, **d**: Transfected early and late spreading ECs were stained for β1 integrin. Exogenous CD93 was imaged as green. Overlay of stained cells and wdc images are shown. Scale bars, 8 μm (**c**) and 7 μm (**d**). **e**, **f**: Immunofluorescent staining of CD93 and active β1 integrin (12G10) in untransfected cells at early and late phases of attachment to the substrate. Merged and wdc images are shown. In **f**, dotted lines indicate cell boundary. Scale bars, 8 μm (**e**) and 13 μm (**f**). For each condition, Manders and Costes quantitative analyses of β1 integrin colocalization with CD93 and vice versa are reported ($n = 4–8$ cells)

contrary, Rab5c silencing dramatically impaired the localization of CD93 in the extending lamellipodia of the migrating front (Fig. 7e lower panels, quantified in Fig. 7g). These findings were further substantiated by internalization assays on migrating control and Rab5c-silenced ECs (Additional file 1: Figure S8). Importantly, in line with the role of CD93 in modulating β1 integrin activation during cell migration [18], Rab5c silencing strongly reduced the amount of β1 integrin as well as its active form at the leading edge of migration (Additional file 1: Figure S9 and Fig. 7f, quantified in Fig. 7g). In keeping with the above results, knocking down Rab5c reduced the ability of HUVECs to migrate in wound closure assays (Fig. 7h and i), indicating that in ECs the Rab5c isoform orchestrates the recycling of endocytosed CD93 involved in the regulation of β1 integrin activation during cell migration.

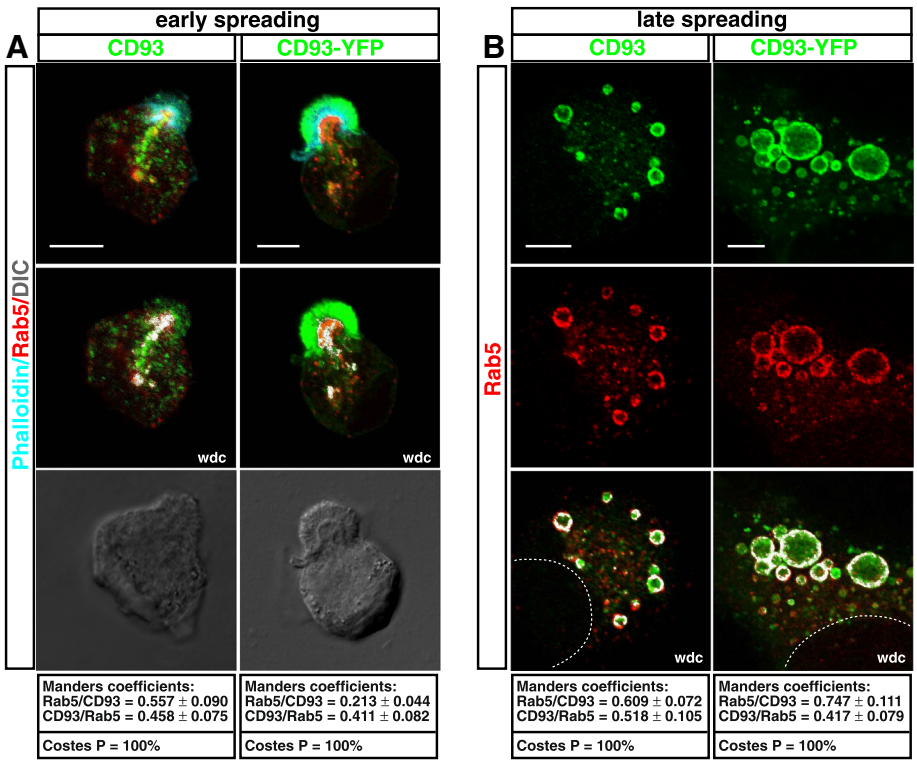

Fig. 6 CD93 colocalizes with the small GTPase Rab5. HUVECs were transfected or not with CD93-YFP, then they were detached from the plate, resuspended in complete growth medium, plated on the substrate, fixed at early (**a**) and late (**b**) degrees of cell spreading, and subjected to immunofluorescence analysis. **a**: Untransfected cells (CD93) were stained with phalloidin, anti-Rab5, and anti-CD93 antibodies. Transfected cells (CD93-YFP) were stained with phalloidin and anti-Rab5 antibodies. Scale bars, 7 μm. **b**: Untransfected cells (CD93) were stained with anti-CD93 and anti-Rab5 antibodies. Transfected cells (CD93-YFP) were stained for Rab5. A dotted line indicates nucleus boundary. Scale bars, 7 μm. In transfected cells, exogenous CD93 was imaged as green. Merged, DIC, and wdc images between CD93 and Rab5 are shown. For each condition, Manders and Costes quantitative analyses of Rab5 colocalization with CD93 and vice versa are reported (n = 5–8 cells)

In adhering and migrating ECs, the cytoplasmic domain of CD93 is critical for CD93 recycling

Since the cytoplasmic tail of CD93 drives the movements of CD93 towards the polarizing apical bud (Fig. 2d), we hypothesized its involvement also in the transport of CD93 to the cell-substrate interface. To explore this hypothesis, HUVECs were transfected with CD93-YFP or CD93ΔC-YFP constructs and the distribution of the chimeric proteins was compared by immunofluorescence analyses at late degrees of cell adhesion. As shown in Fig. 8a (left panel), exogenous CD93 was specifically localized in large vesicles such as the endogenous protein. On the other hand, the CD93ΔC tagged protein showed a diffuse and punctate pattern throughout the cytoplasm and the $CD93^{+ve}$ vesicles showed a strong reduction in size (Fig. 8a, right panel). These observations were sustained by quantitative analysis of $CD93^{+ve}$ vesicle number, highlighting its statistically significant decrease in cells transfected with the deletion mutant in comparison to cells transfected with wild type CD93 (Fig. 8b). Of note, neither the presence of CD93ΔC nor the downregulation of CD93 impaired the formation of large $Rab5c^{+ve}$ vesicles (Fig. 8c and Additional file 1: Figure S10), suggesting that the cytoplasmic random distribution of CD93ΔC is not due to destruction of subcellular structures.

To investigate the role of the cytoplasmic tail in the recycling of CD93 during EC migration, we transfected HUVECs with CD93-YFP or CD93ΔC-YFP constructs, used an in vitro wound healing assay and assessed the subcellular localization of exogenous proteins by confocal microscopy and quantitative analysis of protein localization at the migrating front. While exogenous wild type CD93 was localized in the leading edge of migration, where ECs extended lamellipodia, only low levels of CD93ΔC were observed in the extending lamellipodia of the migrating front, being mainly accumulated in the perinuclear region (Fig. 8d, quantified in Fig. 8e). Altogether, these results suggest that the C-terminus of CD93 controls its retrieval and recycling to the cell surface, and as a result, it regulates cell adhesion and movements of migrating ECs.

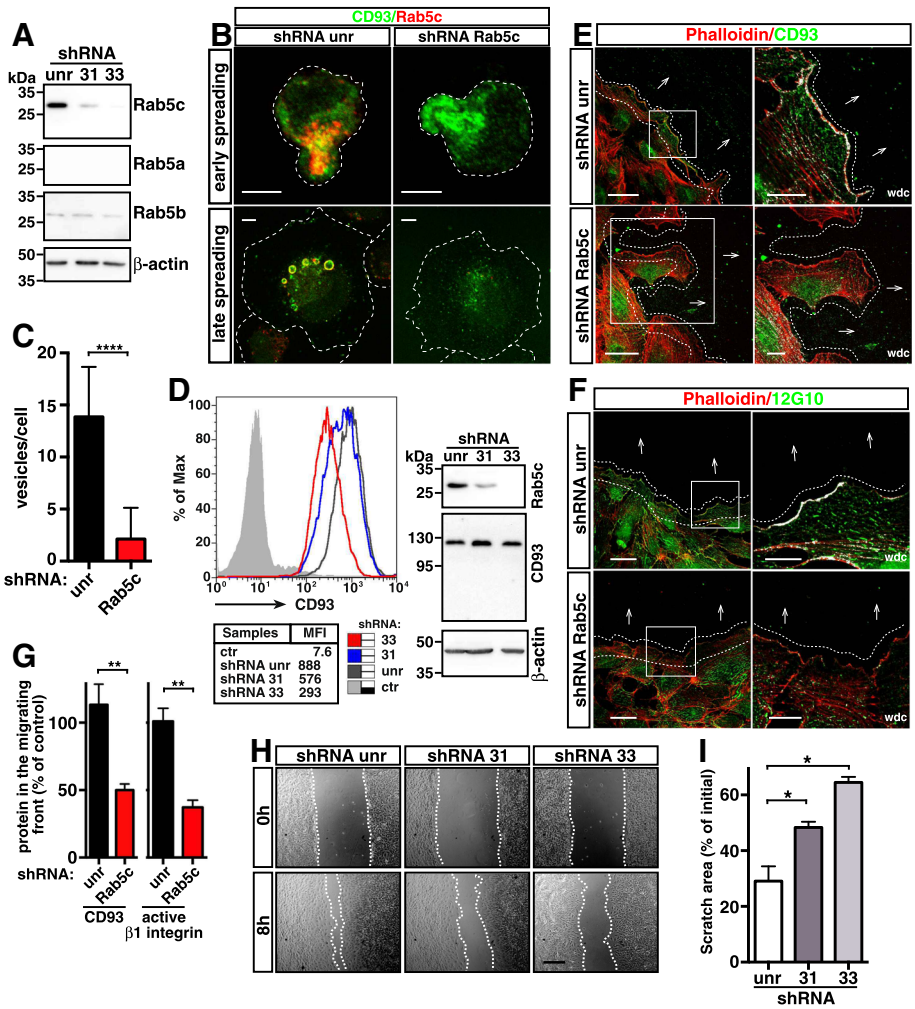

Fig. 7 Rab5c modulates CD93-mediated EC motility. HUVECs were transduced with lentiviral particles expressing unrelated (unr) or Rab5c shRNAs (clone 31 and 33). **a**: Cell lysates from shRNA expressing ECs were analyzed by Western blotting using antibodies against Rab5a, Rab5b, or Rab5c. Anti-β-actin antibodies were used to confirm equal loading. **b**: Representative images of control (shRNA unr) and Rab5c-silenced (shRNA Rab5c, clone 33) HUVECs at early and late phases of spreading. Cells were analyzed by confocal microscopy using anti-CD93 and anti-Rab5c antibodies. Overlay of stained cells is shown. Dashed lines indicate cell boundaries. Scale bars, 6 μm. **c**: Quantitative analysis of $CD93^{+ve}$ vesicles per cell from late spreading ECs treated as in **b**. The vesicle numbers represent the mean ± SD of three independent experiments ($n = 20$ cells). $^{****}P < 0.0001$; unpaired *t*-test. **d**: Flow cytometry analysis of CD93 plasma membrane levels in control (unr) and Rab5c-silenced (clones 31 and 33) HUVECs. Cells stained only with the secondary antibody are shown (ctr). The mean fluorescence intensity (MFI) is reported. Total cell extracts from the same shRNA expressing cells were analyzed by Western blotting using anti-CD93 and anti-Rab5c antibodies. Anti-β-actin antibodies were used to confirm equal loading. **e**, **f**: Representative images of the confocal microscopy analyses of control (shRNA unr) and Rab5c-silenced (shRNA Rab5c, clone 33) HUVECs at 5 h after production of a double-sided scratch in the cell monolayer. Phalloidin and anti-CD93 (**e**) or anti-β1 integrin (12G10) (**f**) antibodies were used to image cells. Arrows indicate direction of migration and dotted lines indicate the migrating front. Overlay of stained cells is shown. Scale bars, 40 μm. Magnifications of the squared areas are shown as wdc images. In wdc images, scale bars are 15 μm. In **b**, **e**, and **f**, same results were obtained when using the clone 31 for Rab5c knockdown. **g**: Quantification of CD93 and active β1 integrin along the migrating front areas indicated by dotted lines in **e** and **f**. Bars represent the percentage of fluorescence intensity of the control. Data are presented as the mean ± SD of three independent experiments ($n = 5$ different areas along the migrating edge). $^{**}P < 0.01$; unpaired *t*-test. **h**: Representative images of wound closure in HUVECs transduced with lentiviral particles expressing control (unr) or Rab5c shRNAs. Cells were photographed at 0 and 8 h. Scale bar, 100 μm. **i**: The percentage of scratch area was calculated from images acquired at time 0 and 8 h following the wound. Analyses were performed using ImageJ. The graph represents the means ± SD, $n = 6$ images per condition pooled from two independent experiments. $^{*}P < 0.05$; unpaired *t*-test

Discussion

In developing blood vessels, ECs exhibit polarity in several axes and polarization of endothelia is essential for morphogenesis of the vascular tree [40]. The establishment of polarity is regulated by the spatiotemporal coordination of different signaling pathways that modulates cytoskeletal

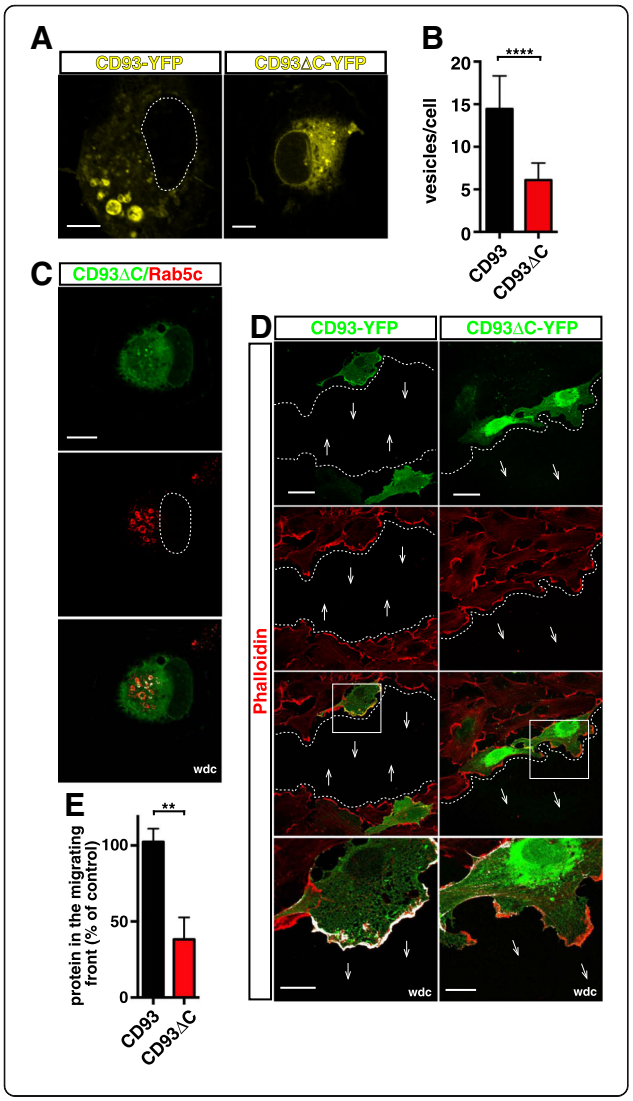

Fig. 8 During EC adhesion and migration, CD93 is recycled through its intracellular domain. YFP-tagged CD93 or CD93ΔC deletion mutant were transfected into HUVECs. **a**: Cells were detached from the plate, resuspended in complete growth medium, plated on the substrate, fixed at late phases of spreading, and analyzed by confocal microscopy. Exogenous proteins were imaged as yellow. Dotted lines indicate nucleus boundary. Scale bars are 7 μm. **b**: Quantitative analysis of $CD93^{+ve}$ vesicles per cell from ECs treated as in **a**. The vesicle numbers represent the mean ± SD of three independent experiments ($n = 20$ cells). $^{****}P < 0.0001$; unpaired *t*-test. **c**: Representative images of transfected HUVECs fixed at late phases of spreading. Cells were analyzed by confocal microscopy using anti-Rab5c antibodies. Exogenous CD93ΔC was imaged as green. A dashed line indicates nucleus boundary. A wdc image between CD93ΔC and Rab5c is shown. Scale bar, 15 μm. **d**: F-actin and wild type or mutant CD93 were imaged at 5 h after production of a double-sided scratch in the cell monolayer. Arrows indicate direction of migration and dotted lines indicate the migrating front. Overlay of stained cells is shown. Scale bar, 40 μm. High-magnification pictures of ECs in the migrating front within the squared area are shown as wdc images. In wdc images, scale bars are 15 μm. **e**: Quantification of CD93 and CD93ΔC along the migrating front of transfected cells. Bars represent the percentage of fluorescence intensity of the control. Data are presented as the mean ± SD of three independent experiments ($n = 7$ transfected cells along the migrating edge). $^{**}P < 0.01$; unpaired *t*-test

remodeling and vesicle trafficking to specify membrane domains [1]. Understanding the underlying mechanisms of EC polarity may help to elucidate the pathophysiology of angiogenic diseases and to improve their treatment [20]. Hence, in this study we investigated the polarized trafficking of CD93, an EC adhesion molecule recently identified as a key regulator of neo-vascularization processes [6, 13, 15].

During cell spreading, a process strictly connected to migration and mitosis, ECs undergo apical-basolateral polarization [41]. We found that at onset of EC spreading CD93 is completely localized to the apical bud, a membrane Moesin-rich domain branching out linear actin cables and able to mediate polarized trafficking [27, 32]. Accordingly, both drug disruption of the actin cytoskeleton and deletion of the CD93 cytoplasmic domain containing the binding site to Moesin severely impair CD93 localization to the apical bud, indicating that hampering the interaction with F-actin prevents a proper CD93 redistribution in the early phases of cell attachment to the substrate. Indeed, it has been shown that Moesin, acting as a bridge between actin microfilaments and plasma membrane, alters cell morphology, motility, and cell polarity [9, 42]. Moesin is maintained in a quiescent state by a masked closed conformation and it is activated following threonine phosphorylation in its C-terminal domain. This phosphorylation is closely associated with cytoskeletal rearrangement and there is now evidence that Moesin phosphorylation can also contribute to enhanced angiogenesis [42, 43]. Of note, in the apical bud, most of Moesin is phosphorylated [27],

suggesting that, in early spreading ECs, activated Moesin and F-actin act synergistically to localize CD93 to the apical bud.

Polarized membrane transport assists continuous reorganization of the cell membrane and it is involved in maintaining polarity and recycling of essential components in spreading and motile cells [20, 44]. Consistent with this, as soon as EC spreading proceeds, we first observed CD93 in cytoplasmic vesicles clustered directly beneath the apical bud and colocalizing with caveolin-1 but not with β-Adaptin, a component of the AP1 and AP2 adapter complexes, indicating that clathrin-independent endocytosis generates $CD93^{+ve}$ vesicles. Of note, clathrin-independent endocytosis, mediated by caveolae, has been linked to cellular spreading, cell polarization, and modulation of intercellular signaling [45]. Next, departing from the apical bud, these $CD93^{+ve}$ vesicles grow in size and, in tight association with F-actin, move towards the cell-substrate interface where they release their cargo. Upon endocytosis, apical and basolateral cargoes enter spatially distinct early or basolateral endosomes, which typically carry Rab5, a small GTPase also involved in the process of homotypic fusion between early endosomes [46, 47]. In line with these findings, we showed that endocytic $CD93^{+ve}$ vesicles strongly colocalize with Rab5c and depletion of Rab5c causes their decrease in size. Importantly, despite bidirectional ER-Golgi transport has emerged as a key regulator of apical transport and lumen morphogenesis [48], CD93 recycling does not transit through the TGN and thus is not tethered to the secretory pathway as previously shown for other adhesion molecules [19]. Furthermore, we found that endocytic $CD93^{+ve}$ vesicles carry MMRN2 and active β1 integrin, suggesting that following cell attachment to the substrate, the internalized CD93/MMRN2/β1 integrin active complex is directly recycled back to the polarized cell surface. Consistently with this assumption, in ECs the reciprocal interaction between CD93, MMRN2 and β1 integrin is essential for activation of β1 integrin [18], an adhesion molecule emerged also as a regulator of EC polarity and lumen formation in the developing vasculature [49]. In this respect, for some cargo the choice of a direct or indirect sorting pathway to the cell surface depends on the degree to which polarity has been established [47]. Here, we showed how in spreading ECs CD93 is retrieved and recycled directly back to the plasma membrane together with MMRN2 and consequently active β1 integrin. This endocytic pathway of CD93, also sustained by previous studies showing that integrins and their ligands exhibit a high traffic-dependent turnover within adhesion sites and that Rab5 controls β1 integrin internalization [50] [51], represents an ideal strategy for enabling cells to sense and rapidly respond to chemical cues from the surrounding extracellular environment.

Since Rab5 is a signaling protein involved in actin remodeling triggered by receptor tyrosine kinases [52], identification of Rab-mediated steps in the CD93 endocytic route argues for a network of interactions that impact on vascular features such as migration. Rab5 is a master regulator of early endosome biogenesis [53]. However, Rab5 has three isoforms, Rab5a, b, c, that have overlapping yet distinct functions [25]. Interestingly, we found that Rab5c is the preferentially expressed isoform in HUVECs and that its depletion causes EC defective migration towards open wound space in a scratch assay by preventing the delivering of CD93 and active β1 integrin to the extending lamellipodia of the migrating front. Intriguingly, recent reports indicate that in HeLa cells Rab5c selectively regulates cell motility and cytoskeletal dynamics and that Rab5c operates semi-independently from the other isoforms by promoting AMAP1-PRKD2 complex formation to enhance a growth factor-stimulated β1 integrin recycling pathway that regulates cancer cell invasion [54, 55].

Several experiments of membrane trafficking inhibition in different cell types reduce cell migration. However, the molecular mechanisms and pathways involved are still elusive [44]. In this study, we identified the CD93 cytotail as an essential domain for the spatiotemporal trafficking of CD93 during EC spreading and migration. Indeed, as happens upon Rab5c function depletion, we observed in a wound-healing assay that CD93 lacking of its cytotail is localized to the perinuclear region and not to the leading edge of migrating cells where F-actin is in active polymerization to form lamellipodia. These results are interesting not only because at the migrating front CD93 interacting with MMRN2 modulates β1 integrin activation, but also because the cytoplasmic domain of CD93 contains a consensus motif for the binding of Cbl, an adapter protein implicated in cell adhesion, organization of the actin cytoskeleton, and migration [12]. However, future work will determine if, by interacting with signaling protein(s), the CD93 cytotail triggers additional biochemical signal(s) promoting cell spreading and migration.

Conclusions

In conclusion, our data, together with the fact that in the plasma membrane CD93 requires ongoing recycling and maintenance of an appropriate diffusional environment for its activity [56, 57], help to clarify the retrieval and recycling pathway of the CD93/MMRN2/β1 integrin complex during cell adhesion and migration, opening up new possibilities to modulate vascular physiology in human health and disease.

Additional file

Additional file 1: Figure S1. Small vesicles containing CD93 colocalize with caveolin-1 in early spreading ECs. **Figure S2.** Disruption of the actin cytoskeleton impairs CD93 intracellular trafficking. **Figure S3.** Microtubule cytoskeleton disruption has no effects on CD93 intracellular trafficking. **Figure S4.** CD93 trafficking does not depend on transport from or to the Golgi complex. **Figure S5.** CD93 is colocalized with MMRN2 in spreading HDBECs. **Figure S6.** CD93 colocalizes strongly with Rab5 and slightly with Rab11, but not with Rab7. **Figure S7.** Rab5c is the predominant isoform in HUVECs. **Figure S8.** Rab5c regulates CD93 recycling to the cell surface. **Figure S9.** β1 integrin protein levels decrease at the leading edge of migrating Rab5c-silenced ECs. **Figure S10.** In CD93 silenced ECs, large Rab5c^{+ve} vesicles form regularly. (PDF 2570 kb)

Abbreviations

CTLD: C-type lectin-like domain; DIC: differential interference contrast; EC: endothelial cell; ECM: extracellular matrix; ERM: Ezrin/Radixin/Moesin; HDBEC: human dermal blood endothelial cell; HUVEC: human umbilical vein endothelial cell; MMRN2: Multimerin-2; TGN: *Trans*-Golgi network; wdc: white dot colocalization

Acknowledgements

The authors thank Dr. M. Mongiat (CRO, Aviano National Cancer Institute, Italy) for providing the rabbit anti-MMRN2 antibody, Dr. C. Ulivieri for the critical reading of the manuscript, and Dr. R. Boccacci for excellent technical assistance. This research was partially supported by MIUR Grant Dipartimento di Eccellenza 2018-2022.

Authors' contributions

SB and MO conceived and designed the experiments. SB, FG, AD, and MO discussed and analyzed the data. SB, FN, IE, GR, and RL performed the experiments. AS and GMT supported the study. AD and FG revised the manuscript. MO wrote the manuscript. All authors read and approved the final manuscript.

Funding

This research was partially supported by MIUR Grant Dipartimento di Eccellenza 2018–2022.

Availability of data and materials

The data generated during this study are included in this article and its supplementary information files are available from the corresponding authors on reasonable request.

Ethics approval and consent to participate

Not applicable.

Consent for publication

Not applicable.

Competing interests

The authors declare that they have no competing interests.

Author details

[1]Department of Biotechnology, Chemistry and Pharmacy, University of Siena, Via A. Moro, 2, 53100 Siena, Italy. [2]Department of Immunology, Genetics and Pathology, Science for Life Laboratory, Rudbeck Laboratory, Uppsala University, SE-751 85 Uppsala, Sweden. [3]Department of Medicine, Surgery and Neuroscience, Ophthalmology Unit, University of Siena, Policlinico "Le Scotte", Viale Bracci, 53100 Siena, Italy.

Received: 26 March 2019 Accepted: 20 May 2019
Published online: 28 May 2019

References

1. Herbert SP, Stainier DYR. Molecular control of endothelial cell behaviour during blood vessel morphogenesis. Nat Rev Mol Cell Biol. 2011;12:551–64.
2. Carmeliet P, Jain RK. Angiogenesis in cancer and other diseases. Nature. 2000;407:249–57.
3. Iozzo RV, Gubbiotti MA. Extracellular matrix: the driving force of mammalian diseases. Matrix Biol. 2018;71-72:1–9.
4. Sennino B, McDonald DM. Controlling escape from angiogenesis inhibitors. Nat Rev Cancer. 2012;12:699–709.
5. Nandini D, Pradip D, Leyland-Jones B. Evading anti-angiogenic therapy: resistance to anti-angiogenic therapy in solid tumors. Am J Transl Res. 2015; 7:1675–98.
6. Orlandini M, Galvagni F, Bardelli M, Rocchigiani M, Lentucci C, Anselmi F, et al. The characterization of a novel monoclonal antibody against CD93 unveils a new antiangiogenic target. Oncotarget. 2014;5:2750–60.
7. Khan KA, Naylor AJ, Khan A, Noy PJ, Mambretti M, Lodhia P, et al. Multimerin-2 is a ligand for group 14 family C-type lectins CLEC14A, CD93 and CD248 spanning the endothelial pericyte interface. Oncogene. 2017;36:6097–108.
8. Yonemura S, Hirao M, Doi Y, Takahashi N, Kondo T, Tsukita S, et al. Ezrin/radixin/Moesin (ERM) proteins bind to a positively charged amino acid cluster in the juxta-membrane cytoplasmic domain of CD44, CD43, and ICAM-2. J Cell Biol. 1998;140:885–95.
9. Neisch AL, Fehon RG. Ezrin, radixin and Moesin: key regulators of membrane–cortex interactions and signaling. Curr Opin Cell Biol. 2011;23: 377–82.
10. McClatchey AI. ERM proteins at a glance. J Cell Sci. 2014;127:3199–204.
11. Zhang M, Bohlson S, S., Dy M, Tenner A, J. Modulated interaction of the ERM protein, moesin, with CD93. Immunology 2005; 115:63–73.
12. Galvagni F, Nardi F, Maida M, Bernardini G, Vannuccini S, Petraglia F, et al. CD93 and dystroglycan cooperation in human endothelial cell adhesion and migration. Oncotarget. 2016;7:10090–103.
13. Langenkamp E, Zhang L, Lugano R, Huang H, Elhassan TEA, Georganaki M, et al. Elevated expression of the C-type lectin CD93 in the glioblastoma vasculature regulates cytoskeletal rearrangements that enhance vessel function and reduce host survival. Cancer Res. 2015;75:4504–16.
14. Du J, Yang Q, Luo L, Yang D. C1qr and C1qrl redundantly regulate angiogenesis in zebrafish through controlling endothelial Cdh5. Biochem Biophys Res Commun. 2017;483:482–7.
15. Tosi GM, Caldi E, Parolini B, Toti P, Neri G, Nardi F, et al. CD93 as a potential target in neovascular age-related macular degeneration. J Cell Physiol. 2016; 232:1767–73.
16. Galvagni F, Nardi F, Spiga O, Trezza A, Tarticchio G, Pellicani R, et al. Dissecting the CD93-Multimerin 2 interaction involved in cell adhesion and migration of the activated endothelium. Matrix Biol. 2017;64:112–27.
17. Kao Y-C, Jiang S-J, Pan W-A, Wang K-C, Chen P-K, Wei H-J, et al. The epidermal growth factor-like domain of CD93 is a potent angiogenic factor. PLoS One. 2012;7:e51647.
18. Lugano R, Vemuri K, Yu D, Bergqvist M, Smits A, Essand M, et al. CD93 promotes β1 integrin activation and fibronectin fibrillogenesis during tumor angiogenesis. J Clin Invest. 2018;128:3280–97.
19. Mana G, Clapero F, Panieri E, Panero V, Böttcher RT, Tseng H-Y, et al. PPFIA1 drives active α5β1 integrin recycling and controls fibronectin fibrillogenesis and vascular morphogenesis. Nat Commun. 2016;7:13546.
20. Cullen PJ, Steinberg F. To degrade or not to degrade: mechanisms and significance of endocytic recycling. Nat Rev Mol Cell Biol. 2018;19:679–96.
21. Yoshioka K, Yoshida K, Cui H, Wakayama T, Takuwa N, Okamoto Y, et al. Endothelial PI3K-C2α, a class II PI3K, has an essential role in angiogenesis and vascular barrier function. Nat Med. 2012;18:1560–9.
22. Margadant C, Monsuur HN, Norman JC, Sonnenberg A. Mechanisms of integrin activation and trafficking. Curr Opin Cell Biol. 2011;23:607–14.
23. Caswell PT, Vadrevu S, Norman JC. Integrins: masters and slaves of endocytic transport. Nat Rev Mol Cell Biol. 2009;10:843–53.
24. Zerial M, McBride H. Rab proteins as membrane organizers. Nat Rev Mol Cell Biol. 2001;2:107–17.
25. Wandinger-Ness A, Zerial M. Rab proteins and the compartmentalization of the endosomal system. Cold Spring Harb Perspect Biol. 2014;6: a022616.
26. Anselmi F, Orlandini M, Rocchigiani M, De Clemente C, Salameh A, Lentucci C, et al. C-ABL modulates MAP kinases activation downstream of VEGFR-2 signaling by direct phosphorylation of the adaptor proteins GRB2 and NCK1. Angiogenesis. 2012;15:187–97.
27. Galvagni F, Baldari CT, Oliviero S, Orlandini M. An apical actin-rich domain drives the establishment of cell polarity during cell adhesion. Histochem Cell Biol. 2012;138:419–33.

28. Orlandini M, Nucciotti S, Galvagni F, Bardelli M, Rocchigiani M, Petraglia F, et al. Morphogenesis of human endothelial cells is inhibited by DAB2 via Src. FEBS Lett. 2008;582:2542–8.
29. Pike JA, Styles IB, Rappoport JZ, Heath JK. Quantifying receptor trafficking and colocalization with confocal microscopy. Methods. 2017; 115:42–54.
30. Galvagni F, Anselmi F, Salameh A, Orlandini M, Rocchigiani M, Oliviero S. Vascular endothelial growth factor receptor-3 activity is modulated by its association with caveolin-1 on endothelial membrane. Biochemistry. 2007; 46:3998–4005.
31. Ulivieri C, Savino MT, Luccarini I, Fanigliulo E, Aldinucci A, Bonechi E, et al. The adaptor protein rai/ShcC promotes astrocyte-dependent inflammation during experimental autoimmune encephalomyelitis. J Immunol. 2016;197: 480–90.
32. Richards M, Hetheridge C, Mellor H. The formin FMNL3 controls early apical specification in endothelial cells by regulating the polarized trafficking of podocalyxin. Curr Biol. 2015;25:2325–31.
33. Grande-García A, del Pozo MA. Caveolin-1 in cell polarization and directional migration. Eur J Cell Biol. 2008;87:641–7.
34. Croisé P, Estay-Ahumada C, Gasman S, Ory S. Rho GTPases, phosphoinositides, and actin. Small GTPases. 2014;5:e29469.
35. Sorkin A, von Zastrow M. Endocytosis and signalling: intertwining molecular networks. Nat Rev Mol Cell Biol. 2009;10:609–22.
36. Green LJ, Mould AP, Humphries MJ. The integrin β subunit. Int J Biochem Cell Biol. 1998;30:179–84.
37. Welz T, Wellbourne-Wood J, Kerkhoff E. Orchestration of cell surface proteins by Rab11. Trends Cell Biol. 2014;24:407–15.
38. Bucci C, Lütcke A, Steele-Mortimer O, Olkkonen VM, Dupree P, Chiariello M, et al. Co-operative regulation of endocytosis by three RAB5 isoforms. FEBS Lett. 1995;366:65–71.
39. El-Brolosy MA, Stainier DYR. Genetic compensation: a phenomenon in search of mechanisms. PLoS Genet. 2017;13:e1006780.
40. Lee CY, Bautch VL. Ups and downs of guided vessel sprouting: the role of polarity. Physiology (Bethesda). 2011;26:326–33.
41. Ebnet K, Kummer D, Steinbacher T, Singh A, Nakayama M, Matis M. Regulation of cell polarity by cell adhesion receptors. Semin Cell Dev Biol. 2018;81:2–12.
42. Zhang Wj, Li Px, Guo Xh, Huang Qb. Role of moesin, Src, and ROS in advanced glycation end product-induced vascular endothelial dysfunction. Microcirculation 2017; 24:e12358.
43. Wang Q, Fan A, Yuan Y, Chen L, Guo X, Huang X, et al. Role of Moesin in advanced glycation end products-induced angiogenesis of human umbilical vein endothelial cells. Sci Rep. 2016;6:22749.
44. Keren K. Cell motility: the integrating role of the plasma membrane. Eur Biophys J. 2011;40:1013–27.
45. Howes MT, Mayor S, Parton RG. Molecules, mechanisms, and cellular roles of clathrin-independent endocytosis. Curr Opin Cell Biol. 2010;22:519–27.
46. Gorvel J-P, Chavrier P, Zerial M, Gruenberg J. rab5 controls early endosome fusion in vitro. Cell. 1991;64:915–25.
47. Apodaca G, Gallo LI, Bryant DM. Role of membrane traffic in the generation of epithelial cell asymmetry. Nat Cell Biol. 2012;14:1235–43.
48. Datta A, Bryant DM, Mostov KE. Molecular regulation of lumen morphogenesis. Curr Biol. 2011;21:R126–36.
49. Zovein AC, Luque A, Turlo KA, Hofmann JJ, Yee KM, Becker MS, et al. β1 integrin establishes endothelial cell polarity and arteriolar lumen formation via a Par3-dependent mechanism. Dev Cell. 2010;18:39–51.
50. De Franceschi N, Hamidi H, Alanko J, Sahgal P, Ivaska J. Integrin traffic – the update. J Cell Sci. 2015;128:839–52.
51. Sandri C, Caccavari F, Valdembri D, Camillo C, Veltel S, Santambrogio M, et al. The R-Ras/RIN2/Rab5 complex controls endothelial cell adhesion and morphogenesis via active integrin endocytosis and Rac signaling. Cell Res. 2012;22:1479–501.
52. Lanzetti L, Palamidessi A, Areces L, Scita G, Di Fiore PP. Rab5 is a signalling GTPase involved in actin remodelling by receptor tyrosine kinases. Nature. 2004;429:309–14.
53. Zeigerer A, Gilleron J, Bogorad RL, Marsico G, Nonaka H, Seifert S, et al. Rab5 is necessary for the biogenesis of the endolysosomal system in vivo. Nature. 2012;485:465–70.
54. Chen P-I, Schauer K, Kong C, Harding AR, Goud B, Stahl PD. Rab5 isoforms orchestrate a "division of labor" in the endocytic network; Rab5C modulates Rac-mediated cell motility. PLoS One. 2014;9:e90384.
55. Onodera Y, Nam J-M, Hashimoto A, Norman JC, Shirato H, Hashimoto S, et al. Rab5c promotes AMAP1–PRKD2 complex formation to enhance β1 integrin recycling in EGF-induced cancer invasion. J Cell Biol. 2012; 197:983–96.
56. Goiko M, de Bruyn JR, Heit B. Short-lived cages restrict protein diffusion in the plasma membrane. Sci Rep. 2016;6:34987.
57. Goiko M, de Bruyn JR, Heit B. Membrane diffusion occurs by continuous-time random walk sustained by vesicular trafficking. Biophys J. 2018;114: 2887–99.

Publisher's Note

3.3 Introduction to article 4

In the following work, we sought to investigate the importance of CD93 in AMD using two CNV models and explored the possibility of targeting the CD93/MMRN2 interaction in nAMD. We demonstrated in the rodent laser trauma model of CNV that CD93 is highly expressed in blood vessels, suggesting a pivotal role of CD93 in driving CNV. Indeed, in CD93-deficient mice, the laser-induced neovascularization of choroidal tissues is impaired and damaged areas have a low vascular density compared to choroidal tissues of wild-type mice. Moreover, we showed that absence of CD93 inhibits EC sprouting in an *ex vivo* model of choroid sprouting assay. Finally, CD93 and MMRN2 were both overexpressed in nAMD patient-derived specimens and inhibiting their binding *via* a mAb impaired EC sprouting *ex vivo*.

ARTICLE 4

The Binding of CD93 to Multimerin-2 Promotes Choroidal Neovascularization

Gian Marco Tosi,[1] Giovanni Neri,[1] Stefano Barbera,[2] Lucia Mundo,[3] Barbara Parolini,[4] Stefano Lazzi,[3] Roberta Lugano,[5] Evelina Poletto,[6] Lorenzo Leoncini,[3] Grazia Pertile,[7] Maurizio Mongiat,[6] Anna Dimberg,[5] Federico Galvagni,[2] and Maurizio Orlandini[2]

[1]Ophthalmology Unit of the Department of Medicine, Surgery and Neuroscience, University of Siena, Siena, Italy
[2]Department of Biotechnology, Chemistry and Pharmacy, University of Siena, Siena, Italy
[3]Department of Medical Biotechnology, Section of Pathology, University of Siena, Siena, Italy
[4]Vitroretinal Unit, Sant'Anna Hospital, Brescia, Italy
[5]Department of Immunology, Genetics and Pathology, Science for Life Laboratory, Rudbeck Laboratory, Uppsala University, Uppsala, Sweden
[6]Department of Research and Diagnosis, Division of Molecular Oncology, Centro di Riferimento Oncologico di Aviano, IRCCS, Aviano, Italy
[7]IRCCS Sacro Cuore Don Calabria Hospital, Negrar (VR), Italy

Correspondence: Maurizio Orlandini, Department of Biotechnology, Chemistry and Pharmacy, University of Siena, Via Aldo Moro, 2, 53100 Siena, Italy; maurizio.orlandini@unisi.it.
Federico Galvagni, Department of Biotechnology, Chemistry and Pharmacy, University of Siena, Via Aldo Moro 2, 53100 Siena, Italy; federico.galvagni@unisi.it.

Received: May 7, 2020
Accepted: June 20, 2020
Published: July 22, 2020

Citation: Tosi GM, Neri G, Barbera S, et al. The binding of CD93 to multimerin-2 promotes choroidal neovascularization. *Invest Ophthalmol Vis Sci.* 2020;61(8):30. https://doi.org/10.1167/iovs.61.8.30

Purpose. The purpose of this study was to investigate the involvement of CD93 and Multimerin-2 in three choroidal neovascularization (CNV) models and to evaluate their contribution in the neovascular progression of age-related macular degeneration (AMD).

Methods. Choroidal neovascular membranes collected during surgery from AMD patients were analyzed by microscopy methods. Laser-induced CNV mouse models and choroid sprouting assays (CSAs) were carried out using the CD93 knockout mouse model. An original ex vivo CSA of vascular angiogenesis, employing choroid tissues isolated from human donors, was developed.

Results. In contrast to healthy choroid endothelium, hyperproliferative choroidal endothelial cells (ECs) of AMD patients expressed high levels of CD93, and Multimerin-2 was abundantly deposited along the choroidal neovasculature. CD93 knockout mice showed a significant reduced neovascularization after laser photocoagulation, and their choroidal ECs displayed a decreased ability to produce sprouts in ex vivo angiogenesis assays. Moreover, the presence of an antibody able to hamper the CD93/Multimerin-2 interaction reduced vascular sprouting in the human CSA.

Conclusions. Our results demonstrate that CD93 and its interaction with Multimerin-2 play an important role in pathological vascularization of the choroid, disclosing new possibilities for therapeutic intervention to neovascular AMD.

Keywords: choriocapillaris, age-related macular degeneration, angiogenesis, neovascularization, retinal degeneration

Age-related macular degeneration (AMD) is the third leading cause (among the elderly, the major cause) of vision loss in industrialized countries.[1] As a result of the global aging of the human population, a significant increase in the number of AMD patients is expected over the next few years.[2] AMD is a heterogeneous disorder and is designated, according to progression and symptoms, as early, intermediate, or advanced disease.[3] Severe vision loss can be mainly attributed to the advanced neovascular form of AMD (nAMD), which occurs when choriocapillaris, the vasculature located posterior to the outer retina, grows and penetrates Bruch's membrane, resulting in vascular leakage, hemorrhage, and, over time, the development of fibrosis.[4] Thus, massive efforts have been dedicated to the development of antineovascular treatments for nAMD. Currently, nAMD is treated by routine intraocular injections of anti-VEGF drugs.[5] Nevertheless, although this therapy has revolutionized the treatment of nAMD providing significant visual benefits, it does not induce a persistent regression of the neovascularization, and frequent intravitreal injections are necessary to limit recurrence of the disorder.[5] Therefore, targeting different nAMD-associated factors represents a novel approach to developing combinatorial therapies that may provide enduring clinical benefits, avoiding the need for multiple treatments for nAMD patients.

The human CD93 is a single-pass transmembrane glycoprotein that belongs to group 14 in the C-type lectin domain (CTLD) superfamily of proteins involved in vascular biology.[6] CD93 expression is upregulated in the hyperproliferative endothelial cells (ECs) of blood vessels in different types of cancer.[7–9] In the activated endothelium, CD93 exhibits proangiogenic activities mainly regulating cell adhesion and

migration. Indeed, CD93 silencing impairs EC proliferation, adhesion, migration, and sprout formation,[10] and the cooperation between CD93 and dystroglycan, an adhesion molecule interacting with the extracellular matrix (ECM) protein laminin, promotes EC migration and tube formation.[11] Moreover, the cytoplasmic interaction between CD93 and moesin, which anchors CD93 to the actin cytoskeleton, is crucial for stabilizing cell adhesion and CD93 recycling, both necessary for proper EC migration.[12–14]

CD93 contributes to cell adhesion and migration through its interaction with Multimerin-2, an ECM endothelial-specific member of the EDEN family consistently deposited along the blood vessels of tumor vasculature.[9,15–17] In tumor angiogenesis, the CD93/Multimerin-2 interaction stabilizes the cell surface expression of CD93 and promotes β1 integrin activation and the fibrillar organization of fibronectin, leading to filopodia formation during the angiogenic process.[18] Therefore, CD93 neutralization may represent a new target for neovascularization inhibition in pathological contexts. In fact, we have formerly reported that an anti-CD93 monoclonal antibody (clone 4E1) was able to inhibit the formation of new blood vessels in both in vitro and in vivo experiments without affecting EC survival.[10]

Previously, we have shown that CD93 is overexpressed in ECs within choroidal neovascular membranes and that the aqueous humor of nAMD patients displays a high concentration of soluble CD93.[8] Here, we investigate the involvement of CD93 and Multimerin-2 in the neovascular progression of AMD. We show that the choriocapillaris of nAMD patients, in addition to expressing high levels of CD93, also exhibits strong Multimerin-2 deposition in the extracellular environment. Using both animal and ex vivo models, we demonstrate the important role of CD93 in the formation of new blood vessels in the choroid and highlight the relevance to hampering the CD93/Multimerin-2 interaction to block AMD-associated neoangiogenesis.

Methods

Subjects

The described research adhered to the tenets of the Declaration of Helsinki and received Institutional Review Board/Ethics Committee approval. The included patients presented with active choroidal neovascularization (CNV) secondary to AMD. As they could not benefit from anti-VEGF therapy, they were offered autologous retinal pigment epithelium–choroid graft transplantation. CNV membranes were collected during submacular surgery as previously described.[8] Patients were treated after being informed of the nature of the treatment being offered and the potential risks, benefits, adverse effects, and possible treatment outcomes. All patients signed consent forms. Demographics and clinical characteristics of patients are reported (see Supplementary Table S1).

Animals

C57BL/6 wild-type mice were purchased from Envigo (Indianapolis, IN, USA). CD93 knockout (*CD93*$^{-/-}$) mice on the C57BL/6 background[19] were housed in a pathogen-free animal facility at the Nuovi Istituti Biologici di San Miniato, University of Siena, Italy, in accordance with the Institutional Animal Welfare Guidelines, Italian legislation, and the ARVO Statement for the Use of Animals in Ophthalmic and Vision Research. The animal experiments conformed with the Guiding Principles for Research Involving Animals and Human Beings[20] and were approved by the Local Ethics Committee of the University of Siena and the Italian Ministry of Health.

Immunofluorescent and Immunohistochemical Staining

CNV membranes were collected from neovascular AMD patients during submacular surgery. Healthy choroid tissues were obtained from two retinoblastoma female patients during surgery and a whole eye from the corpse of a male who died in a car accident. Samples were processed as previously described.[8,21] Immunofluorescent staining was performed with antibodies against human Multimerin-2[22] and human CD34 (QBEnd/10; Ventana Medical Systems, Inc., Oro Valley, AZ, USA). Mouse laser-injured choroids were flatmounted and stained with anti-C1qR1/CD93 (R&D Systems, Minneapolis, MN, USA) and anti-Pecam-1 (H-3; Santa Cruz Biotechnology, Dallas, TX, USA) antibodies. Primary antibodies were identified with Alexa Fluor 488 or 568 secondary antibodies (Thermo Fisher Scientific, Waltham, MA, USA). Fluorescent images were captured using a Leica TCS SP2 AOBS (Wetzlar, Germany) confocal laser-scanning microscope, and overlaid images were produced. To show colocalization events by white dots, images were processed using ImageJ software (National Institutes of Health, Bethesda, MD, USA) and the ImageJ Colocalization plug-in (threshold channel green and red 90%; ratio setting value 50%). Immunohistochemical staining was performed as previously described.[8] The primary antibodies used were against human Multimerin-2, CD34, or CD93 (monoclonal antibody 4E1).[10] Samples were counterstained with hematoxylin and images obtained with a Zeiss microscope (Carl Zeiss Meditec, Jena, Germany).

Laser-Induced CNV and Choroidal Flatmount Analyses

CNV was induced by laser photocoagulation with rupture of the Bruch's membrane as previously described.[23] Briefly, mice 8 to 10 weeks old were anesthetized by intraperitoneal injection of 2,2,2-tribromoethanol (Avertin; Sigma-Aldrich, St. Louis, MO, USA), and their pupils were dilated with 1% tropicamide. Photocoagulation lesions (100-µm spot size, 100-ms duration, 200-mW power) were delivered by the PurePoint ophthalmic diode laser system (Alcon, Irvine, CA, USA), wavelength 532 nm, coupled to a slit lamp. A coverslip was placed on the cornea as a contact lens to view the retina, and each eye received four burns centered around the optic nerve at the 3, 6, 9, and 12 o'clock positions located equidistance from the optic disk and between the major retinal vessels. The morphologic end point of the laser injury was the appearance of a bubble, which confirmed disruption of the Bruch's membrane.[23,24] Lesions in which bubbles were not observed and eyes showing hemorrhage were excluded from the study.

Seven days after laser injury, the CNV lesions were characterized using immunofluorescent staining or size measured using FITC-dextran staining in choroidal flatmounts. Briefly, mice were anesthetized and euthanized either directly for characterization or 5 minutes after a 50-µL injection of FITC-conjugated dextran (2×10^6 average molecular weight;

Sigma-Aldrich), dissolved in water at a concentration of 50 mg/mL, into the mouse's orbital venous sinus using a 30-gauge needle attached to a 0.3-mL syringe.[25,26] Eyes were enucleated and fixed in paraformaldehyde (3% solution) for 2 hours. The anterior segment and retina were removed from the eyecup. The remaining retinal pigment epithelium (RPE)–choroid–sclera complex was either processed for confocal immunofluorescent analysis or flatmounted in Mowiol 4-88 (Calbiochem, San Diego, CA, USA) and examined by fluorescence microscopy using an Eclipse E600 microscope equipped with a DS-Fi1c digital camera (Nikon Instruments, Melville, NY, USA). The total area of CNV associated with each rupture site was measured using Nikon NIS-Elements image analysis software. A default and constant threshold in pixels was used to quantify CNV. An operator masked to the identity of the experimental groups performed the analysis.

Mouse and Human Choroid Sprouting Assays

Dissection and culture preparation of mouse tissue were performed as previously described.[27] Briefly, 5- to 6-week-old C57BL/6J and *CD93*$^{-/-}$ mice were sacrificed and their eyes immediately enucleated. The RPE–choroid–sclera was separated from the retina, cut into pieces, and embedded with 30 µL of growth factor-reduced Matrigel (BD Biosciences, San Jose, CA, USA) in 24-well plates. For human assay, choroid–sclera was obtained from the nasal scleral edge of eyes from the corpses of males 59, 69, and 55 years old who died of natural causes (car crash for one, heart attack for the other two). Choroids were quickly dissected, within 6 hours from the death of the individuals, and stored in M199 without supplements at 4°C until their use in the choroid sprouting assay (CSA) experiments, which were usually performed within 12 hours from collection. The choroid was cut into small pieces and embedded into 40 µL of growth factor-reduced Matrigel, in which was incorporated the monoclonal antibody 4E1 or unrelated antibodies (Mouse IgG Isotype Control, cat. no. 10400C; Thermo Fisher Scientific) at the concentration of 500 nM. Mouse and human choroidal explants were kept in a cell culture incubator (37°C and 5% CO_2) in the presence of Endothelial Cell Growth Medium 2 with supplements (PromoCell, Heidelberg, Germany). The culture medium was changed every 3 days, and on days 7 to 8 phase-contrast photographs of individual explants were captured. For immunofluorescence analysis, mouse and human choroidal explants were fixed with paraformaldehyde (3% solution) for 30 minutes and processed as previously described,[28] the only modification being that sample washes were performed on a rocker. Quantification analyses were performed in blind and measured the area of sprouting (subtracted from the explanted area) and the maximal extension of angiogenesis (from the choroid tissue edge) using the NIS-Elements image analysis software.

Statistics

Data analyses were performed with Prism 6 software (GraphPad Software, Inc., San Diego, CA, USA), and the values represent the mean ± SD obtained from at least three measurements on randomized samples. The statistical significance of the differences was determined by Student's *t*-test and the nonparametric Mann–Whitney *U* test for comparisons between two groups. All *P* values reported were two-tailed, and $P < 0.05$ was considered statistically significant.

Results

Blood Vessels of Human CNV Membranes Display Increased CD93 and Multimerin-2 Expression

It has been shown that the vascular expression of CD93, as well as its binding partner, Multimerin-2, are upregulated in several human tumor samples.[8,9,17,29–32] Similar to tumor blood vessels, choroidal neovessels from AMD patients show strong upregulation of CD93.[8] We thus wondered if Multimerin-2, the only known extracellular binding partner for CD93, was also highly deposited along the choriocapillaris of AMD patients. To address this issue, sections of CNV membranes from AMD patients already known to exhibit upregulation of vascular CD93[8] were processed for immunofluorescence analyses. Interestingly, compared to normal choroidal tissue, the choriocapillaris of AMD patients displayed a stronger expression of Multimerin-2, which overlapped that of CD34, used as a vascular marker (Figs. 1A, 1B). The differential expression of Multimerin-2 between normal and neovascular choroidal vessels and the strong CD93 expression in the choroidal neovasculature of AMD patients were confirmed by immunohistochemical analyses (Figs. 1C, 1D), indicating that Multimerin-2 is strongly deposited along blood vessels of the CNV membranes, which are characterized by the presence of proliferating ECs expressing high levels of CD93.

In Mice, the Ablation of CD93 Hinders Choroidal Angiogenesis

Because CD93 displays proangiogenic activities and its depletion impairs migration, adhesion, tube formation, and cytoskeletal organization of proliferating ECs,[7,10] we asked whether it also played a key role during the pathological vascularization of the choroid. To address this question, we exploited the *CD93*$^{-/-}$ murine model in two different assays of choroidal neovascularization. First, we used the laser-induced CNV (LI-CNV) mouse model, which led to the formation of vascular complexes that recapitulate the main features of the exudative form of human AMD.[23] After laser photocoagulation, quantitative analysis of FITC–dextran-stained choroidal flatmounts revealed a significantly reduced neovascularization in *CD93*$^{-/-}$ mice compared to wild-type animals (Figs. 2A, 2B). Of note, fluorescence microscopy analyses showed that, in the laser-injured regions, blood vessels from wild-type mice displayed strong CD93 staining (Fig. 2C). Strikingly, in *CD93*$^{-/-}$ mice, no CD93 signal was observed in the laser-damaged areas, despite these regions being highly vascularized, as indicated by Pecam-1 staining (Fig. 2D). Next, to test whether the effect of CD93 knockdown on choroidal angiogenesis was a phenomenon limited to LI-CNV or could be reproduced in a different model, we employed the ex vivo choroid sprouting assay, which has been shown to be a reproducible model of choroidal angiogenesis[27] (Fig. 3A). Interestingly, the ability of the choroidal tissues to form sprouts was significantly reduced in explants from *CD93*$^{-/-}$ mice compared to tissues explanted from control mice (Fig. 3B), as measured by a significant reduction in the area of choroid sprouting (Fig. 3C) and also in the longest vessel growth (Fig. 3D).

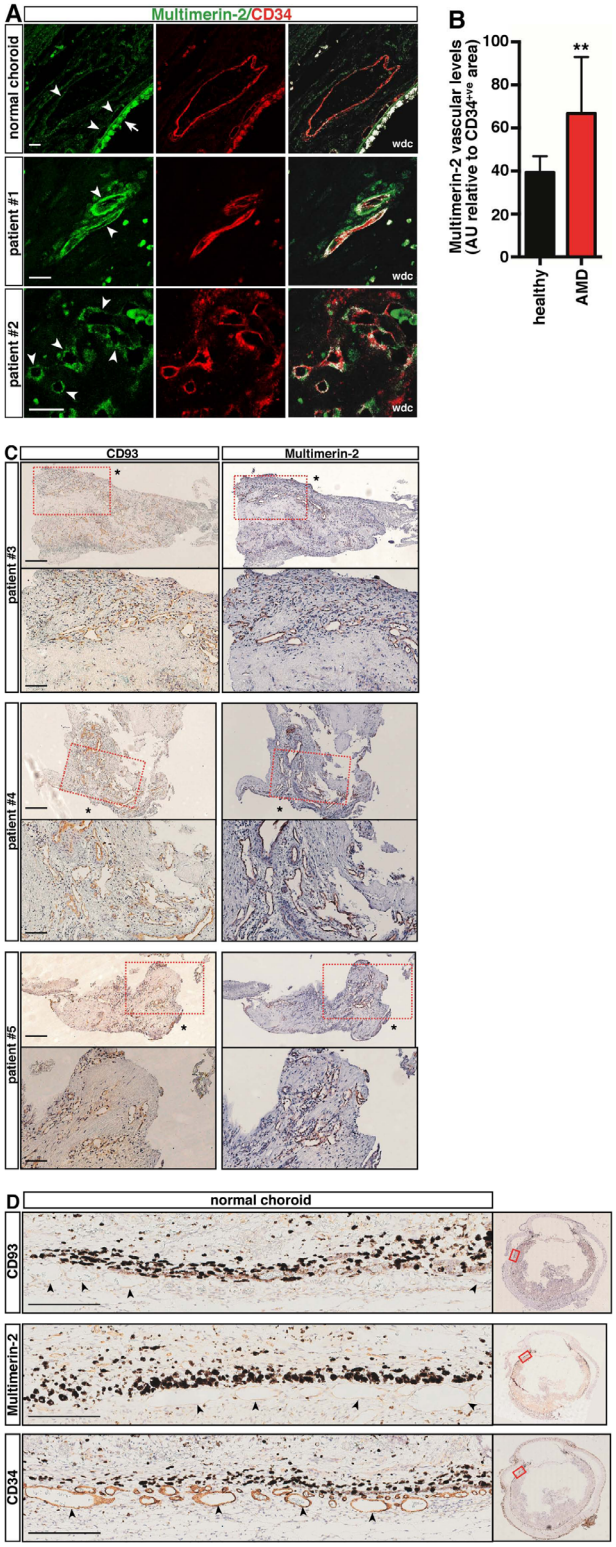

Figure 1. In contrast to normal choroidal tissue, CD93 and Multimerin-2 are highly expressed in blood vessels within CNV membranes. (**A**) CNV membrane sections obtained from AMD patients were analyzed by confocal imaging using antibodies to Multimerin-2 and the endothelial marker CD34. White dot colocalization (wdc) images are shown. *Arrowheads* indicate blood vessels. An *arrow* indicates the autofluorescent retinal pigment epithelium. *Scale bars*: 20 µm. (**B**) Multimerin-2 quantification in choriocapillaris from healthy ($n = 7$) and AMD ($n = 9$) patients. Values, measured using ImageJ software, represent mean ± SD expressed as arbitrary units (AUs) of Multimerin-2^{+ve} area normalized by CD34^{+ve} area. $^{**}P < 0.01$; unpaired *t*-test. (**C**) Serial CNV membrane sections were analyzed by immunohistochemistry using anti-CD93 and anti-Multimerin-2 antibodies. High magnifications of stained sections displayed in the *red dashed rectangles* are shown beneath each section. An *asterisk* indicates the most likely position of the retinal pigment epithelium, based on the presence of its small fragments. *Scale bars*: 250 µm; 100 µm for magnifications. (**D**) Serial paraffin-embedded sections from human normal choroids were analyzed by immunohistochemical staining using anti-CD93, anti-Multimerin-2, and anti-CD34 antibodies. In the left panels, *arrowheads* indicate choroidal blood vessels beneath the retinal pigment epithelium. Right panels show entire eye sections, and a *red rectangle* indicates the magnification area shown in the left panels. *Scale bars*: 250 µm.

Blockage of the CD93/Multimerin-2 Interaction Prevents Endothelial Sprouting in Human Choroids

Because the binding of CD93 to Multimerin-2 has recently been demonstrated to play a pivotal role in the activation of the quiescent endothelium,[9,18] we wondered if this interaction could also promote the formation of new blood vessels in the human choroid. To address this possibility, we sought

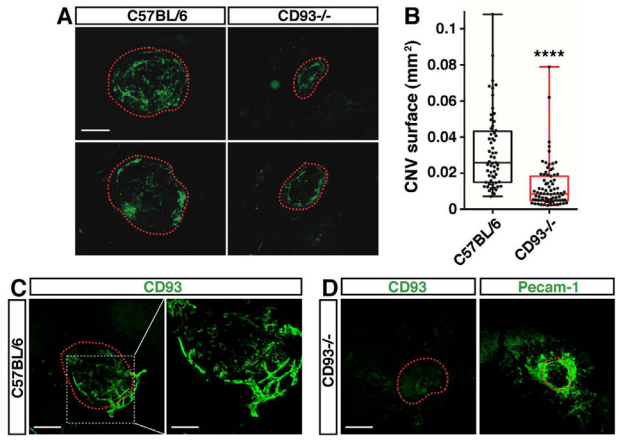

Figure 2. CD93 deficiency in mice associates with reduced LI-CNV. (**A**) Two representative fluorescent images of LI-CNV lesions from control (C57BL/6J) and *CD93*$^{-/-}$ mice, captured 7 days after laser exposure. In flatmounted choroids, *red dashed lines* show the extent of the LI-CNV lesions fluorescently labeled with FITC–dextran. *Scale bar*: 150 µm. (**B**) Quantification of FITC–dextran^{+ve} area in choroidal flatmounts of control (C57BL/6J, $n = 60$ impacts from 16 mice) and *CD93*$^{-/-}$ ($n = 79$ impacts from 21 mice) mice on day 7 after laser photocoagulation. Data are presented as box-and-whiskers plots and scatterplots displaying median, lower, and upper quartiles (boxes) and minimum–maximum (whiskers) for each lesion. $^{****}P < 0.0001$; unpaired *t*-test. (**C**) Choroid flatmount preparations from 7-day laser-injured regions of C57BL/6 mice were analyzed by immunofluorescence using an anti-CD93 antibody. A representative image of laser-injured areas (11 in total) from three eyes of different mice is shown. A *red dotted line* marks the LI-CNV lesion. High magnification of the stained region displayed into the *white dashed square* is shown in the right panel. *Scale bars*: 150 µm; 75 µm for the magnification. (**D**) Seven days after laser exposure, flatmounted choroids from *CD93*$^{-/-}$ mice were fluorescently labeled with anti-CD93 and anti-Pecam-1 antibodies and analyzed by confocal microscopy. Representative images of CD93-stained (seven from two eyes of two different mice) and Pecam-1-stained (eight from the remaining two eyes of the same mice) laser-injured areas are shown. The fluorescent staining in the CD93 panel represents background noise due to secondary antibodies. *Red dotted lines* indicate the laser-injured areas. *Scale bar*: 150 µm.

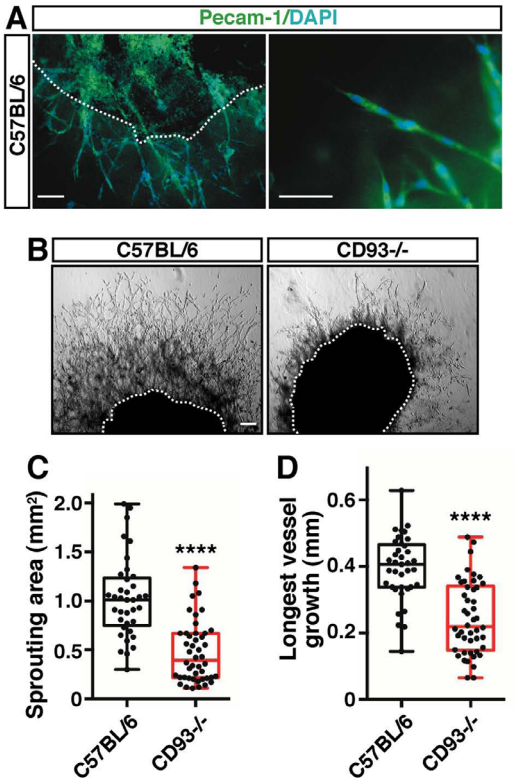

Figure 3. Choroidal tissue explanted from CD93$^{-/-}$ mice displays reduced EC sprouting. (**A**) Immunofluorescence analysis of choroidal sprouts from C57BL/6 mouse tissue, stained with an anti-Pecam-1 antibody and 4′,6-diamidino-2-phenylindole (DAPI) for nuclei labeling. A *dotted line* highlights the implant boundary. Images were captured using a fluorescent microscope. Details of choroidal sprouts are shown in the right panel. *Scale bars*: 50 µm. (**B**) Representative images of sprouts elicited from RPE–choroid–sclera of control (C57BL/6J) and CD93$^{-/-}$ mice. A *dashed line* indicates explant edge. *Scale bar*: 50 µm. (**C**, **D**) Quantitative analyses of sprouting area and maximal extension of angiogenesis from the mouse choroidal tissue edge. Data are presented as box-and-whiskers plots and scatterplots (n = 37 explants from four control mice; n = 46 explants from four CD93$^{-/-}$ mice). $^{****}P < 0.0001$; unpaired t-test.

to block the binding between CD93 and Multimerin-2 in an ex vivo choroid sprouting model using the anti-CD93 monoclonal antibody 4E1, which, as we previously showed, is able to interfere with this interaction (Fig. 4A).[9] To perform the experiment, we set up a novel assay employing human tissues obtained from healthy cornea donors. Because in different mouse strains the CSA may vary significantly,[27] we compared the choroid sprouting response of human tissues with that obtained using choroids explanted from wild-type C57BL/6J mice. As observed in the mouse model, the use of the EC marker Pecam-1 highlighted the presence of vascular sprouting emerging from human explants (Fig. 4B). However, the vessel areas and vessel lengths developed from human choroids were smaller compared to those developed from the murine choroids in the same time frame (compare quantifications in Figs. 3 and 4), suggesting that both the different species and aging may be factors to slow down vascular growth we observed in human choroid. Importantly, human endothelial sprouts displayed typical tip cell features on the extending growth cones, which resemble vascular tube formation in vivo (Fig. 4C).[33] Next, to verify

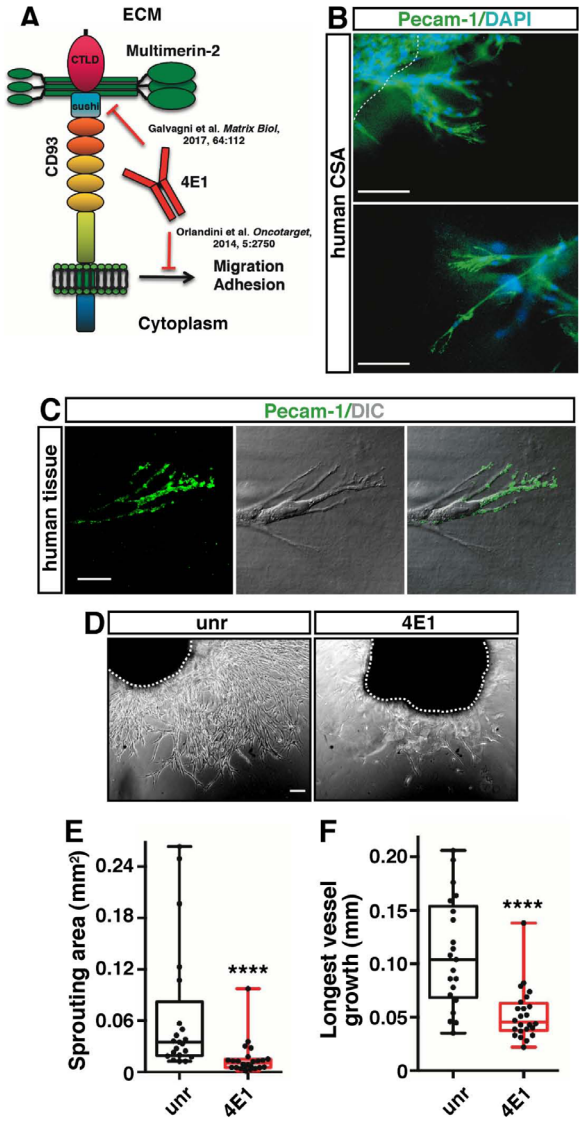

Figure 4. The CD93/Multimerin-2 interaction regulates human choroidal vessel sprouting. (**A**) Schematic representation of the CD93/Multimerin-2 interaction inhibition by the monoclonal antibody 4E1. The CD93 CTLD and sushi domains involved in the binding to Multimerin-2 are indicated. (**B**) Immunofluorescence staining of choroidal sprouts from human tissue, stained with an anti-Pecam-1 antibody and DAPI for nuclei labeling. A *dotted line* highlights the implant edge. Images were captured using a fluorescent microscope. Details of choroidal sprouts are shown in the lower panel. *Scale bars*: 50 µm. (**C**) Human sprouts from CSAs analyzed by confocal immunofluorescence using an anti-Pecam-1 antibody. Differential interference contrast (DIC) and overlaid images are shown. *Scale bar*: 18 µm. (**D**) Representative images of sprouts elicited from human choroids embedded into Matrigel containing the neutralizing anti-CD93 (4E1) or unrelated (unr) antibodies (500 nM). *White dashed lines* highlight the edge of choroid explants. *Scale bars*: 50 µm. (**E**, **F**) Quantification of sprouting area and maximal extension of endothelial sprouts from the human choroidal tissue edge. Data are presented as box-and-whiskers plots and scatterplots (n = 21 untreated and n = 24 4E1-treated choroid explants from three cornea donors). $^{****}P < 0.0001$; unpaired t-test.

the possible role of the CD93/Multimerin-2 interaction in this context, we employed the antibody 4E1 to interfere with this interaction. Importantly, and in contrast to the use of an unrelated control antibody, the presence of 4E1 significantly inhibited the ability of the choroidal tissues to form endothelial sprouts, in terms of both reduced sprouting areas and vessel length (Figs. 4D–4F).

Discussion

Following the identification of VEGF as an important regulator of nAMD, the development of anti-VEGF drugs has revolutionized the field of AMD treatment.[34] However, despite the initial therapeutic benefits, most patients develop refractory disease characterized by resumed neovascularization, eliciting the need to develop new therapeutic strategies.[35] As such, the use of combinatorial antineovascular drugs could prevent escape mechanisms and provide more effective, long-term disease control.[36]

CD93 has recently emerged as a potential target for antineovascular therapy.[16,18] Of note, CD93, along with its only currently known binding partner, Multimerin-2, were included as important components of a tumor angiogenesis signature and were found highly expressed in blood vessels within several tumor tissues of different origin.[9,37] Consistent with the aforementioned data on pathological neovascularization, we showed that CD93 and Multimerin-2 were also strongly coexpressed in blood vessels within CNV membranes of AMD patients, indicating that, during pathological vascularization of the choroid, CD93 and Multimerin-2 contribute to blood vessel growth. Importantly, CD93 and Multimerin-2 were faintly expressed in quiescent vessels of the healthy choroid. Along with our findings, a large amount of evidence suggests that the engagement of CD93 by Multimerin-2 plays a role in proliferative rather than in quiescent ECs.[9,16,18] In light of these results, low-affinity and high-avidity therapeutic agents that preferentially bind to highly target-expressing ECs could be successfully used to impair proliferative but not quiescent ECs, as has been applied to breast cancer treatment through the design of efficient, highly selective anticancer agents able to minimize toxicity.[38]

The rodent laser trauma model has contributed greatly to the present knowledge of nAMD pathogenesis, and the reproducibility of its response has encouraged studies in novel pharmacological treatments of CNV.[24] Accordingly, using the LI-CNV model in wild-type and *CD93*$^{-/-}$ mice, we observed not only that the CD93 knockdown impaired the formation of new blood vessels in injured areas but also that ECs strongly expressed CD93 in wild-type laser-damaged regions, suggesting the pivotal role of CD93 during the growth of blood vessels in the process of CNV.

The relevance of Multimerin-2 in angiogenesis has been previously described, stressing its dual role as an angiostatic or a proangiogenic molecule.[16,18,22,31] These conflicting roles could be context dependent, as recently suggested by a study using the *Multimerin-2* knockout model, which highlights its role in maintaining proper blood vessel homeostasis and stabilization.[17] Therefore, through the engagement of CD93, Multimerin-2 expression may be required for vessel development in specific steps of the angiogenic process.[9,18] Accordingly, inhibiting the CD93/Multimerin-2 interaction may disrupt vascular integrity, thus retarding angiogenesis and tumor growth. In fact, the use of a Multimerin-2 recombinant peptide containing the CD93 binding site decreased tumor growth in mouse models.[16] Also, the antiangiogenic antibody 4E1 binds between the CTLD and sushi domains, the CD93 region involved in the interaction with Multimerin-2 (Fig. 4A).[9,10] Current rodent models of CNV are still limited by the anatomical lack of a macula and by the inability to recapitulate the complex chain of events from early to late AMD.[24] In light of these observations, the possibility of inhibiting CD93/Multimerin-2 binding on human choroidal proliferative endothelium could provide important information regarding the role of this interaction in human CNV. To this end, we set up a novel experimental model based on CSA, employing human eye tissue from postmortem donors and, as a consequence, primary and not immortalized human choroidal ECs.[39] In order to maximally reduce the postmortem deterioration, human choroids were processed as quickly as possible. In all cases, despite the different ages and causes of death, in our experimental settings we observed the emergence of endothelial sprouts. Of note, blockage of the CD93/Multimerin-2 interaction by the antibody 4E1 impaired the ability of human choroidal tissues to form endothelial sprouts, reinforcing the hypothesis that hampering the CD93/Multimerin-2 interaction in the neovascularized choroid may be of potential benefit in the treatment of nAMD patients.

In conclusion, we demonstrated that choroidal human tissues obtained from healthy cornea donors might be exploited in choroid sprouting assays as effectively as the employment of rodent tissues for microvascular disease research.[27] It is currently unknown whether or not rodent models are an appropriate choice for testing humanized antibodies, and it is difficult in a preclinical setting to evaluate the toxicity and safety of potentially effective drugs for the treatment of human patients.[24,40] However, the novel experimental approach based on choroidal sprouting from postmortem eyes proposed in this study may represent a platform for appropriate testing of new pharmacological compounds for AMD treatment.

Acknowledgments

Supported by a Grant Dipartimento di Eccellenza (2018–2022) grant; I.Ri.Fo.R Onlus (Institute for Research, Training, and Rehabilitation); Italian Association for the Blind and Visually Impaired; Italian Association for Cancer Research (grant IG-23643, MM); and the Italian Ministry of Health (grant RF-2018-12365425, MM).

Disclosure: **G.M. Tosi,** None; **G. Neri,** None; **S. Barbera,** None; **L. Mundo,** None; **B. Parolini,** None; **S. Lazzi,** None; **R. Lugano,** None; **E. Poletto,** None; **L. Leoncini,** None; **G. Pertile,** None; **M. Mongiat,** None; **A. Dimberg,** None; **F. Galvagni,** None; **M. Orlandini,** None

References

1. Flaxman SR, Bourne RRA, Resnikoff S, et al. Global causes of blindness and distance vision impairment 1990–2020: a systematic review and meta-analysis. *Lancet Glob Health*. 2017;5:e1221–e1234.
2. Wong WL, Su X, Li X, et al. Global prevalence of age-related macular degeneration and disease burden projection for 2020 and 2040: a systematic review and meta-analysis. *Lancet Glob Health*. 2014;2:e106–e116.
3. Coleman HR, Chan C-C, Ferris FL, Chew EY. Age-related macular degeneration. *Lancet* 2008;372:1835–1845.

4. Handa JT, Bowes Rickman C, Dick AD, et al. A systems biology approach towards understanding and treating non-neovascular age-related macular degeneration. *Nat Commun*. 2019;10:3347.
5. Mammadzada P, Corredoira PM, André H. The role of hypoxia-inducible factors in neovascular age-related macular degeneration: a gene therapy perspective. *Cell Mol Life Sci*. 2020;77:819–833.
6. Khan KA, McMurray JL, Mohammed F, Bicknell R. C-type lectin domain group 14 proteins in vascular biology, cancer and inflammation. *FEBS J*. 2019;286:3299–3332.
7. Langenkamp E, Zhang L, Lugano R, et al. Elevated expression of the C-type lectin CD93 in the glioblastoma vasculature regulates cytoskeletal rearrangements that enhance vessel function and reduce host survival. *Cancer Res*. 2015;75:4504–4516.
8. Tosi GM, Caldi E, Parolini B, et al. CD93 as a potential target in neovascular age-related macular degeneration. *J Cell Physiol*. 2017;232:1767–1773.
9. Galvagni F, Nardi F, Spiga O, et al. Dissecting the CD93-Multimerin 2 interaction involved in cell adhesion and migration of the activated endothelium. *Matrix Biol*. 2017;64:112–127.
10. Orlandini M, Galvagni F, Bardelli M, et al. The characterization of a novel monoclonal antibody against CD93 unveils a new antiangiogenic target. *Oncotarget* 2014;5:2750–2760.
11. Galvagni F, Nardi F, Maida M, et al. CD93 and dystroglycan cooperation in human endothelial cell adhesion and migration. *Oncotarget*. 2016;7:10090–10103.
12. Zhang M, Bohlson SS, Dy M, Tenner AJ. Modulated interaction of the ERM protein, moesin, with CD93. *Immunology*. 2005;115:63–73.
13. Galvagni F, Baldari CT, Oliviero S, Orlandini M. An apical actin-rich domain drives the establishment of cell polarity during cell adhesion. *Histochem Cell Biol*. 2012;138:419–433.
14. Barbera S, Nardi F, Elia I, et al. The small GTPase Rab5c is a key regulator of trafficking of the CD93/Multimerin-2/β1 integrin complex in endothelial cell adhesion and migration. *Cell Comm Signal*. 2019;17:55.
15. Zanivan S, Maione F, Hein MY, et al. SILAC-based proteomics of human primary endothelial cell morphogenesis unveils tumor angiogenic markers. *Mol Cell Proteomics*. 2013;12:3599–3611.
16. Khan KA, Naylor AJ, Khan A, et al. Multimerin-2 is a ligand for group 14 family C-type lectins CLEC14A, CD93 and CD248 spanning the endothelial pericyte interface. *Oncogene*. 2017;36:6097–6108.
17. Pellicani R, Poletto E, Andreuzzi E, et al. Multimerin-2 maintains vascular stability and permeability. *Matrix Biol*. 2020;87:11–25.
18. Lugano R, Vemuri K, Yu D, et al. CD93 promotes β1 integrin activation and fibronectin fibrillogenesis during tumor angiogenesis. *J Clin Invest*. 2018;128:3280–3297.
19. Norsworthy PJ, Fossati-Jimack L, Cortes-Hernandez J, et al. Murine CD93 (C1qRp) contributes to the removal of apoptotic cells in vivo but is not required for C1q-mediated enhancement of phagocytosis. *J Immunol*. 2004;172:3406–3414.
20. American Physiological Society, World Medical Association General Assembly. Guiding principles for research involving animals and human beings. *Am J Physiol Cell Physiol*. 2002;282:R281–R283.
21. Tosi GM, Neri G, Caldi E, et al. TGF-β concentrations and activity are down-regulated in the aqueous humor of patients with neovascular age-related macular degeneration. *Sci Rep*. 2018;8:8053.
22. Lorenzon E, Colladel R, Andreuzzi E, et al. MULTIMERIN2 impairs tumor angiogenesis and growth by interfering with VEGF-A/VEGFR2 pathway. *Oncogene*. 2012;31:3136–3147.
23. Lambert V, Lecomte J, Hansen S, et al. Laser-induced choroidal neovascularization model to study age-related macular degeneration in mice. *Nat Protoc*. 2013;8:2197–2211.
24. Pennesi ME, Neuringer M, Courtney RJ. Animal models of age related macular degeneration. *Mol Aspects Med*. 2012;33:487–509.
25. Li S, Li T, Luo Y, et al. Retro-orbital injection of FITC-dextran is an effective and economical method for observing mouse retinal vessels. *Mol Vis*. 2011;17:3566–3573.
26. Yardeni T, Eckhaus M, Morris HD, Huizing M, Hoogstraten-Miller S. Retro-orbital injections in mice. *Lab Anim*. 2011;40:155–160.
27. Shao Z, Friedlander M, Hurst CG, et al. Choroid sprouting assay: an ex vivo model of microvascular angiogenesis. *PLoS One*. 2013;8:e69552.
28. Orlandini M, Nucciotti S, Galvagni F, et al. Morphogenesis of human endothelial cells is inhibited by DAB2 via Src. *FEBS Lett*. 2008;582:2542–2548.
29. Bao L, Tang M, Zhang Q, et al. Elevated expression of CD93 promotes angiogenesis and tumor growth in nasopharyngeal carcinoma. *Biochem Biophys Res Commun*. 2016;476:467–474.
30. Olsen R, Lindh M, Vorkapic E, et al. CD93 gene polymorphism is associated with disseminated colorectal cancer. *Int J Colorectal Dis*. 2015;30:883–890.
31. Colladel R, Pellicani R, Andreuzzi E, et al. MULTIMERIN2 binds VEGF-A primarily via the carbohydrate chains exerting an angiostatic function and impairing tumor growth. *Oncotarget*. 2016;7:2022–2037.
32. Andreuzzi E, Capuano A, Pellicani R, et al. Loss of Multimerin-2 and EMILIN-2 expression in gastric cancer associate with altered angiogenesis. *Int J Mol Sci*. 2018;19:E3983.
33. Eelen G, de Zeeuw P, Treps L, Harjes U, Wong BW, Carmeliet P. Endothelial cell metabolism. *Physiol Rev*. 2017;98:3–58.
34. Bressler SB. Introduction: understanding the role of angiogenesis and antiangiogenic agents in age-related macular degeneration. *Ophthalmology*. 2009;116(suppl):S1–S7.
35. Jager RD, Mieler WF, Miller JW. Age-related macular degeneration. *N Engl J Med*. 2008;358:2606–2617.
36. Solomon SD, Lindsley K, Vedula SS, Krzystolik MG, Hawkins BS. Anti-vascular endothelial growth factor for neovascular age-related macular degeneration. *Cochrane Database Syst Rev*. 2019;3:CD005139.
37. Masiero M, Simões Filipa C, Han Hee D, et al. A core human primary tumor angiogenesis signature identifies the endothelial orphan receptor ELTD1 as a key regulator of angiogenesis. *Cancer Cell*. 2013;24:229–241.
38. Slaga D, Ellerman D, Lombana TN, et al. Avidity-based binding to HER2 results in selective killing of HER2-overexpressing cells by anti-HER2/CD3. *Sci Transl Med*. 2018;10:eaat5775.
39. Loeven MA, van Gemst JJ, Schophuizen CMS, et al. A novel choroidal endothelial cell line has a decreased affinity for the age-related macular degeneration-associated complement factor H variant 402H. *Invest Ophthalmol Vis Sci*. 2018;59:722–730.
40. Lu F, Adelman RA. Are intravitreal bevacizumab and ranibizumab effective in a rat model of choroidal neovascularization? *Graefes Arch Clin Exp Ophthalmol*. 2009;247:171–177.

Investigative Ophthalmology & Visual Science

4 UNPUBLISHED RESULTS: The characterization of the CD93 dimeric form in ECs.

4.1 Introduction

With the aim to gain insights into the molecular structure of a recombinant form of CD93 comprising the CTLD and the sushi domain, which together form the protein fragment named D1L, implicated in the CD93/MMRN2 interaction (Galvagni et al., 2017), we characterized the formation and analyzed the functional meaning of the CD93 dimerization.

First, we expressed and purified the recombinant D1L protein in *E. coli* and assessed the correct protein folding by means of both an anti-CD93 monoclonal antibody that recognizes a conformational epitope and the binding to MMRN2.

Previous work on the CD93 CTLD domain has revealed the formation of CD93's CTLD dimers in *E.* coli (Nativel et al., 2016). Therefore, we characterized the dimer formation in HUVECs and expressed the longer recombinant form of CD93 spanning from the CTLD to the Mucin like domain in HEK 293 cells. We showed the formation of the CD93 dimer and observed its sensitivity to reducing agents suggesting that dimerization might occur *via* swapping of two monomeric CTLDs as it happens for other CTLD-containing proteins (Liu and Eisenberg, 2002). Finally, we demonstrated that in immunoprecipitation experiments the CD93 dimers strongly bind to MMRN2 in comparison to monomers.

To complete these preliminary results, we are currently working to obtain the crystal structure of the monomeric CD93 known as D1L, which is critical in mediating CD93 functions through MMRN2 binding. Next, by means of more accurate techniques that analyze the interaction of endogenous proteins in ECs, we will better characterize the binding of the dimer to MMRN2 and calculate the affinity of both the monomer and the dimer for the MMRN2.

4.2 Results

Expression and purification of recombinant CD93 in E. coli

Due to the presence of four disulfide bonds in the CD93 CTLD that are instrumental for the proper protein folding and the highly reducing environment of *E.coli* cytoplasm, we co-expressed the pTIFA vector encoding the Erv1p and DsbC enzymes together with the pET28a-His-TEV-CD93-D1L in BL21 cells (Nativel et al., 2016). Coomassie staining confirmed soluble expression of the recombinant protein (Figure 1A). Proper protein folding was validated by immunoblotting experiments that compared D1L expression in HEK 293 cells using a monoclonal antibody able to bind a conformational epitope (Figure 1B). Interestingly, we observed formation of protein dimers in both eukaryotic and prokaryotic cell extracts (Figure 1B).

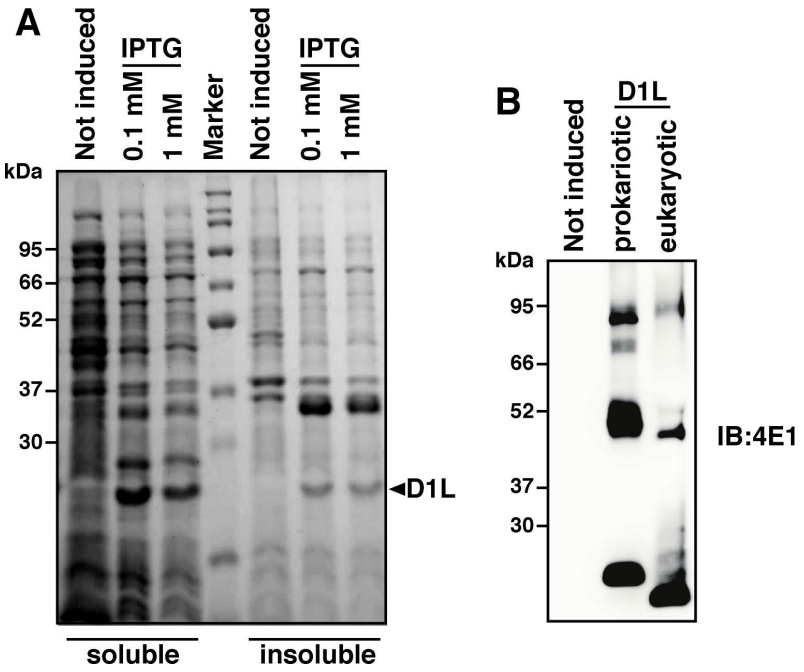

Figure 1. Expression of recombinant D1L in *E. Coli.*

A) *Soluble and insoluble fractions of cell lysates from non-induced and induced with 0.1 or 1mM IPTG BL21 cells were analyzed by non-reducing SDS-PAGE and stained using Coomassie dye.* ***B)*** *Non-reducing immunoblotting analysis of prokaryotic and eukaryotic D1L. Proteins were detected using the anti-CD93 monoclonal antibody 4E1.*

In conclusion, these experimental procedures allowed us to obtain a soluble bacterial recombinant protein, which reflects key features of its eukaryotic counterpart. We therefore carried out its purification for further analyses (Figure 2).

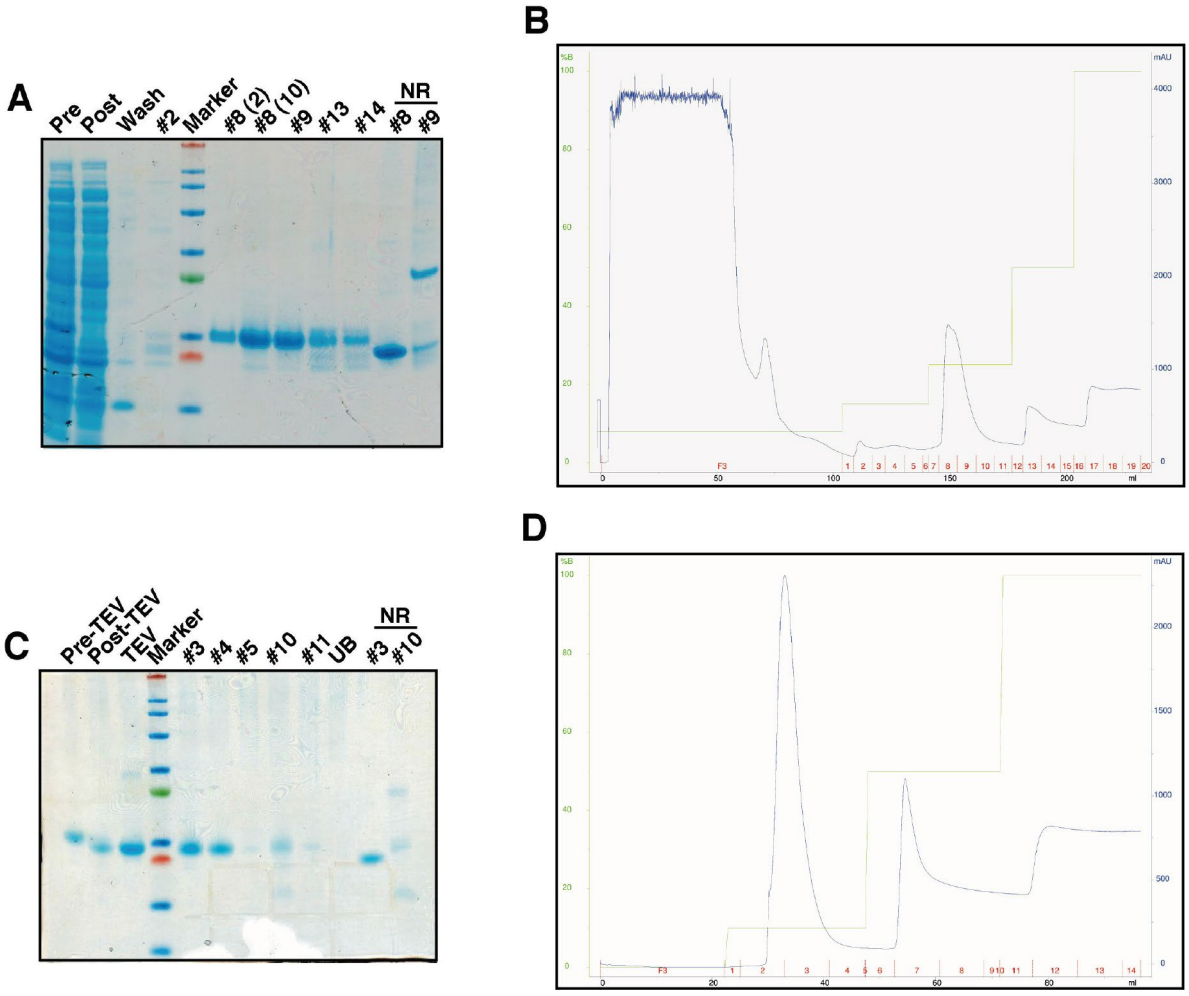

Figure 2. Purification of recombinant D1L.

A) *Fractions of post affinity purification from E. coli cell extracts were stained with Coomassie dye. Numbers indicate the relative fraction showed in B.* ***B)*** *Chromatogram of affinity purification. The y-axis on the left indicates percentage of 0.5M imidazole-containing solution relative to the binding solution. The y-axis on the right indicates U.V. reading expressed in arbitrary units (mAU). The x-axis indicates elution fractions.* ***C)*** *Protein fractions were cleaved using His^6-tagged TEV enzyme, subjected to affinity purification and stained with Coomassie staining, numbers indicate the relative fraction showed in D.* ***D)*** *Chromatogram of affinity purification. The y-axis on the left indicates percentage of 0.5M imidazole-containing solution relative to the binding solution. The y-axis on the right indicates U.V. reading expressed in arbitrary units (mAU). The x-axis indicates elution fractions.*

CD93 dimers in HUVECs

To better characterize the formation of CD93 dimers, we employed the soluble CD93 mutant spanning from the CTLD to the Mucin-like domain (named D1D3), expressed it in HEK 293 cells, and performed immunoblotting analyses under reducing, non-reducing and native conditions (Figure 3A). Importantly, in the presence of 10mM DTT the dimer band disappeared suggesting that sulfur bridges play a role in the dimer formation and stabilization. Hence, to evaluate whether CD93 dimerization occurred in HUVECs, we performed immunoblotting analyses of HUVEC lysates in the absence or presence of 10mM DTT and blotted with different anti-CD93 antibodies. As shown in Figure 3B, every antibody was able to recognize monomeric and dimeric CD93 under non-reducing conditions, while two of them failed to recognize the proteins when 10mM DTT was added to the lysate. Finally, to corroborate the CD93 dimer formation in HUVECs we used a lentiviral construct to overexpress a membrane bound Myc-tagged D1L (D1L-TM) and performed co-immunoprecipitation experiments. Surprisingly, the D1L-TM mutant was able to interact with endogenous CD93 in HUVECs (Figure 3C), suggesting that in human ECs CD93 forms a dimer stabilized by sulfur bridges.

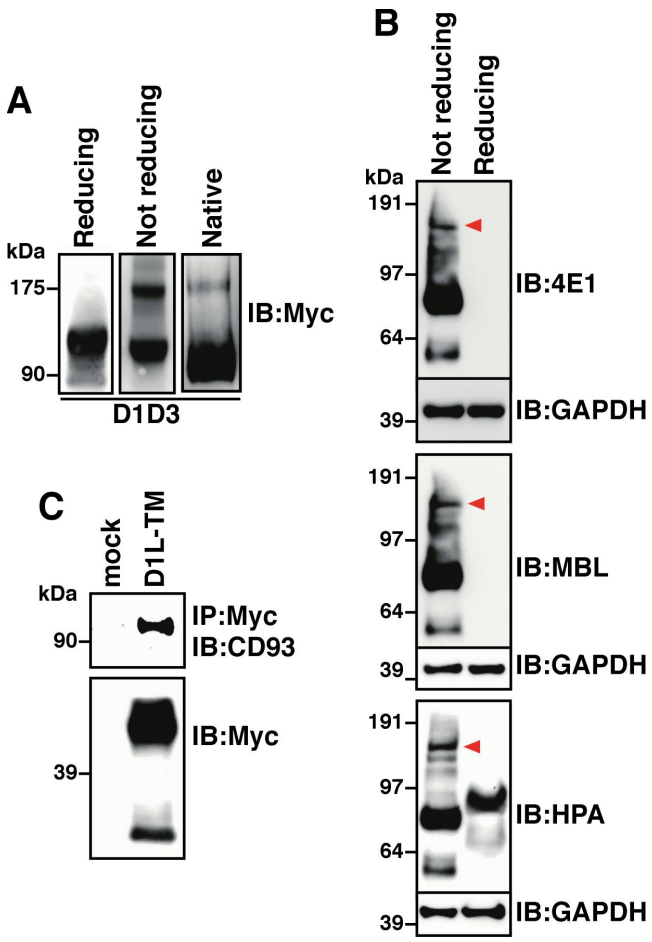

Figure 3. Characterization of CD93 dimers in HUVECs.

A) *Immunoblotting analysis of soluble D1D3 CD93 mutants in reducing, non-reducing and native conditions using anti-Myc tag antibodies.* ***B)*** *HUVEC extracts were treated (reducing) or not (not reducing) with 10mM DTT and subjected to immunoblotting analysis using different anti-CD93 specific antibodies, red arrowheads indicate CD93 dimers. To confirm equal loading, cell extracts were analyzed using anti-GAPDH antibodies.* ***C)*** *Cell extracts of HUVECs transduced with the D1L-TM mutant were immunoprecipitated using anti-Myc antibodies. Immunoprecipitates were analyzed by immunoblotting using anti-CD93 specific antibodies.*

The CD93 dimer binds to MMRN2

To gain functional insights of the dimeric form of CD93, we tested whether CD93 dimers could bind to MMRN2. We exogenously expressed MMRN2 in HEK 293 cells, incubated the supernatant of MMRN2-transfected cells with either bacterial or mammalian-expressed D1L, and performed co-immunoprecipitation experiments. Both the prokaryotic and the eukaryotic proteins were able to interact with the MMRN2, however, D1L dimers showed higher affinity to MMRN2 compared to the monomeric forms (Figure 4A, quantified in 4B).

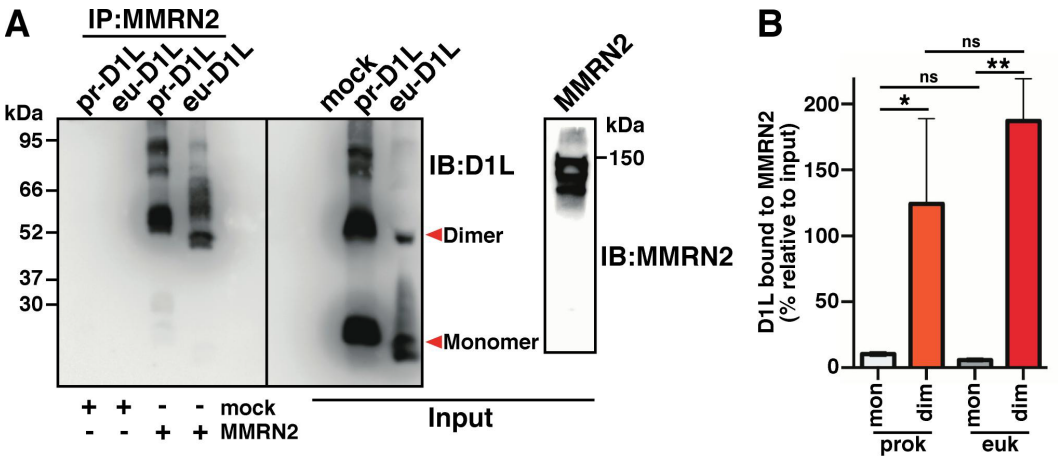

Figure 4. CD93 dimers bind to MMRN2.

A) *E. coli cell extracts (pr-D1L) or D1L-containing supernatants of transfected HEK 293 cells (eu-D1L) were mixed with supernatants of MMRN2-expressing HEK 293 or mock, and immunoprecipitated using anti-MMRN2 antibodies. Immunoprecipitates were analyzed by immunoblotting using anti-CD93 antibodies. Red arrowheads indicate bands corresponding to D1L monomers or dimers.* ***B)****. Quantitative analysis of the D1L protein levels bound to MMRN2 from experiments performed as in A. Values represent the percentage of the ratio between D1L monomer or dimer levels in the IP over their respective input levels. *P < 0.05 and **P < 0.01; Ordinary one-way ANOVA.*

4.3 Materials and methods

DNA constructs and cloning

pET28a-His-TEV-CD93-D1L was purchased by Genscript (Piscataway, NJ, USA). The pTIFA vector, encoding the Erv1p and DsbC enzymes necessary for the proper formation of sulphur bridges and protein folding in the *E. coli* cytoplasm, was a generous gift from Dr. W. Viranaicken (UMR PIMIT, France). MMRN2-expressing plasmid was a generous gift from Dr. M. Mongiat (CRO IRCCS, Italy). To obtain His^6-tagged D1L for eukaryotic expression the His^6 tag was introduced by PCR and the CD93 sequence was amplified using the following primers: For1 5'-GAGAGGATCCGACACGGAGGCGGTGGTCTG and Rev1 5'-GAGAGAATTCTCAGTGGTGATGGTGATGATGACAGAGGGGGCCCGAG. PCR fragments were then digested using BamHI and EcoRI and subcloned into a pCS2 vector containing the CD93 leader sequence as previously described (Galvagni et al., 2017). The lentiviral vector containing the Myc-tagged D1L-TM sequence was obtained by amplification with the following primers: For2 5'-GAGATCTAGAGCCACCATGGCCACCTCCATGGGC and Rev2 5'-GAGATCTAGAGGCTCGAGAGGCCTTG. Fragments were digested using the XbaI restriction enzyme and subcloned into an EF1a-CD93TM-P2A-GFP lentiviral vector containing the CD93 transmembrane domain. All plasmids were checked by sequencing.

Cell cultures and transfection

HUVECs from single donors were purchased from PromoCell (Heidelberg, Germany) and grown on gelatin-coated plates in antibiotic-free Endothelial Cell Basal Medium (EBM-MV2) with supplements (PromoCell) as previously described (Orlandini et al., 2008). For lentiviral particles production, human Lenti-X 293T cells (Takara Bio Inc, Kusatsu, Japan) were grown in DMEM containing 2% FBS and 1 mM sodium butyrate (Merck KGaA, Darmstadt, Germany), which increases viral titer (Cribbs et al., 2013). Transient transfection of Lenti-X 293T cells was obtained by using Transporter 5 transfection reagent (Polysciences, Warrington, PA, USA).

Protein expression and purification

BL21 (DE3) (Novagen) were co-transformed with pET28a-His-TEV-CD93-D1L and pTIFA as previously described (Nativel et al., 2016), and grown in Luria-Bertani (LB) 1.5% agar plates containing 25µg/ml Kanamycin and 35µg/ml Chloramphenicol. Single colonies were pre-inoculated in 20ml LB containing 25ug/ml Kanamycin and 35ug/ml Chloramphenicol and let grow overnight. 20 mL of bacterial cells were inoculated in 1L of LB medium without antibiotics and protein expression was induced at 0.4 OD_{600} using 0.25mM isopropyl-b-D-thiogalactoside (IPTG) for 24h at 18°C in continuous shaking. Bacterial pellets were obtained by centrifugation at 4000*g* and resuspended in PBS containing 25mM imidazole. Bacterial lysis was performed by adding 0.5mg/ml lysozyme (Thermo Fisher Scientific, Waltham, MA, USA) followed by sonication. Lysates were centrifuged 11000*g* for 60min at 8°C to obtain supernatants and pellets. Samples of

total cell lysates, supernatants and pellets were subsequently analyzed by non-reducing SDS-PAGE and stained with Simplyblue (Thermo Fisher Scientific) coomassie solution to check recombinant protein expression.

Protein purification was obtained using a fast protein liquid chromatograph (FPLC) Akta purifier system endowed of a UV-900 Detector and a Frac-900 fraction collector (Amersham Pharmacia Biotech Inc, Piscataway, NJ, USA). Cell supernatants were loaded into a Cytiva 5ml His Trap FF Crude (Thermo Fisher Scietific) nickel affinity chromatography column, washed with 10 volumes of PBS containing 25mM imidazole, then eluted with a solution of 125mM imidazole in PBS. Aliquots were analyzed by non-reducing SDS-PAGE analysis and pure fractions were pooled and dialyzed once against 100 volumes of PBS overnight using a 10 kDa cutoff Spectra/Por dialysis membrane (Thermo Fisher Scientific). To achieve His-tag cleavage, we added directly to the dialysis membrane an in-house produced His^6-tagged TEV protease (HT-TEV) at a ratio of 0.05mg TEV *per* mg of target protein at 4°C. Complete cleavage was obtained after overnight incubation and the resulting protein sample was applied to a 5ml His Trap FF Crude nickel affinity chromatography column to separate the mature D1L (eluted with a solution of PBS containing 50mM imidazole) from the His^6-tagged TEV (eluted at a concentration of 250mM imidazole in PBS). Next, fractions containing D1L protein were subjected to a second round of dialysis as described above. Finally, protein concentration was calculated using the bicinchoninic acid assay (BCA) (Thermo Fisher Scientific).

Antibodies

The following primary antibodies were used: rabbit anti-CD93 (HPA009300, Atlas Antibodies, Bromma, Sweden); mouse anti-CD93 (D198-3, MBL International Corporation, Ottawa, IL, USA); mouse monoclonal anti-CD93 (clone 4E1) (Orlandini et al., 2014) rabbit anti-GAPDH (ab9485), rabbit anti-Myc tag (ab9106, Abcam, Cambridge, United Kingdom); rabbit anti-Multimerin-2 (Lorenzon et al., 2012).

Immunoprecipitation and Immunoblotting analyses

Co-immunoprecipitation experiments were carried out using the protein A conjugated dynabeads (Thermo Fisher Scientific) according to the manufacturer's instructions. Cell lysates were immunoprecipitated using the primary antibody, and analyzed by immunoblotting as previously described (Galvagni et al., 2007). Densitometric analyses were performed using the gel analyzer tool of ImageJ2.

Statistical analysis

Data analyses were performed using Prism 6 statistical software (GraphPad, San Diego, CA, USA) and the values represent the mean +/- SD obtained from at least three independent experiments. The statistical significance of the differences between two groups was determined using the two-tailed Student t-test. All P values reported were two-tailed and $P < 0.05$ was considered statistically significant.

5 DISCUSSION

EC cell migration represents a critical step of sprouting angiogenesis and therefore is an appealing target for vascular growth inhibition. CD93 regulates EC migration in different ways. First, the binding to MMRN2 activates β1 integrin which, in turn, regulates matrix composition through the deposition of fibronectin fibrils (Lugano et al., 2018). Second, upon Src family kinases-dependent phosphorylation of two tyrosine residues (Galvagni et al., 2016), CD93 triggers a signaling pathway that controls actin cytoskeleton dynamics *via* the Cbl/Crk/DOCK180 signaling pathway that culminates in the modulation of Rho GTPases (Barbera et al., 2021a, 2021b). Indeed, live imaging and immunofluorescence analyses of CD93-depleted cells show high stress fiber content and slow actin dynamics accounting for the reduced EC migratory capability. These studies suggest that CD93 might redundantly regulate EC migration by convergent mechanisms. On one hand, following MMRN2 binding, mediates the activation of β1 integrin, with consequent FAK activation, and, on the other, by regulating the phosphorylation of Cbl on the tyrosine residue 774. Interestingly, the cooperation of FAK and Cbl is known to promote focal adhesion turnover and actin remodeling in pro-migratory stress fibers and lamellipodia (Rafiq et al., 2012; Wozniak et al., 2004), leading to the speculation that, in ECs, CD93 might be a point of connection between the FAK- and Cbl-mediated signaling pathways. In migrating cells the establishment of apical-basal cell polarity allows to functionally orchestrate protein distribution (Ebnet et al., 2018; Polo and Di Fiore, 2006). We demonstrated that CD93 polarized distribution is regulated by its cytoplasmic domain and interaction with filamentous actin (F-actin). Although a direct connection between CD93 and the F-actin occurs *via* Moesin (Zhang et al., 2005) and accounts for CD93 distribution, plasma membrane regions containing CD93 are transported across the cell by Rab5C^{+ve} endosomes and recycled on strategic cell areas where pro-migratory proteins are needed. Importantly, in these endosomal compartments, CD93 remains associated with both MMRN2 and β1 integrin suggesting that the complex is shuttled to specific regions of the plasma membrane subjected to specific cues (Barbera et al., 2019).

Due to its ability to regulate EC migration, the CD93/MMRN2 interaction is considered an appealing target to prevent neovascularization (Galvagni et al., 2017; Khan et al., 2017). Using *in vivo* and *ex vivo* CNV mouse models we showed that CD93 itself guides the progression of vascularization in injured choroids. Importantly, since rodent models of CNV present anatomical differences with the human counterparts, we employed *ex vivo* CSA of human tissues to evaluate the effects of blocking the CD93/MMRN2 interaction by the 4E1 mAb, which competes with MMRN2 for CD93 binding (Galvagni et al., 2017), showing that blocking this interaction reduces EC sprouting (Tosi et al., 2020). These results open for interesting therapeutic avenues of targeting the CD93/MMRN2 interaction to prevent choroidal neovascularization, although other *in vivo* models are still needed to better define the effects of targeting CD93 in nAMD.

CD93 has always been considered a monomeric protein. Our preliminary biochemical studies have shown that CD93 can form a dimer *via* interaction of the CTLD domain of two monomers. Although other groups have shown that recombinant CD93's CTLD can form monomers in *E. coli* (Nativel et al., 2016), a better characterization of CD93 dimers has never been attempted in more physiological contexts such as in ECs. We showed that CD93 forms a dimer in eukaryotic cells and more specifically in HUVECs. Interestingly, the dimeric form of CD93 mutants comprising the CTLD and sushi domains showed a higher affinity for the MMRN2 compared to their monomeric counterpart. These findings need to be corroborated in more accurate models as they might have important repercussion on the development of inhibitory molecules that aim to block the CD93 activity. Indeed, due to its multifaceted functions in ECs, aiming for the solely CD93/MMRN2 blockade can take advantage on developing molecules that selectively inhibit the dimeric form of CD93 thus reducing unpredictable effects. On the other hand, inhibiting the solely CD93 monomers can be challenging due to the fact that CD93 dimers seem to be formed by the entire domains of two monomers. To gain insights on how CD93 dimers form, our research is also pointing to define the crystal structure of recombinant CD93 monomers and dimers. These findings not only will increase our understanding of CD93's biochemical properties, but also will clarify the nature of CD93 dimerization in light of developing selective inhibitors.

Neovascularization is implicated in several pathologies such as cancer and nAMD. In the last decades, the scientific community has pointed towards vascular remodeling for cancer treatment in the attempt to normalize the tumor vasculature. Conceptually, instead of starving the tumor by vascular pruning, a normalized vasculature reacquires physiological features that improve tumor perfusion, facilitating drug delivery and providing a less hostile environment for immune cell infiltration and function. However, if for cancer vascular normalization seems to be the road to follow, in nAMD the strategy could be to aim for vessel pruning to prevent exudation and halt the progression of the disease. Therefore, the approach of targeting the vasculature must be different and dependent on the pathological context. In this scenario, CD93 represents an ideal target. Being expressed mainly in the activated endothelium and being a regulator of EC migration, CD93 blockade should minimize unwanted side effects on other tissues and has already shown the potential of being suitable for both anti-angiogenic therapy and vascular normalization (Tosi et al., 2020; Sun et al., 2021).

REFERENCES

Adams, R.H., Alitalo, K., 2007. Molecular regulation of angiogenesis and lymphangiogenesis. Nat. Rev. Mol. Cell Biol. 8, 464–478. https://doi.org/10.1038/nrm2183

Al-Zamil, W., Yassin, S., 2017. Recent developments in age-related macular degeneration: a review. Clin. Interv. Aging Volume 12, 1313–1330. https://doi.org/10.2147/CIA.S143508

Baeriswyl, V., Christofori, G., 2009. The angiogenic switch in carcinogenesis. Semin. Cancer Biol. 19, 329–337. https://doi.org/10.1016/j.semcancer.2009.05.003

Bao, L., Tang, M., Zhang, Q., You, B., Shan, Y., Shi, S., Li, L., Hu, S., You, Y., 2016. Elevated expression of CD93 promotes angiogenesis and tumor growth in nasopharyngeal carcinoma. Biochem. Biophys. Res. Commun. 476, 467–474. https://doi.org/10.1016/j.bbrc.2016.05.146

Barbera, S., Lugano, R., Pedalina, A., Mongiat, M., Santucci, A., Tosi, G.M., Dimberg, A., Galvagni, F., Orlandini, M., 2021a. The C-type lectin CD93 controls endothelial cell migration via activation of the Rho family of small GTPases. Matrix Biol. 99, 1–17. https://doi.org/10.1016/j.matbio.2021.05.006

Barbera, S., Nardi, F., Elia, I., Realini, G., Lugano, R., Santucci, A., Tosi, G.M., Dimberg, A., Galvagni, F., Orlandini, M., 2019. The small GTPase Rab5c is a key regulator of trafficking of the CD93/Multimerin-2/β1 integrin complex in endothelial cell adhesion and migration. Cell Commun. Signal. 17, 55. https://doi.org/10.1186/s12964-019-0375-x

Barbera, S., Raucci, L., Lugano, R., Tosi, G.M., Dimberg, A., Santucci, A., Galvagni, F., Orlandini, M., 2021b. CD93 Signaling via Rho Proteins Drives Cytoskeletal Remodeling in Spreading Endothelial Cells. Int. J. Mol. Sci. 22, 12417. https://doi.org/10.3390/ijms222212417

Carmeliet, P., 2003. Angiogenesis in health and disease. Nat. Med. 9, 8.

Carmeliet, P., Jain, R.K., 2011a. Molecular mechanisms and clinical applications of angiogenesis. Nature 473, 298–307. https://doi.org/10.1038/nature10144

Carmeliet, P., Jain, R.K., 2011b. Principles and mechanisms of vessel normalization for cancer and other angiogenic diseases. Nat. Rev. Drug Discov. 10, 417–427. https://doi.org/10.1038/nrd3455

Carmeliet, P., Jain, R.K., 2000. Angiogenesis in cancer and other diseases. Nature 407, 249–257. https://doi.org/10.1038/35025220

Challa, J.K., Gillies, M.C., Penfold, P.L., Gyory, J.F., Hunyor, A.B., Billson, F.A., 1998. Exudative macular degeneration and intravitreal triamcinolone: 18 month follow up. Aust. N. Z. J. Ophthalmol. 26, 277–281. https://doi.org/10.1111/j.1442-9071.1998.tb01330.x

Cribbs, A.P., Kennedy, A., Gregory, B., Brennan, F.M., 2013. Simplified production and concentration of lentiviral vectors to achieve high transduction in primary human T cells. BMC Biotechnol. 13, 98. https://doi.org/10.1186/1472-6750-13-98

Danet, G.H., Luongo, J.L., Butler, G., Lu, M.M., Tenner, A.J., Simon, M.C., Bonnet, D.A., 2002. C1qRp defines a new human stem cell population with hematopoietic and hepatic potential. Proc. Natl. Acad. Sci. 99, 10441–10445. https://doi.org/10.1073/pnas.162104799

Daniel, E., Toth, C.A., Grunwald, J.E., Jaffe, G.J., Martin, D.F., Fine, S.L., Huang, J., Ying, G., Hagstrom, S.A., Winter, K., Maguire, M.G., 2014. Risk of Scar in the Comparison of Age-related Macular Degeneration Treatments Trials. Ophthalmology 121, 656–666. https://doi.org/10.1016/j.ophtha.2013.10.019

Day, S., Acquah, K., Mruthyunjaya, P., Grossman, D.S., Lee, P.P., Sloan, F.A., 2011. Ocular Complications After Anti–Vascular Endothelial Growth Factor Therapy in Medicare Patients With Age-Related Macular Degeneration. Am. J. Ophthalmol. 152, 266–272. https://doi.org/10.1016/j.ajo.2011.01.053

De Palma, M., Biziato, D., Petrova, T.V., 2017. Microenvironmental regulation of tumour angiogenesis. Nat. Rev. Cancer 17, 457–474. https://doi.org/10.1038/nrc.2017.51

De Smet, F., Segura, I., De Bock, K., Hohensinner, P.J., Carmeliet, P., 2009. Mechanisms of Vessel Branching: Filopodia on Endothelial Tip Cells Lead the Way. Arterioscler. Thromb. Vasc. Biol. 29, 639–649. https://doi.org/10.1161/ATVBAHA.109.185165

Dieterich, L.C., Mellberg, S., Langenkamp, E., Zhang, L., Zieba, A., Salomäki, H., Teichert, M., Huang, H., Edqvist, P.-H., Kraus, T., Augustin, H.G., Olofsson, T., Larsson, E., Söderberg, O., Molema, G., Pontén, F., Georgii-Hemming, P., Alafuzoff, I., Dimberg, A., 2012. Transcriptional profiling of human glioblastoma vessels indicates a key role of VEGF-A and TGFβ2 in vascular abnormalization: Transcriptional characterization of blood vessels in glioblastoma. J. Pathol. 228, 378–390. https://doi.org/10.1002/path.4072

Du, J., Yang, Q., Luo, L., Yang, D., 2017. C1qr and C1qrl redundantly regulate angiogenesis in zebrafish through controlling endothelial Cdh5. Biochem. Biophys. Res. Commun. 483, 482–487. https://doi.org/10.1016/j.bbrc.2016.12.118

Ebnet, K., Kummer, D., Steinbacher, T., Singh, A., Nakayama, M., Matis, M., 2018. Regulation of cell polarity by cell adhesion receptors. Semin. Cell Dev. Biol. 81, 2–12. https://doi.org/10.1016/j.semcdb.2017.07.032

Filipowska, J., Tomaszewski, K.A., Niedźwiedzki, Ł., Walocha, J.A., Niedźwiedzki, T., 2017. The role of vasculature in bone development, regeneration and proper systemic functioning. Angiogenesis 20, 291–302. https://doi.org/10.1007/s10456-017-9541-1

Folkman, F., 1971. Tumor angiogenesis: therapeutic implications. N Engl J Med 285, 1182–1186. https://doi.org/10.1056/NEJM197111182852108

Frank Billson, M.C.G., 2003. A Randomized Clinical Trial of a Single Dose of Intravitreal Triamcinolone Acetonide for Neovascular Age-Related Macular Degeneration: One-Year Results. ARCH OPHTHALMOL 121, 7.

Galvagni, F., Anselmi, F., Salameh, A., Orlandini, M., Rocchigiani, M., Oliviero, S., 2007. Vascular Endothelial Growth Factor Receptor-3 Activity Is Modulated by Its Association with Caveolin-1 on Endothelial Membrane. Biochemistry 46, 3998–4005. https://doi.org/10.1021/bi061400n

Galvagni, F., Nardi, F., Maida, M., Bernardini, G., Vannuccini, S., Petraglia, F., Santucci, A., Orlandini, M., 2016. CD93 and dystroglycan cooperation in human endothelial cell adhesion and migration. Oncotarget 7, 10090–10103. https://doi.org/10.18632/oncotarget.7136

Galvagni, F., Nardi, F., Spiga, O., Trezza, A., Tarticchio, G., Pellicani, R., Andreuzzi, E., Caldi, E., Toti, P., Tosi, G.M., Santucci, A., Iozzo, R.V., Mongiat, M., Orlandini, M., 2017. Dissecting the CD93-Multimerin 2 interaction involved in cell adhesion and migration of the activated endothelium. Matrix Biol. 64, 112–127. https://doi.org/10.1016/j.matbio.2017.08.003

Gerhardt, H., Golding, M., Fruttiger, M., Ruhrberg, C., Lundkvist, A., Abramsson, A., Jeltsch, M., Mitchell, C., Alitalo, K., Shima, D., Betsholtz, C., 2003. VEGF guides angiogenic sprouting utilizing endothelial tip cell filopodia. J. Cell Biol. 161, 1163–1177. https://doi.org/10.1083/jcb.200302047

Greenlee, M.C., Sullivan, S.A., Bohlson, S.S., 2009. Detection and characterization of soluble CD93 released during inflammation. Inflamm. Res. 58, 909–919. https://doi.org/10.1007/s00011-009-0064-0

Grunwald, J.E., Pistilli, M., Daniel, E., Ying, G.-S., Pan, W., Jaffe, G.J., Toth, C.A., Hagstrom, S.A., Maguire, M.G., Martin, D.F., 2017. Incidence and Growth of Geographic Atrophy during 5 Years of Comparison of Age-Related Macular Degeneration Treatments Trials. Ophthalmology 124, 97–104. https://doi.org/10.1016/j.ophtha.2016.09.012

Harburger, D.S., Calderwood, D.A., 2009. Integrin signalling at a glance. J. Cell Sci. 122, 1472–1472. https://doi.org/10.1242/jcs.052910

Herbert, S.P., Stainier, D.Y.R., 2011. Molecular control of endothelial cell behaviour during blood vessel morphogenesis. Nat. Rev. Mol. Cell Biol. 12, 551–564. https://doi.org/10.1038/nrm3176

Hida, K., Hida, Y., Amin, D.N., Flint, A.F., Panigrahy, D., Morton, C.C., Klagsbrun, M., 2004. Tumor-Associated Endothelial Cells with Cytogenetic Abnormalities. Cancer Res. 64, 8249–8255. https://doi.org/10.1158/0008-5472.CAN-04-1567

Hida, K., Maishi, N., Torii, C., Hida, Y., 2016. Tumor angiogenesis—characteristics of tumor endothelial cells. Int. J. Clin. Oncol. 21, 206–212. https://doi.org/10.1007/s10147-016-0957-1

Hurwitz, H., Fehrenbacher, L., Novotny, W., Cartwright, T., Hainsworth, J., Heim, W., Berlin, J., Baron, A., Griffing, S., Holmgren, E., Ferrara, N., Fyfe, G., Rogers, B., Ross, R., Kabbinavar, F., 2004. Bevacizumab plus Irinotecan, Fluorouracil, and Leucovorin for Metastatic Colorectal Cancer. N. Engl. J. Med. 350, 2335–2342. https://doi.org/10.1056/NEJMoa032691

Ikewaki, N., Yamao, H., Kulski, J.K., Inoko, H., 2010. Flow Cytometric Identification of CD93 Expression on Naive T Lymphocytes (CD4+CD45RA+ Cells) in Human Neonatal Umbilical Cord Blood. J. Clin. Immunol. 30, 723–733. https://doi.org/10.1007/s10875-010-9426-1

Jonas, J.B., Degenring, R.F., Kreissig, I., Friedemann, T., Akkoyun, I., 2005. Exudative age-related macular degeneration treated by intravitreal triamcinolone acetonide. A prospective comparative nonrandomized study. Eye 19, 163–170. https://doi.org/10.1038/sj.eye.6701438

Kao, Y.-C., Jiang, S.-J., Pan, W.-A., Wang, K.-C., Chen, P.-K., Wei, H.-J., Chen, W.-S., Chang, B.-I., Shi, G.-Y., Wu, H.-L., 2012. The Epidermal Growth Factor-like Domain of CD93 Is a Potent Angiogenic Factor. PLoS ONE 7, e51647. https://doi.org/10.1371/journal.pone.0051647

Khan, K.A., McMurray, J.L., Mohammed, F., Bicknell, R., 2019. C-type lectin domain group 14 proteins in vascular biology, cancer and inflammation. FEBS J. 286, 3299–3332. https://doi.org/10.1111/febs.14985

Khan, K.A., Naylor, A.J., Khan, A., Noy, P.J., Mambretti, M., Lodhia, P., Athwal, J., Korzystka, A., Buckley, C.D., Willcox, B.E., Mohammed, F., Bicknell, R., 2017. Multimerin-2 is a ligand for group 14 family C-type lectins CLEC14A, CD93 and CD248 spanning the endothelial pericyte interface. Oncogene 36, 6097–6108. https://doi.org/10.1038/onc.2017.214

Lai, K., Landa, G., 2015. Current choice of treatments for neovascular AMD. Expert Rev. Clin. Pharmacol. 8, 135–140. https://doi.org/10.1586/17512433.2015.990379

Langenkamp, E., Zhang, L., Lugano, R., Huang, H., Elhassan, T.E.A., Georganaki, M., Bazzar, W., Lööf, J., Trendelenburg, G., Essand, M., Pontén, F., Smits, A., Dimberg, A., 2015. Elevated Expression of the C-Type Lectin CD93 in the Glioblastoma Vasculature Regulates Cytoskeletal Rearrangements That Enhance Vessel Function and Reduce Host Survival. Cancer Res. 75, 4504–4516. https://doi.org/10.1158/0008-5472.CAN-14-3636

Liu, C., Cui, Z., Wang, S., Zhang, D., 2014. CD93 and GIPC expression and localization during central nervous system inflammation. Neural Regen. Res. 9, 0. https://doi.org/10.4103/1673-5374.145383

Liu, Y., Eisenberg, D., 2002. 3D domain swapping: As domains continue to swap. Protein Sci. 11, 1285–1299. https://doi.org/10.1110/ps.0201402

Lorenzon, E., Colladel, R., Andreuzzi, E., Marastoni, S., Todaro, F., Schiappacassi, M., Ligresti, G., Colombatti, A., Mongiat, M., 2012. MULTIMERIN2 impairs tumor angiogenesis and growth by interfering with VEGF-A/VEGFR2 pathway. Oncogene 31, 3136–3147. https://doi.org/10.1038/onc.2011.487

Løvik, G., Larsen Sand, K., Iversen, J.G., Rolstad, B., 2001. C1qRp Elicits a Ca^{++} Response in Rat NK Cells but Does not Influence NK-Mediated Cytotoxicity: C1qRp Influence on NK Cell Function. Scand. J. Immunol. 53, 410–415. https://doi.org/10.1046/j.1365-3083.2001.00895.x

Lugano, R., Ramachandran, M., Dimberg, A., 2020. Tumor angiogenesis: causes, consequences, challenges and opportunities. Cell. Mol. Life Sci. 77, 1745–1770. https://doi.org/10.1007/s00018-019-03351-7

Lugano, R., Vemuri, K., Yu, D., Bergqvist, M., Smits, A., Essand, M., Johansson, S., Dejana, E., Dimberg, A., 2018. CD93 promotes β1 integrin activation and fibronectin fibrillogenesis during tumor angiogenesis. J. Clin. Invest. 128, 3280–3297. https://doi.org/10.1172/JCI97459

Lupo, G., Caporarello, N., Olivieri, M., Cristaldi, M., Motta, C., Bramanti, V., Avola, R., Salmeri, M., Nicoletti, F., Anfuso, C.D., 2017. Anti-angiogenic Therapy in Cancer: Downsides and New Pivots for Precision Medicine. Front. Pharmacol. 07. https://doi.org/10.3389/fphar.2016.00519

Magnussen, A.L., Mills, I.G., 2021. Vascular normalisation as the stepping stone into tumour microenvironment transformation. Br. J. Cancer 125, 324–336. https://doi.org/10.1038/s41416-021-01330-z

Mahabeleshwar, G.H., Feng, W., Reddy, K., Plow, E.F., Byzova, T.V., 2007. Mechanisms of Integrin–Vascular Endothelial Growth Factor Receptor Cross-Activation in Angiogenesis. Circ. Res. 101, 570–580. https://doi.org/10.1161/CIRCRESAHA.107.155655

McGreal, E.P., Ikewaki, N., Akatsu, H., Morgan, B.P., Gasque, P., 2002. Human C1qRp Is Identical with CD93 and the mNI-11 Antigen But Does Not Bind C1q. J. Immunol. 168, 5222–5232. https://doi.org/10.4049/jimmunol.168.10.5222

Merajver, S.D., Usmani, S.Z., 2005. Multifaceted Role of Rho Proteins in Angiogenesis. J. Mammary Gland Biol. Neoplasia 10, 291–298. https://doi.org/10.1007/s10911-006-9002-8

Monahan-Earley, R., Dvorak, A.M., Aird, W.C., 2013. Evolutionary origins of the blood vascular system and endothelium. J. Thromb. Haemost. 11, 46–66. https://doi.org/10.1111/jth.12253

Nativel, B., Figuester, A., Andries, J., Planesse, C., Couprie, J., Gasque, P., Viranaicken, W., Iwema, T., 2016. Soluble expression of disulfide-bonded C-type lectin like domain of human CD93 in the cytoplasm of Escherichia coli. J. Immunol. Methods 439, 67–73. https://doi.org/10.1016/j.jim.2016.10.003

Nepomuceno, R.R., Tenner, A.J., 1998. C1qRP, the C1q Receptor That Enhances Phagocytosis, Is Detected Specifically in Human Cells of Myeloid Lineage, Endothelial Cells, and Platelets. J Immunol 160, 1929–1935.

Neve, A., Cantatore, F.P., Maruotti, N., Corrado, A., Ribatti, D., 2014. Extracellular Matrix Modulates Angiogenesis in Physiological and Pathological Conditions. BioMed Res. Int. 2014, 1–10. https://doi.org/10.1155/2014/756078

Ng, E.W.M., Adamis, A.P., 2005. Targeting angiogenesis, the underlying disorder in neovascular age-related macular degeneration. Can. J. Ophthalmol. 40, 352–368. https://doi.org/10.1016/S0008-4182(05)80078-X

Norsworthy, P.J., Fossati-Jimack, L., Cortes-Hernandez, J., Taylor, P.R., Bygrave, A.E., Thompson, R.D., Nourshargh, S., Walport, M.J., Botto, M., 2004. Murine CD93 (C1qRp) Contributes to the Removal of Apoptotic Cells In Vivo but Is Not Required for C1q-Mediated Enhancement of Phagocytosis. J. Immunol. 172, 3406–3414. https://doi.org/10.4049/jimmunol.172.6.3406

Orlandini, M., Galvagni, F., Bardelli, M., Rocchigiani, M., Lentucci, C., Anselmi, F., Zippo, A., Bini, L., Oliviero, S., 2014. The characterization of a novel monoclonal antibody against CD93 unveils a new antiangiogenic target. Oncotarget 5, 2750–2760. https://doi.org/10.18632/oncotarget.1887

Orlandini, M., Nucciotti, S., Galvagni, F., Bardelli, M., Rocchigiani, M., Petraglia, F., Oliviero, S., 2008. Morphogenesis of human endothelial cells is inhibited by DAB2 via Src. FEBS Lett. 582, 2542–2548. https://doi.org/10.1016/j.febslet.2008.06.025

Otrock, Z., Mahfouz, R., Makarem, J., Shamseddine, A., 2007. Understanding the biology of angiogenesis: Review of the most important molecular mechanisms. Blood Cells. Mol. Dis. 39, 212–220. https://doi.org/10.1016/j.bcmd.2007.04.001

Plow, E.F., Haas, T.A., Zhang, L., Loftus, J., Smith, J.W., 2000. Ligand Binding to Integrins. J. Biol. Chem. 275, 21785–21788. https://doi.org/10.1074/jbc.R000003200

Pober, J.S., Tellides, G., 2012. Participation of blood vessel cells in human adaptive immune responses. Trends Immunol. 33, 49–57. https://doi.org/10.1016/j.it.2011.09.006

Polo, S., Di Fiore, P.P., 2006. Endocytosis Conducts the Cell Signaling Orchestra. Cell 124, 897–900. https://doi.org/10.1016/j.cell.2006.02.025

Rafiq, K., Guo, J., Vlasenko, L., Guo, X., Kolpakov, M.A., Sanjay, A., Houser, S.R., Sabri, A., 2012. c-Cbl Ubiquitin Ligase Regulates Focal Adhesion Protein Turnover and Myofibril Degeneration Induced by Neutrophil Protease Cathepsin G. J. Biol. Chem. 287, 5327–5339. https://doi.org/10.1074/jbc.M111.307009

Reynolds AR, K.E., 2019. Vessel co-option in cancer. Nat Rev Clin Oncol 469–493. https://doi.org/10.1038/s41571-019-0181-9.

Seano, G., Jain, R.K., 2020. Vessel co-option in glioblastoma: emerging insights and opportunities. Angiogenesis 23, 9–16. https://doi.org/10.1007/s10456-019-09691-z

Somanath, P.R., Malinin, N.L., Byzova, T.V., 2009. Cooperation between integrin αvβ3 and VEGFR2 in angiogenesis. Angiogenesis 12, 177–185. https://doi.org/10.1007/s10456-009-9141-9

Steinberger, P., Szekeres, A., Wille, S., Prager, E., 2002. Identification of human CD93 as the phagocytic C1q receptor (C1qRp) by expression cloning. J Leukoc Biol 71, 133–40.

Sun, Y., Chen, W., Torphy, R.J., Yao, S., Zhu, G., Lin, R., Lugano, R., Miller, E.N., Fujiwara, Y., Bian, L., Zheng, L., Anand, S., Gao, F., Zhang, W., Ferrara, S.E., Goodspeed, A.E., Dimberg, A., Wang, X.-J., Edil, B.H., Barnett, C.C., Schulick, R.D., Chen, L., Zhu, Y., 2021. Blockade of the CD93 pathway normalizes tumor vasculature to facilitate drug delivery and immunotherapy. Sci. Transl. Med. 13, eabc8922. https://doi.org/10.1126/scitranslmed.abc8922

Tosi, G.M., Caldi, E., Parolini, B., Toti, P., Neri, G., Nardi, F., Traversi, C., Cevenini, G., Marigliani, D., Nuti, E., Bacci, T., Galvagni, F., Orlandini, M., 2017. CD93 as a Potential Target in Neovascular Age-Related Macular Degeneration: CD93 EXPRESSION AND SHEDDING IN AMD. J. Cell. Physiol. 232, 1767–1773. https://doi.org/10.1002/jcp.25689

Tosi, G.M., Neri, G., Barbera, S., Mundo, L., Parolini, B., Lazzi, S., Lugano, R., Poletto, E., Leoncini, L., Pertile, G., Mongiat, M., Dimberg, A., Galvagni, F., Orlandini, M., 2020. The Binding of CD93 to Multimerin-2 Promotes Choroidal Neovascularization. Investig. Opthalmology Vis. Sci. 61, 30. https://doi.org/10.1167/iovs.61.8.30

Tunica, D.G., Yin, X., Sidibe, A., Stegemann, C., Nissum, M., Zeng, L., Brunet, M., Mayr, M., 2009. Proteomic analysis of the secretome of human umbilical vein endothelial cells using a combination

of free-flow electrophoresis and nanoflow LC-MS/MS. PROTEOMICS 9, 4991–4996. https://doi.org/10.1002/pmic.200900065

Viallard, C., Larrivée, B., 2017. Tumor angiogenesis and vascular normalization: alternative therapeutic targets. Angiogenesis 20, 409–426. https://doi.org/10.1007/s10456-017-9562-9

Wozniak, M.A., Modzelewska, K., Kwong, L., Keely, P.J., 2004. Focal adhesion regulation of cell behavior. Biochim. Biophys. Acta BBA - Mol. Cell Res. 1692, 103–119. https://doi.org/10.1016/j.bbamcr.2004.04.007

Yerramothu, P., 2018. New Therapies of Neovascular AMD—Beyond Anti-VEGFs. Vision 2, 31. https://doi.org/10.3390/vision2030031

Yeung, C.K., Chan, K.P., Chan, C.K.M., Pang, C.P., Lam, D.S.C., 2004. Cytotoxicity of Triamcinolone on Cultured Human Retinal Pigment Epithelial Cells: Comparison with Dexamethasone and Hydrocortisone. Jpn. J. Ophthalmol. 48, 236–242. https://doi.org/10.1007/s10384-003-0053-8

Zhang, M., Bohlson, S.S., Dy, M., Tenner, A.J., 2005. Modulated interaction of the ERM protein, moesin, with CD93. Immunology 115, 63–73. https://doi.org/10.1111/j.1365-2567.2005.02120.x

Zimna, A., Kurpisz, M., 2015. Hypoxia-Inducible Factor-1 in Physiological and Pathophysiological Angiogenesis: Applications and Therapies. BioMed Res. Int. 2015, 1–13. https://doi.org/10.1155/2015/549412